

SMIP12

SMIP12 SEMINAR ON UTILIZATION OF STRONG-MOTION DATA

Sacramento, California
October 2, 2012

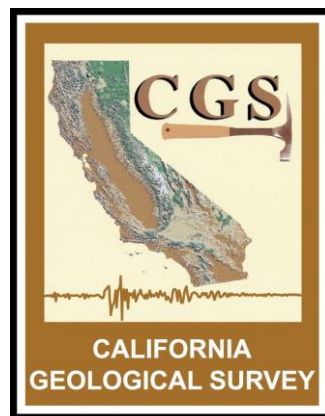
PROCEEDINGS

Sponsored by

California Strong Motion Instrumentation Program
California Geological Survey
California Department of Conservation

Co-Sponsors

California Seismic Safety Commission
California Emergency Management Agency
California Department of Transportation
Office of Statewide Health Planning and Development



The California Strong Motion Instrumentation Program (CSMIP), a program within the California Geological Survey (CGS) of the California Department of Conservation, records the strong shaking of the ground and structures during earthquakes for analysis and utilization by the engineering and seismology communities through a statewide network of strong motion instruments (www.conservation.ca.gov/CGS/smip). CSMIP is advised by the Strong Motion Instrumentation Advisory Committee (SMIAC), a committee of the California Seismic Safety Commission. Major program funding is provided by an assessment on construction costs for building permits issued by cities and counties in California, with additional funding from the California Emergency Management Office (CalEMA, formerly California Office of Emergency Services), the California Department of Transportation (Caltrans) and the Office of Statewide Health Planning and Development (OSHPD).

In July 2001, the California Office of Emergency Services (OES) began funding for the California Integrated Seismic Network (CISN), a newly formed consortium of institutions engaged in statewide earthquake monitoring that grew out of TriNet, funded by FEMA, and includes CGS, USGS, Caltech and UC Berkeley. The goals are to record and rapidly communicate ground shaking information in California, and to analyze the data for the improvement of seismic codes and standards (www.cisn.org). CISN produces ShakeMaps of ground shaking, based on shaking recorded by stations in the network, within minutes following an earthquake. The ShakeMap identifies areas of greatest ground shaking for use by OES and other emergency response agencies in the event of a damaging earthquake.

The Center for Engineering Strong Motion Data (CESMD) is operated by the CSMIP Program of the CGS in cooperation with the National Strong-Motion Project (NSMP) and the Advanced National Seismic System (ANSS) of the U.S. Geological Survey (USGS). The CESMD builds on and incorporates the CISN Engineering Data Center and will continue to serve the California region while expanding to serve other ANSS regions. The Data Center provides strong-motion data rapidly after a significant earthquake in the United States. Users also have direct access to data from previous earthquakes and detailed information about the instrumented structures and sites. The Data Center is co-hosted by CGS and USGS at www.strongmotioncenter.org

DISCLAIMER

Neither the sponsoring nor supporting agencies assume responsibility for the accuracy of the information presented in this report or for the opinions expressed herein. The material presented in this publication should not be used or relied upon for any specific application without competent examination and verification of its accuracy, suitability, and applicability by qualified professionals. Users of information from this publication assume all liability arising from such use.

SMIP12

SMIP12 SEMINAR ON UTILIZATION OF STRONG-MOTION DATA

Sacramento, California
October 2, 2012

PROCEEDINGS

Edited by

Moh Huang

Sponsored by

California Strong Motion Instrumentation Program
California Geological Survey
California Department of Conservation

Co-Sponsors

California Seismic Safety Commission
California Emergency Management Agency
California Department of Transportation
Office of Statewide Health Planning and Development

PREFACE

The California Strong Motion Instrumentation Program (CSMIP) in the California Geological Survey of the California Department of Conservation established a Data Interpretation Project in 1989. Each year CSMIP Program funds several data interpretation contracts for the analysis and utilization of strong-motion data. The primary objectives of the Data Interpretation Project are to further the understanding of strong ground shaking and the response of structures, and to increase the utilization of strong-motion data in improving post-earthquake response, seismic code provisions and design practices.

As part of the Data Interpretation Project, CSMIP holds annual seminars to transfer recent research findings on strong-motion data to practicing seismic design professionals, earth scientists and post-earthquake response personnel. The purpose of the annual seminar is to provide information that will be useful immediately in seismic design practice and post-earthquake response, and in the longer term, useful in the improvement of seismic design codes and practices. Proceedings and individual papers for each of the previous annual seminars are available in PDF format at <http://www.consrv.ca.gov/CGS/smip/proceedings.htm>. Due to the State budget restraints, CSMIP did not fund as many projects as in other years and did not hold an annual seminar in 2010 or 2011. The SMIP12 Seminar is the twenty-first in this series of annual seminars.

The SMIP12 Seminar is divided into two sessions in the morning and two sessions in the afternoon. The sessions in the morning include four presentations on CSMIP-funded projects. These include analysis of building response data for improvement of seismic design for non-structural components, soil-structure interactions, dampings in buildings, and computer models for seismic response of buildings. The first afternoon session includes a presentation of the project on wave propagation and site effects in the Humboldt Bay area, and two presentations on the extensive instrumentation of a 62-story building in San Francisco and analysis of the ambient vibration data from the building. The last session includes invited presentations by Chris Tokas of OSHPD on seismic safety and instrumentation of hospital buildings and by Brian Maroney of Caltrans on the construction of the new San Francisco-Oakland Bay Bridge East Span. Individual papers and the proceedings are available to the SMIP12 participants in an USB flash drive.

Moh Huang
CSMIP Data Interpretation Project Manager

Appreciation to Members of the Strong Motion Instrumentation Advisory Committee

Main Committee

Chris Poland, Chair, Degenkolb Engineers
Norman Abrahamson, Pacific Gas & Electric Company
Anil Chopra, UC Berkeley
Bruce Clark, Leighton & Associates
Martin Eskijian, California State Lands Commission (retired)
Wilfred Iwan, California Institute of Technology
Tom Ostrom, Caltrans
Farzad Naeim, John A. Martin & Associates
Marshall Lew, AMEC
Daniel Shapiro, SOHA Engineers
Robert Anderson (ex-officio), Seismic Safety Commission

Ground Response Subcommittee

Marshall Lew, Chair, AMEC
Abbas Abghari, Caltrans
Yousef Bozorgnia, PEER
Brian Chiou, Caltrans
Geoffrey Martin, Univ. of Southern California
Maurice Power, AMEC Geomatics
Ben Tsai, Pacific Gas & Electric Company (retired)

Buildings Subcommittee

Farzad Naeim, Chair, John A. Martin & Associates
Lucie Fougner, Degenkolb Engineers
Donald Jephcott, Structural Engineer
David Leung, City of San Francisco
Bret Lizundia, Rutherford & Chekene
Eduardo Miranda, Stanford University
John Robb, Structural Engineer
Daniel Shapiro, SOHA Engineers
Chris Tokas, Office of Statewide Health Planning and Development
Chia-Ming Uang, UC San Diego

Lifelines Subcommittee

Martin Eskijian, Chair, California State Lands Commission
Craig Davis, Los Angeles Dept. of Water and Power
David Gutierrez, DWR Division of Safety of Dams
Marsha McLaren, Pacific Gas & Electric Company
Tom Ostrom, Caltrans

Data Utilization Subcommittee

Wilfred Iwan, Chair, California Institute of Technology
Representatives from each Subcommittee

TABLE OF CONTENTS

Seminar Program.....	v
Evaluation of ASCE/SEI 7 Equations for Seismic Design of Nonstructural Components Using CSMIP Records	1
Saeed Fathali and Bret Lizundia	
Earthquake Record Interpretation for Soil-Structure Interactions Effects of Two Instrumented Buildings	19
Christine Goulet, Atsushi Mikami and Jonathan Stewart	
Damping Identification in Buildings from Earthquake Records.....	39
Dionisio Bernal, Salma Mozaffari Kojidi, Kenny Kwan and Michael Dohler	
Calibrating Computer Models for Seismic Analysis: Case Studies Using Instrumented Building Records.....	57
Daniel Swensen and Sashi Kunnath	
3D Wave Propagation and Site Effects in the Humboldt Bay Area Using Ground Motion Records from the M6.5 2010 Ferndale Earthquake	69
Arben Pitarka, Hong Kie Thio and Paul Somerville	
Strong Motion Instrumentation of a 62-story Concrete Core Residential Building in San Francisco	81
Moh Huang, Anthony Shakal, Carl Petersen, Mehmet Celebi, John Hooper and Ron Klemencic	
Ambient Response of a Unique Performance-Based Design Building with Dynamic Response Modification Features	97
Mehmet Celebi, Moh Huang, Anthony Shakal, John Hooper and Ron Klemencic	
Hospital Seismic Safety Program and Strong Motion Instrumentation	111
Chris Tokas and Roy Lobo	
San Francisco-Oakland Bay Bridge New East Span: Construction Progress and Challenges	125
Brian Maroney	

**SMIP12 SEMINAR ON
UTILIZATION OF STRONG-MOTION DATA**

October 2, 2012

Secretary of State Auditorium
1500 11th Street, Sacramento, California

PROGRAM

8:00 am **REGISTRATION**

9:15 am **WELCOMING REMARKS**

Farzad Naeim, Strong Motion Instrumentation Advisory Committee (SMIAC)
John Parrish, State Geologist, California Geological Survey
Mark Nechodom, Director, Department of Conservation

INTRODUCTION

Anthony Shakal, Manager, California Strong Motion Instrumentation Program
Moh Huang, California Strong Motion Instrumentation Program

Session I

Moderator: *Marshall Lew*, AMEC and SMIAC

9:35 am **Evaluation of ASCE/SEI 7 Equations for Seismic Design of Nonstructural Components Using CSMIP Records**

Saeed Fathali and *Bret Lizundia*, Rutherford + Chekene, San Francisco

10:05 am **Earthquake Record Interpretation for Soil-Structure Interactions Effects of Two Instrumented Buildings**

Christine Goulet, PEER, Berkeley, *Atsushi Mikami*, Univ. of Tokushima, and
Jonathan Stewart, UCLA,

10:35 am Break

Session II

Moderator: *Farzad Naeim*, John A. Martin & Assoc. and SMIAC

11:05 am **Damping Identification in Buildings from Earthquake Records**

Dionisio Bernal, *Salma Mozaffari Kojidi*, *Kenny Kwan* and *Michael Dohler*, Northeastern Univ., Boston

11:35 pm **Calibrating Computer Models for Seismic Analysis: Case Studies Using Instrumented Building Records**

Daniel Swensen and *Sashi Kunnath*, Univ. of California, Davis

12:05 pm **Lunch**

Box lunch will be provided

Session III

Moderator: *Wilfred Iwan*, Caltech and SMIAC

1:00 pm **3D Wave Propagation and Site Effects in the Humboldt Bay Area Using Ground Motion Records from the M6.5 2010 Ferndale Earthquake**

Arben Pitarka, Lawrence Livermore Natl. Lab., *Hong Kie Thio* and *Paul Somerville*, URS Corp., Los Angeles

1:30 pm **Strong Motion Instrumentation of a 62-story Concrete Core Residential Building in San Francisco**

Moh Huang, *Anthony Shakal*, *Carl Petersen*, CSMIP, *Mehmet Celebi*, USGS, *John Hooper* and *Ron Klemencic*, Magnusson Klemencic Assoc.

Ambient Response of a Unique Performance-Based Design Building with Dynamic Response Modification Features

Mehmet Celebi, USGS, *Moh Huang*, *Anthony Shakal*, CSMIP, *John Hooper* and *Ron Klemencic*, Magnusson Klemencic Assoc.

2:10 pm Break

Session IV

Moderator: *Martin Eskijian*, California State Lands Commission and SMIAC

2:40 pm **Hospital Seismic Safety Program and Strong Motion Instrumentation**

Chris Tokas and *Roy Lobo*, Office of Statewide Health Planning and Development (OSHPD)

3:10 pm **San Francisco-Oakland Bay Bridge New East Span: Construction Progress and Challenges**

Brian Maroney, California Department of Transportation (Caltrans)

3:40 pm **Adjourn**

EVALUATION OF ASCE/SEI 7 EQUATIONS FOR SEISMIC DESIGN OF NONSTRUCTURAL COMPONENTS USING CSMIP RECORDS

Saeed Fathali and Bret Lizundia

Rutherford + Chekene, San Francisco, CA

Phone: (415)568-4400, *E-mail:* sfathali@ruthchek.com; blizundia@ruthchek.com

Abstract

A recently completed California Strong Motion Instrumentation Program (CSMIP) data interpretation project used recorded ground and floor motion data to evaluate a key ASCE/SEI 7-05 (and 7-10) equation for seismic design of acceleration-sensitive building nonstructural components. CSMIP motions from 73 earthquakes recorded in 151 fixed-base buildings were used in the evaluation. An improved equation was developed with two categories of revisions. First, the current code formula considers a linear relationship between the peak floor acceleration (PFA) and relative height of the component in the building with a roof PFA that is three times that of the peak ground acceleration. The analyses of the recorded motions showed that improved results could be obtained by using a nonlinear relationship and by considering both the building approximate period, T_a , and the level of ground motion. Second, the code formula considers a component amplification factor, a_p , that takes values between 1.0 and 2.5 depending on the flexibility of the nonstructural component. Analyses showed that component amplification factor can be better represented using a three-segment spectrum composed of a linear rise from 1.0 to maximum value of a_p at short periods, a flat segment with the maximum value of a_p at medium range periods, and a nonlinear decaying segment at longer periods. The shape and amplitude of the spectrum was found to vary depending on T_a .

Objectives

In a CSMIP-sponsored study, Fathali and Lizundia (2011a) compared the response data recorded from instrumented buildings with the equations in ASCE/SEI 7-05 used for seismic design of acceleration-sensitive nonstructural components and recommended modifications for improvement. These equations are unchanged in ASCE/SEI 7-10. The study focused on two primary tasks. The first was to compare the relationship $[1 + 2(z/h)]$ in Equation 13.3-1 that relates upper floor acceleration to ground level acceleration. The second primary task was to study the a_p parameter of Equation 13.3-1 that is essentially the ratio between the peak acceleration response of the elastic component to the peak floor acceleration. A large database was created from available recorded motions, and a proposed equation was developed as a result of the study that involves changes to both aspects of the equation.

The paper is organized with the following sections: a brief review of relevant literature, a description of the current code equations used in seismic design of nonstructural components, a summary of the earthquake records in our database, the methodology used to evaluate the code equations and recorded response, a summary of the revised equation proposed in Fathali and

Lizundia (2011a), and our conclusions. The majority of the work presented in this paper was previously published by Fathali and Lizundia (2011b).

Literature Review

Extensive research can be found in the literature on the history and development of various equations that have been used for seismic design of nonstructural components. A more detailed review is contained in Fathali and Lizundia (2011a). A brief summary of some key studies is provided here.

Uniform Building Code: The first Uniform Building Code (UBC) in 1927 (ICBO, 1927) makes reference to designing “parts and portions” of the building for seismic forces and provided force levels to use that were the same as the overall lateral force-resisting system. The next edition in 1935 (ICBO, 1935) provides explicit seismic design provisions for general nonstructural building components. Only architectural components are addressed. Noteworthy changes were made in the 1961, 1976, 1979 and 1997 editions of the UBC, including the addition of mechanical, electrical and plumbing (MEP) components in 1976.

ATC 3-06: One of earthquake engineering’s seminal documents is ATC 3-06 (ATC, 1978 and 1984). It was a large effort by a multi-disciplinary team to develop new seismic design provisions. Chapter 8 contains provisions for seismic design of nonstructural components. Requirements for mechanical and electrical components were included and had a slightly different equation than the equation for architectural components. Per the ATC 3-06 commentary, the forces used in nonstructural seismic design were based in part on the UBC. The form of the equation, though, is substantially different than the UBC equation at the time and includes additional variables. In 1985, the BSSC published the first *NEHRP Recommended Provisions for the Development of Seismic Regulations for New Buildings* (BSSC, 1985). The ATC 3-06 provisions were used as a basis for NEHRP Provisions. For nonstructural seismic design, ATC 3-06 and the 1985 NEHRP Provisions are identical.

NCEER-93-0003: Another key early publication is the *NCEER-93-0003* (Soong, et al., 1993) report which reviewed the seismic design requirements for nonstructural components in the 1991 NEHRP Provisions (BSSC, 1992) and made recommended revisions. Many of the concepts proposed in the NCEER-93-0003 study were incorporated in the 1994 NEHRP Provisions (Bachman and Drake, 1994).

Bachman and Drake (1995): The most comprehensive early work involving strong motion records was done by Robert Bachman, Richard Drake and John Gillengerten. It is summarized in several related papers, including Drake and Gillengerten (1994), Bachman and Drake (1994), Drake and Bachman (1995), Bachman and Drake (1995), and Drake and Bachman (1996). Detailed information is contained in Bachman and Drake (1995), including tables listing the data sets. 405 data sets were compiled, taken from 16 California earthquakes, ranging from the 1971 San Fernando Earthquake to the 1994 Northridge Earthquake. A dataset was derived by taking the peak acceleration at a floor (PFA) in each direction and then averaging the values from each direction. This average peak floor acceleration was then divided by a similar average peak ground acceleration (PGA) to derive a relationship of PFA to PGA. A series of plots were made

of the ratio of upper floor response to ground floor response, and the plots were compared with equations in the 1994 NEHRP Provisions.

Gillengerten and Bachman (2003): A major change in the NEHRP Provisions was made with the 1997 edition (BSSC, 1998). Equations are the same as three of those in ASCE/SEI 7-05. The background on the development of these provisions is provided in Gillengerten and Bachman (2003). They note that “while there is considerable scatter in the data, the amplification term of...” $[1 + 2(z/h)]$ “...bounds the mean plus standard deviation of the peak accelerations well.” Gillengerten and Bachman (2003) also note that “the simplifying assumption that the force increases linearly with height was necessary to keep the complexity of the method at a reasonable level.”

They also discuss the code range of 1.0 to 2.5 for the component amplification factor, a_p . They acknowledged that “amplification factors greater than 2.5 may occur, depending upon the period of the component, the dynamic characteristics of the supporting structure, and the amount of damping present in the component or its supports.” However, they point out that “the value of 2.5 for most flexible components appears reasonable, since in strong shaking, neither the period of the structure nor the period of the component is likely to remain constant. The shift in period is likely to drive the component response off of the peak.”

The Influence of Period: Many papers have investigated the influence of building period on component response, including Schroeder and Bachman (1994), Horne and Burton (2003), Singh, et al. (2006a, b), and Miranda and Taghavi (2009). They all show the influence of the dynamic properties of the building, such as the fundamental period of vibration, on component response.

Component Amplification Factor: The component amplification factor, a_p , has evolved in the various code provisions and research studies. The split into rigid and flexible components using the 0.06 second fundamental component period has been in UBC provisions since the 1988 edition. Similar definitions were added to the NEHRP Provisions in the 1994 edition. The initial NEHRP Provisions had a component amplification factor a_c that varied depending on the ratio of the component to structural periods. This was eliminated in the 1994 edition. The commentary to the 2003 NEHRP Provisions (BSSC, 2004b) describes a study for NCEER by Bachman, Drake and Richter (1993) which recommended a spectral shape.

Current Code Equations

ASCE/SEI 7-05 (ASCE, 2006) was adopted by model codes such as the 2009 International Building Code (ICC, 2009) and the 2010 California Building Code (CBSC, 2010). The next edition of ASCE/SEI 7 is ASCE/SEI 7-10 (ASCE, 2010). It represents the current source document for the seismic design of nonstructural components in the United States. It is referenced in model codes such as the 2012 International Building Code (ICC, 2012). In Section 13.3.1 of ASCE/SEI 7-05, there are four equations which provide the forces for use in determining the seismic design demands for nonstructural components. They are provided below. Note that they are unchanged in ASCE/SEI 7-10; this paper, for consistency with Fathali and Lizundia (2011a), uses the ASCE/SEI 7-05 references.

$$F_p = \{0.4 S_{DS} a_p (1 + 2(z/h))(I_p/R_p)\}W_p \quad (\text{ASCE/SEI 7-05 Equation 13.3-1})$$

$$F_p \leq 1.6 S_{DS} I_p W_p \quad (\text{ASCE/SEI 7-05 Equation 13.3-2})$$

$$F_p \geq 0.3 S_{DS} I_p W_p \quad (\text{ASCE/SEI 7-05 Equation 13.3-3})$$

In these equations, F_p is the lateral seismic force at the LRFD force design level, W_p is the weight of component, a_p is the component amplification factor that ranges from 1.0 to 2.5 and accounts for amplification due to component flexibility, S_{DS} is the site-specific short period spectral acceleration, z is the component elevation in structure relative to grade, h is the roof elevation in structure relative to grade, R_p is the component response modification factor which represents the ability of the component to absorb energy, and I_p is the component importance factor.

When a modal analysis is performed using $R = 1.0$, nonstructural seismic design forces can be determined from the following Equation 13.3-4 in lieu of Equation 13.3-1. The upper and lower limits of Equations 13.3-2 and 13.3-3 still apply.

$$F_p = ((a_i a_p)(I_p/R_p)) A_x W_p \quad (\text{ASCE/SEI 7-05 Equation 13.3-4})$$

In this equation, a_i is the acceleration at level i obtained from modal analysis, A_x is the torsional amplification factor, and the remaining values are the same as those used in the previous equations.

The vast majority of seismic design efforts in practice use Equations 13.3-1, 13.3-2, and 13.3-3, rather than Equation 13.3-4 since Equation 13.3-4 requires a dynamic analysis to determine the component a_i . Equations 13.3-2 and 13.3-3 set maximum and minimum limits on the forces used, depending on the short period spectral acceleration, S_{DS} , assigned to the site.

Summary of Database Characteristics

The database developed for this study included entries from 169 CSMIP building stations (151 fixed base and 18 seismically isolated), and 73 earthquakes occurred in the period of 1978 to 2010 in California. The buildings of the database are in the range of one to 54 stories with a roof elevation of 10 to 716 ft, and approximate period of 0.11 to 5.22 sec. 11 different types of lateral-force-resisting systems are found in the buildings of the database.

The 73 earthquakes of the database had a PGA in the range of 0.01 to 0.86g. Figure 1 shows the distribution of fixed-base buildings of the database in terms of the experience PGA. Some of the building stations provided us with more than one set of records (at least one pair of ground and floor acceleration along the same direction); thus, the database included 541 sets of “building-earthquake records” from fixed-base buildings. Each set of building-earthquake records provided at least one point for the study of PFA/PGA profile over the building height, and at least one floor spectrum for the study of floor amplification factor.

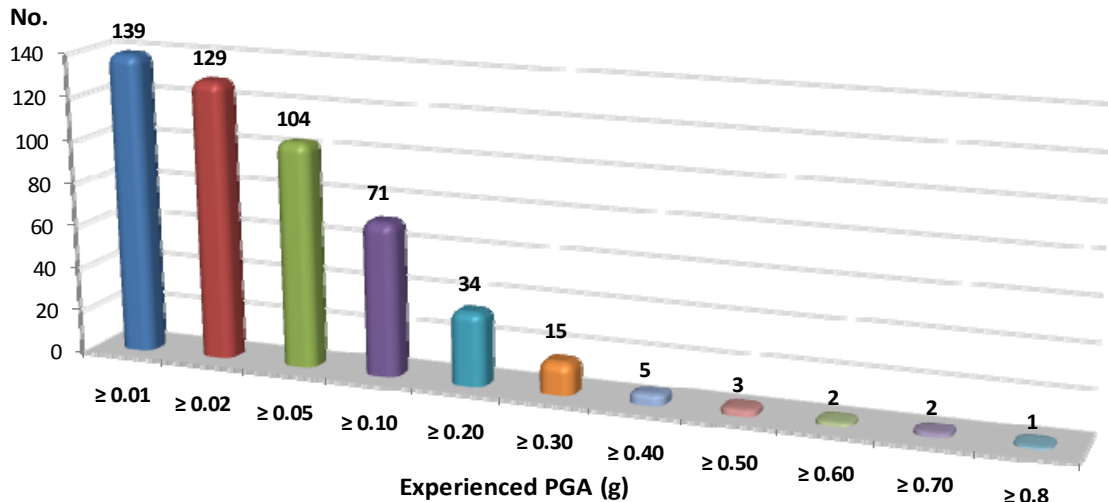


Figure 1. Distribution of Fixed-Base Buildings of Database in Terms of Experienced PGA

Methodology

The current code formula implicitly simplifies the variation of PFA over the building height to a linear relationship between two dimensionless ratios: the ratio of PFA to PGA and the ratio of the floor to roof elevations from the building grade (z/h). Therefore, each pair of ground and floor acceleration histories recorded in a CSMIP building station can provide a data point to validate the current code formula as long as the following four parameters are available: peak acceleration recorded by the floor accelerometer/channel (PFA), peak acceleration recorded by the ground-level accelerometer/channel (PGA), and elevations of the roof and floor (h and z) from the building grade.

The database of PFA/PGA versus z/h for this study was developed such that each data point has a series of attributes including the building height, number of stories, lateral force-resisting system type, approximate period, and the ground motions properties. None of these attributes is explicitly included in the code formula. The developed database permitted investigating whether these attributes influence the relationship between the PFA/PGA and z/h ratios.

The calculation of PFA/PGA ratio at any floor of a building under an earthquake ground motion was straightforward only if the building is instrumented only in one direction and there is only one accelerometer at each level. However, for the typical situation, when the building is instrumented along both directions and there are multiple recorded acceleration histories at the floor or ground level, the decision of how to calculate the PFA/PGA ratio can become rather complicated. For such cases, different answers to the following questions would result in different methodologies to calculate the PFA/PGA ratio:

- (a) Should responses along the two orthogonal principal axes of the building be considered separately or collectively?
- (b) Which recorded response should be used in the calculation of PFA/PGA ratio: the response at the vicinity of the center of rigidity of the floor plate or responses near the perimeter of the floors?

- (c) If there is no recorded response available at the preferred locations (the answer to the previous question), is it permissible and possible to calculate virtual acceleration histories based on the available recorded acceleration histories at other locations of the floor?
- (d) If the responses along the two orthogonal principal axes are not combined, should the minimum, mean, maximum (or some other statistical function) of the individual recorded peak acceleration values be used in the calculation of PFA/PGA ratio?
- (e) If the responses along the two orthogonal principal axes are combined, should the resultant acceleration histories, or a combination of the PFA/PGA ratios calculated along the two orthogonal principal axes, be used in the calculation of PFA/PGA ratio?
- (f) If the combined PFA/PGA ratio is calculated based on the PFA/PGA ratios along the two orthogonal principal axes, should the minimum, mean, maximum (or other statistical functions) of the two PFA/PGA ratios be used in the calculation of PFA/PGA ratio?

Based on the recommendation from the SMIP Building Subcommittee of the Strong Motion Instrumentation Advisory Committee (compromised of practicing engineers and academicians), it was decided to use the following two rules when calculating the PFA/PGA ratio:

- I. Only actual/recorded acceleration histories along the same direction were used to calculate the PFA/PGA ratios (no virtual/calculated records, and no combination of response along the two orthogonal principal directions).
- II. If at one of the building floors along a given direction there was more than one recorded acceleration history, the mean of the peak acceleration values of those records was used to calculate the PFA/PGA ratio.

These rules were selected for the following three reasons. First, several CSMIP building stations have different lateral force-resisting systems type, and fundamental period, and consequently different seismic behavior along their two orthogonal principal axes. Moreover, for a large portion of the database, the ground motions along the two principal axes of the building stations are considerably different in terms of the amplitude and frequency content. Therefore, it was decided that the methods that do not combine the response along the two orthogonal principal axes are preferable for this research study. Second, calculations of virtual acceleration histories need a fairly precise knowledge of the locations of the existing channels and the center of rigidity of the floor plate, and are possible only for the buildings with rigid diaphragms. Lastly, compared to the maximum value, the mean of the peak acceleration values recorded through different channels at a building floor is more representative of the peak response at that floor since it uses all of the recorded acceleration histories.

The study compiled 2224 data points from above ground level ($z/h > 0$) data, as shown in Figure 2. In this figure, the solid and dashed lines represent the 1997 UBC and ASCE/SEI 7-05

equations for the relationship between PFA/PGA and z/h . At any given z/h value, the PFA/PGA ratios established based on the CSMIP floor motions can be compared to the corresponding value predicted by the current and previous code formula.

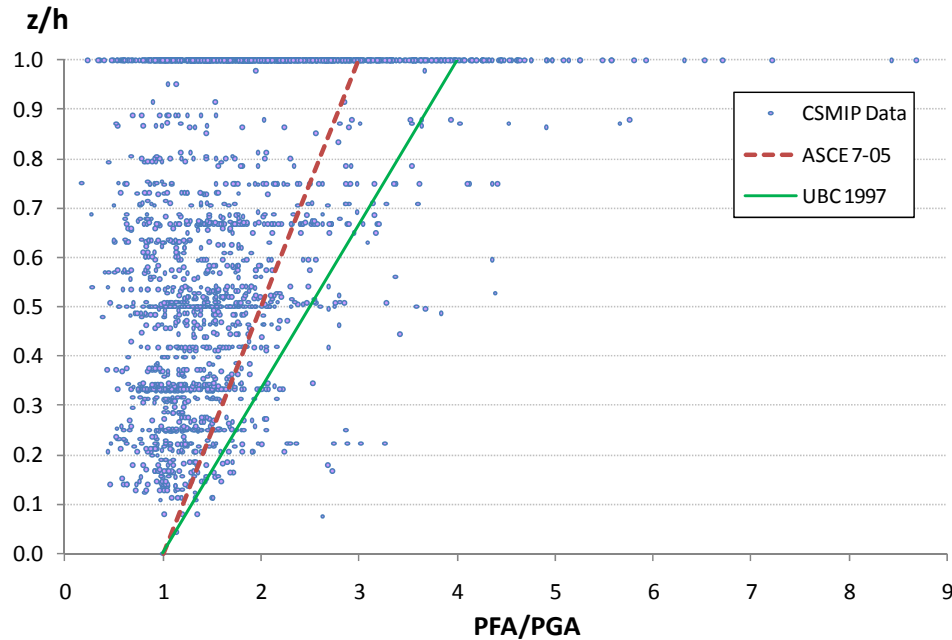


Figure 2. Data Points vs. Building Code Formula for Relationship between PFA/PGA and z/h (2224 above-Ground Level Data Points from 151 Fixed-Base Building Stations)

After development of the database of PGA/PFA versus z/h ratios, establishing the best-fit equation to between these two ratios could be undertaken by linear or nonlinear regression analyses. Equations established by linear regression analyses through the database would be in the general form of Equation 1. Figure 3(a) shows how variations of parameter α affect the shape of the profile of peak floor acceleration over the building. As indicated in this figure, larger values of parameter α correspond to larger amplifications of peak floor accelerations over the building height, and α equal to 2 corresponds to the ASCE/SEI 7-05 code formula.

$$\text{PFA/PGA} = 1 + \alpha (z/h) \quad (1)$$

However, reviewing the actual responses recorded in CSMIP buildings during past earthquakes shows that in several cases the profile of PFA/PGA over the building height is significantly different from a straight line and can be much better presented by Equation 2, which is a nonlinear equation that allows z/h ratio takes exponents smaller or larger than 1.

$$\text{PFA/PGA} = 1 + \alpha (z/h)^\beta \quad (2)$$

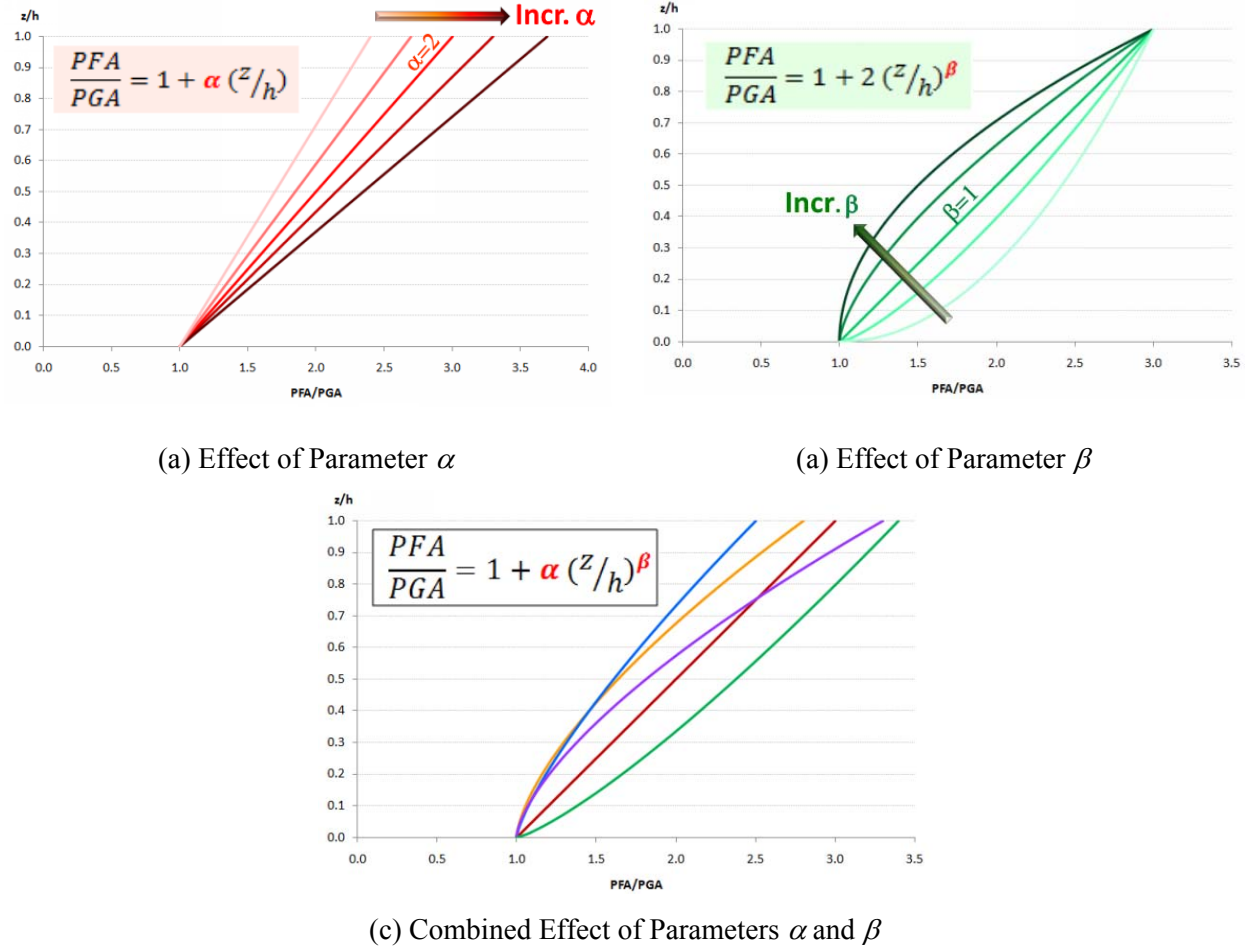


Figure 3. General Nonlinear Relationship Between PFA/PGA and z/h Ratios

Figure 3(b) shows how variations of parameter β , the exponent of the z/h ratio, change the shape of the profile of the peak floor acceleration over the building height. β values larger than 1 suggest that the rate of increase in the amplification of floor acceleration is proportional to the floor height. β values smaller than 1, on the other hand, produce profiles such that the rate of increase in the amplification of floor acceleration is inversely proportional to the floor height. Therefore, very small values of parameter β can produce profiles with almost constant peak floor acceleration over the building height. Figure 3(c) shows how combined variations of parameters α and β of Equation 2 result in different shapes for the profile of PFA/PGA ratio over the building height. Since Equation 1 is a special case of Equation 2 ($\beta=1$) the search for the best-fit equation through the database of PFA/PGA versus z/h ratios was pursued by nonlinear regression analyses to establish values of parameters α and β .

Since a large portion of the data points established based on the CSMIP records are located at the roof level ($z/h = 1$), the parameter α of Equation 2 will be mainly governed by the response at the roof level of the buildings. To reduce this effect, a weighted window averaging technique can be used. To do so, a series of imaginary windows are considered that cover the entire database without any overlaps. Each window has finite, arbitrary width in terms of the z/h ratio,

but an unlimited width in terms of PFA/PGA ratio. Then, all of the data points within each window are presented by a single data point whose PFA/PGA ratio is equal to the mean plus standard deviation of PFA/PGA ratio of all the data points in that window. The z/h ratio of the two data points representing the lowest and highest windows are considered as 0 and 1, respectively. For the other windows, on the other hand, the z/h ratio of the representative point is equal to the z/h ratio at the center of the window.

Estimating the peak floor acceleration is only the first step in calculating the seismic demand of acceleration-sensitive components. A given floor acceleration history would induce different seismic forces in nonstructural components with different dynamic properties. The peak acceleration response of elastic, rigid nonstructural components that are rigidly anchored to the building floors is equal to the peak floor acceleration. For flexible nonstructural components (or any flexibly-mounted nonstructural components), on the other hand, the peak acceleration response could be smaller or larger than the peak floor acceleration.

The current code formula addresses this issue by using the parameter a_p , the component amplification factor, which is the ratio between the peak acceleration of elastic response of a component to the peak floor acceleration. Per Table 13.2-1 of ASCE/SEI 7-05 which lists the a_p values of different nonstructural components, a_p can take three different values: 1 for rigid nonstructural components that rigidly attached to the floor, 2.5 for all flexible or flexibly mounted nonstructural components, and 1.25 for the fasteners of the connecting system for exterior nonstructural wall elements and connections. For other components that are not listed in that table, the code requires the designer use the period of the mounted nonstructural component to decide whether it is rigid ($a_p=1$) or flexible ($a_p=2.5$). Per Section 11.2 of ASCE/SEI 7-05, rigid and flexible nonstructural components are separated at the component period of 0.06 sec. The code allows using dynamic analyses to find a_p of a component as long as it is not smaller than 1.

One of the major objectives of this study was to compare the current code values for the a_p parameters to the a_p of different nonstructural components under actual floor accelerations recorded by CSMIP. The a_p values of nonstructural components with different periods can be presented in a spectrum format. To calculate the a_p spectrum of a floor acceleration history, the absolute acceleration response spectrum is calculated first, and then it is normalized by the peak floor acceleration (which is equal to the spectral acceleration at the infinitely small period). This process was repeated for each spectra.

Figure 4 shows the mean, mean plus standard, and maximum of all of the 3742 5%-damped a_p spectra. The red dashed line shows values of 1 and 2.5 for component periods shorter and longer than 0.06 seconds, respectively, and it represents the a_p value per ASCE/SEI 7-05.

As it can be seen in Figure 4, a_p of flexible components under some of the floor accelerations recorded in the past has been much larger than 2.5 (the maximum is about 8.2). The maximum a_p spectrum shows that for a wide range of component periods (0.1 to 3 sec.), a_p could take values larger than 5. However, the intention of the building codes is usually to design for approximately the mean plus standard deviation of the demand.

The comparison of the code values for a_p and the mean plus standard deviation a_p spectrum shows that for a range of component period between 0.1 and 0.75 seconds the established a_p spectrum exceeds the code value of 2.5 and reaches a maximum value of 3.3 at the component period of 0.3 seconds. Outside this range of period, on the other hand, the code value is conservative. Contrary to what the code formula implies that any nonstructural component with a period of longer than 0.06 seconds experiences the maximum value of a_p (2.5), the results show that in the range of component period of 0.06 to 0.3 seconds, a_p can take values smaller than 2.5. As it is shown in Figure 4, over the entire range of periods for flexible components, the mean a_p spectrum is smaller than 2.5. The mean a_p spectrum reaches a value of about 2.5 at the component period of 0.3 seconds.

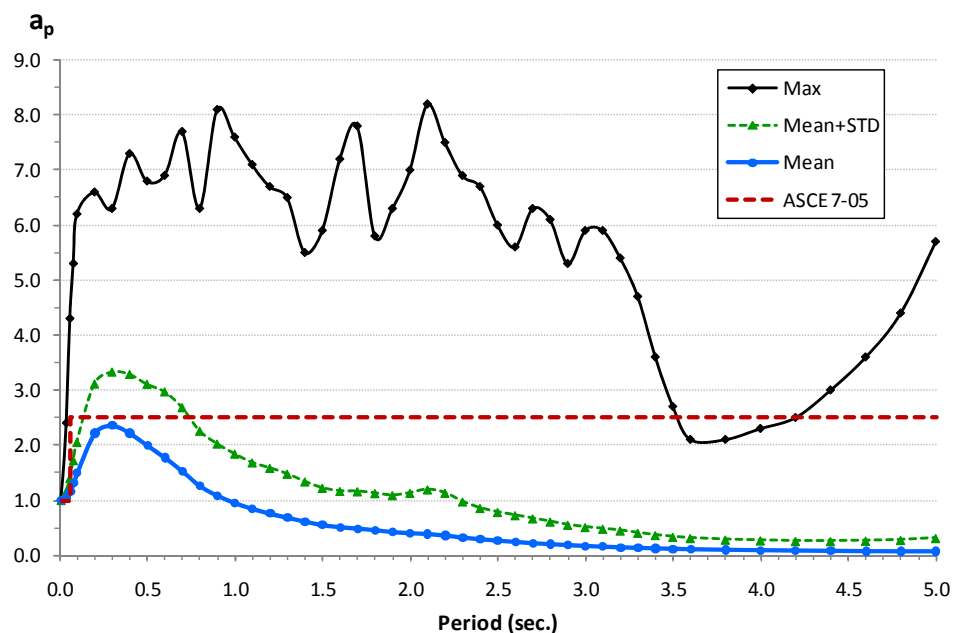


Figure 4. Comparison of Code Values for Component Amplification Factor, a_p , and Mean, Mean Plus Standard Deviation, and Maximum 5%-Damped a_p Spectra Calculated Based on 3742 CSMIP Floor Acceleration Histories from Fixed-Base Buildings

Reviewing the a_p spectra of several CSMIP recorded responses showed that the a_p spectrum typically consists of three segments: first, it rises from a_p of 1 for rigid components to a maximum value of a_p ; then it remains relatively constant over a range of component periods; and finally, it begins to decay for long component periods. This pattern, which was consistently seen across the existing database, suggested that a simplified three-segment spectrum similar to the code response spectrum used for seismic design of buildings would be a good fit for the general floor a_p spectrum. Therefore, a search was undertaken in this study by searching for the parameters that govern the shape of a general three-segment floor a_p spectrum that is the best fit to the building responses recorded by CSMIP during the past earthquakes.

Modified Equations Proposed by Fathali and Lizundia (2011a)

In a CSMIP research study, Fathali and Lizundia (2011a) proposed Equation 3 as a modified version of Equation 13.3-1 of ASCE/SEI 7-05 to calculate F_p :

$$F_p = \{0.4 S_{DS} a_p (1 + \alpha (z/h)^\beta)(I_p/R_p)\}W_p \quad (3)$$

In this equation, α and β are coefficients that depend on building approximate period (T_a) and peak ground acceleration ($0.4S_{DS}$), and a_p is the component amplification factor that is defined based on the proposed floor a_p spectrum shown in Figure 5. Remaining parameters of Equation 3 have the same definition as the corresponding parameters in Equation 13.3-1 of ASCE/SEI 7-05.

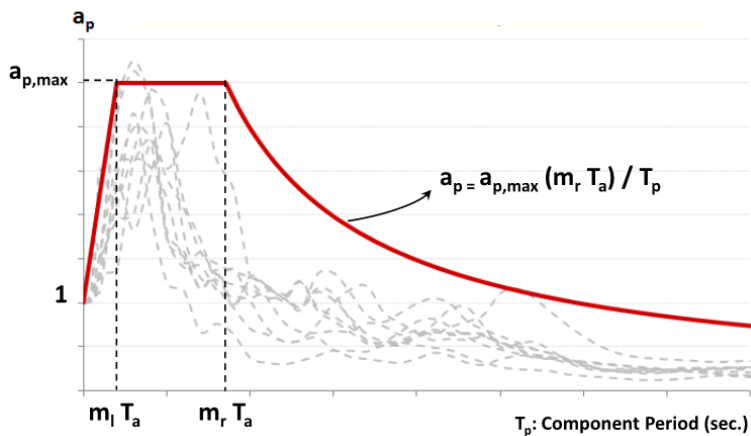


Figure 5. Floor a_p Spectrum Proposed by Fathali and Lizundia (2011a)

To establish values of parameters α and β and the spectrum of a_p used in Equation 3, Fathali and Lizundia (2011a) performed two series of nonlinear regression analyses through data points corresponding to the mean and to the mean plus one standard deviation of the response recorded in the past earthquakes. The results corresponding to the mean of the response recorded in the past are presented in Tables 1 through 3. These results are recommended for the seismic evaluation of acceleration-sensitive nonstructural components in existing buildings. Figure 6 shows how different values of parameters α and β established for different ranges of building approximate period and PGA change the shape of the profile of peak floor acceleration over the building height.

The results corresponding to the mean plus one standard deviation of the response recorded in the past are presented in Tables 4 through 6. These results are recommended for the seismic design of acceleration-sensitive nonstructural components in new construction.

The profiles of peak floor acceleration shown in Figure 7 demonstrate that compared to the code formula that assumes a threefold amplification at the roof level, the established equations for the short-, medium- and long-range period buildings under strong earthquakes with $PGA \geq 0.20g$ suggest about 10%, 70% and 100% less amplification, respectively. Note that at the design level, PGA equals $0.4 S_{DS}$, and $PGA \geq 0.20g$ corresponds to Seismic Design Category D buildings of Occupancy Category I through III per Table ASCE/SEI 7-05).

Table 1. Values of Parameter α of Equation 1 Recommended for Seismic Evaluation of Acceleration-Sensitive Nonstructural Components in Existing Buildings

	$0.4 S_{DS} = \text{PGA} < 0.067 \text{ g}$	$0.067 \leq 0.4 S_{DS} = \text{PGA} < 0.20 \text{ g}$	$0.4 S_{DS} = \text{PGA} \geq 0.20 \text{ g}$
$T_a < 0.5 \text{ sec.}$	1.26	1.04	0.99
$0.5 \leq T_a < 1.5 \text{ sec.}$	1.52	1.02	0.65
$T_a \geq 1.5 \text{ sec.}$	0.90	0.72	0.00

Table 2. Values of Parameter β of Equation 1 Recommended for Seismic Evaluation of Acceleration-Sensitive Nonstructural Components in Existing Buildings

	$0.4 S_{DS} = \text{PGA} < 0.067 \text{ g}$	$0.067 \leq 0.4 S_{DS} = \text{PGA} < 0.20 \text{ g}$	$0.4 S_{DS} = \text{PGA} \geq 0.20 \text{ g}$
$T_a < 0.5 \text{ sec.}$	1.09	1.29	0.89
$0.5 \leq T_a < 1.5 \text{ sec.}$	1.57	1.63	1.55
$T_a \geq 1.5 \text{ sec.}$	1.69	3.00	1.00

Table 3. Parameters of General 5%-Damped Floor a_p Spectrum Recommended for Seismic Evaluation of Acceleration-Sensitive Nonstructural Components in Existing Buildings

	m_l	m_r	$a_{p,\max}$
$T_a < 0.5 \text{ sec.}$	0.9	1.2	2.5
$0.5 \leq T_a < 1.5 \text{ sec.}$	0.3	0.8	2.1
$T_a \geq 1.5 \text{ sec.}$	0.1	0.3	2.1

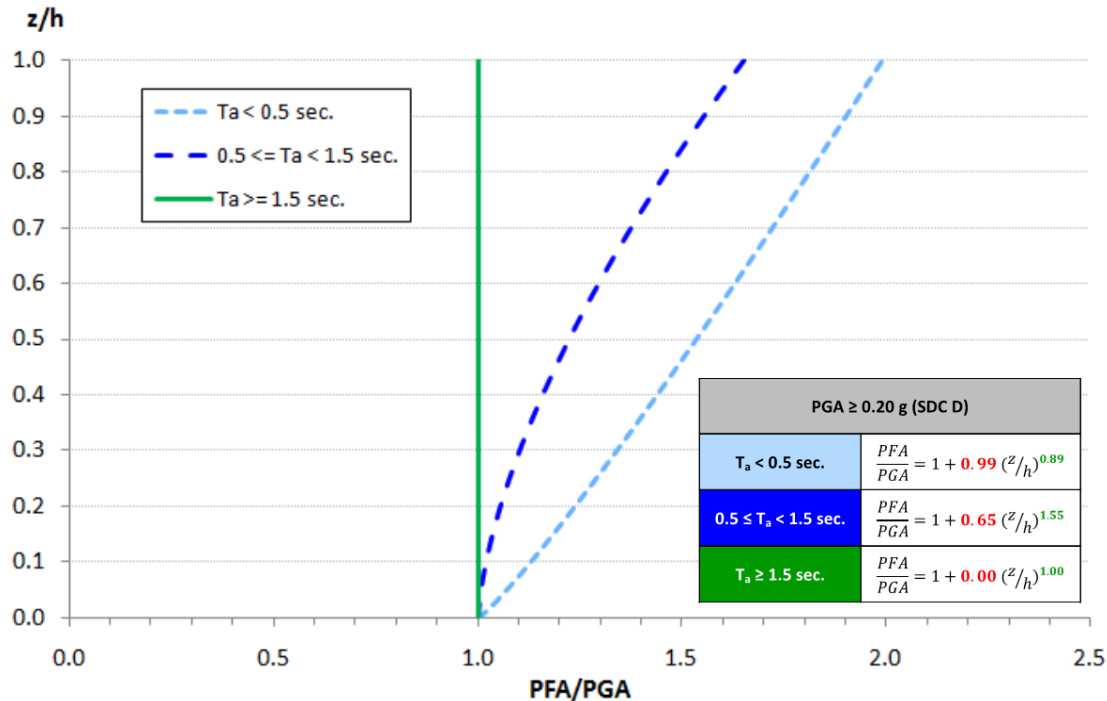


Figure 6. Profile of PFA/PGA over Building Height Recommended for Seismic Evaluation of Acceleration-Sensitive Nonstructural Components in Existing Buildings under Earthquakes with $\text{PGA} \geq 0.20 \text{ g}$ (SDC D or Higher of Occupancy Category I through III)

Table 4. Values of Parameter α of Equation 1 Recommended for Seismic Design of Acceleration-Sensitive Nonstructural Components in New Constructions

	$\text{PGA}=0.4 S_{DS} < 0.067 \text{ g}$	$0.067 \leq \text{PGA}=0.4 S_{DS} < 0.20 \text{ g}$	$\text{PGA}=0.4 S_{DS} \geq 0.20 \text{ g}$
$T_a < 0.5 \text{ sec.}$	2.12	1.93	1.75
$0.5 \leq T_a < 1.5 \text{ sec.}$	2.61	1.55	1.01
$T_a \geq 1.5 \text{ sec.}$	2.52	1.53	0.50

Table 5. Values of Parameter β of Equation 1 Recommended for Seismic Design of Acceleration-Sensitive Nonstructural Components in New Constructions

	$\text{PGA}=0.4 S_{DS} < 0.067 \text{ g}$	$0.067 \leq \text{PGA}=0.4 S_{DS} < 0.20 \text{ g}$	$\text{PGA}=0.4 S_{DS} \geq 0.20 \text{ g}$
$T_a < 0.5 \text{ sec.}$	0.78	1.25	0.92
$0.5 \leq T_a < 1.5 \text{ sec.}$	1.16	0.75	0.69
$T_a \geq 1.5 \text{ sec.}$	1.64	1.65	3.00

Table 6. Parameters of General 5%-Damped Floor a_p Spectrum Recommended for Seismic Design of Acceleration-Sensitive Nonstructural Components in New Constructions

	m_l	m_r	$a_{p,\max}$
$T_a < 0.5 \text{ sec.}$	0.8	1.4	3.3
$0.5 \leq T_a < 1.5 \text{ sec.}$	0.3	1.0	2.9
$T_a \geq 1.5 \text{ sec.}$	0.1	0.3	2.5

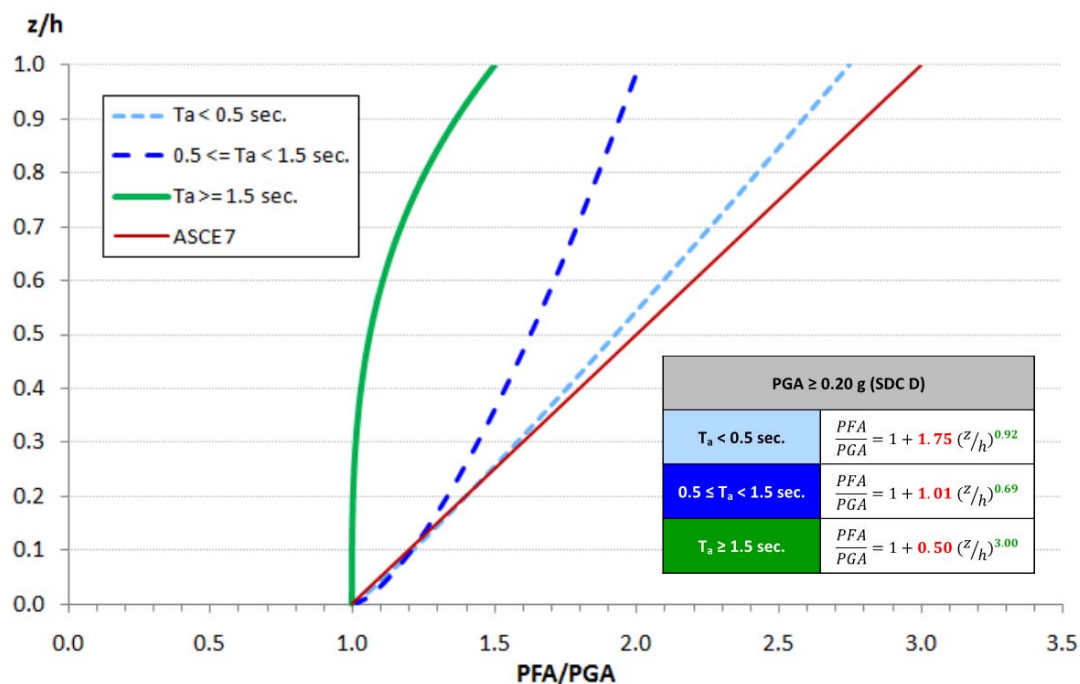


Figure 7. Profile of PFA/PGA over Building Height Recommended for Seismic Design of Acceleration-Sensitive Nonstructural Components in New Constructions under Earthquakes with $\text{PGA} \geq 0.20 \text{ g}$ (SDC D or Higher of Occupancy Category I through III)

The profiles of peak floor acceleration over the building height for different ranges of PGA and building approximate period shown in Figures 6 and 7 demonstrate that the amplification of peak floor acceleration is inversely proportional to the building period and the effect of building period on the profile of peak floor acceleration over the building height is stronger under the strong ground motions than it is under moderate and minor earthquakes.

The results presented for parameters α and β in Tables 4 and 5 show that for some ranges of PGA and building period the proposed nonlinear profile for the PFA/PGA ratio over the building height is significantly different from the linear equation used by the code formula. To quantify how much this significant difference results in improvement in the goodness of the fit to the data points obtained from the CSMIP records, Coefficient of Determination or R^2 (R -squared) Error was used. It should be noted that contrary to what the name implies, the larger values of the R^2 Error correspond to better fits (the maximum value of the R^2 Error corresponding to a perfect fit equals one), and for poorer fits the index can take negative values. For different ranges of PGA and T_a , the R^2 Error of the proposed nonlinear equation and ASCE/SEI 7 formula are compared to each other in Table 7. Note that the “Best Fit” in Table 7 refers to the trendline through mean plus one standard deviation data points established by window averaging method that was previously explained in Methodology Section of this paper. As it can be seen in this table, for all different ranges of PGA and T_a , using the nonlinear equation instead of the linear equation of the code improved the goodness of the fit (results in larger values of R^2 Error). This improvement is particularly significant for longer building period and larger PGA values. Using the proposed nonlinear equation instead of the linear equation of the current code formula for those ranges of PGA increases the value of the R^2 error from negative values to values close to 0.6.

Table 7. Comparison of R^2 Error (Coefficient of Determination) of Proposed Equation and ASCE/SEI 7-05 equation for Profile of PFA/PGA Ratio over Building Height

	PGA < 0.067 g (SDC A)		0.067 ≤ PGA < 0.20 g (SDC B&C)		PGA ≥ 0.20 g (SDC D)	
	Best Fit	ASCE 7	Best Fit	ASCE 7	Best Fit	ASCE 7
$T_a < 0.5$ sec.	0.65	0.50	0.89	0.80	0.46	0.40
$0.5 \leq T_a < 1.5$ sec.	0.80	0.65	0.58	0.38	0.54	-2.62
$T_a \geq 1.5$ sec.	0.67	0.60	0.50	-0.08	0.59	-12.79

Conclusions and Summary

Fathali and Lizundia (2011a) provided a general evaluation of the key Equation 13.3-1 used by ASCE/SEI 7-05 for the seismic design of nonstructural components. This equation is unchanged in the current ASCE/SEI 7-10. A proposed revision to the equation was developed and was provided as Equation 3 above.

PFA/PGA Relationship: The code relationship between z/h and PFA/PGA is linear and amplifies PFA up to a value of three times that of the PGA. Our conclusions include the following.

- Equation 13.3-1 is a good fit for short-period buildings (fundamental period less than 0.5 seconds) in low-to-moderate seismicity areas such as those characterized by Seismic Design Category (SDC) B and C.
- Equation 13.3-1 was found to be significantly conservative (up to 100%) for medium-range period buildings (period between 0.5 seconds and 1.5 seconds) and long period buildings (period over 1.5 seconds).
- Equation 13.3-1 does not explicitly account for parameters found to be influential in this study, including building period, and PGA. Damping is likely to be influential as well, but was not directly investigated in this study.
- Simple improvements can be made to Equation 13.3-1 that will provide a better fit for the recorded data, using the code equation for fundamental period and USGS mapped values for site seismicity as reflected in the parameter S_{DS} .

Component Amplification Factor: The component amplification factor, a_p , used in Equation 13.3-1 accounts for the dynamic amplification of the component response as compared to the PFA. The code sets the value for a_p to be 1.0 for rigid components (defined as those with a fundamental period of 0.06 seconds or less) and 2.5 for flexible components (defined as those with a fundamental period greater than 0.06 seconds). Our conclusions include the following.

- The code values for a_p are conservative when the component fundamental period is longer than the building fundamental period.
- The code values for a_p are conservative when the component fundamental period is away from the range of periods that include the periods of the building modes that participate in the building response.
- The code values for a_p is less than the a_p value obtained from recorded values for flexible components located in short-period buildings (period less than 0.5 seconds) and medium-range period buildings (period between 0.5 seconds and 1.5 seconds). All our studies were done with 5% damped spectra. For components that have less damping, the difference would be even larger.
- The ASCE/SEI formulation for a_p does not consider the building fundamental period, which is expected from structural dynamics to have a significant influence and which was confirmed in our study.
- The ASCE/SEI formulation can be improved by use of a proposed a_p spectrum that is based on the building fundamental period as calculated using the standard code formula for building period.
- The improved formulation for a_p is relatively simple, inherently addresses the effect of the building lateral force-resisting system (through the use of building period), permits

values of $a_p < 1$ where relevant, and permits use of values between the maximum and 1.0 for flexible components.

Acknowledgments

The contents of this report were developed under Contract No. 1008-921 from the California Department of Conservation, California Geological Survey, Strong Motion Instrumentation Program. However, these contents do not necessarily represent the policy of that agency nor are they endorsement by the State Government. The authors are grateful to Anthony Shakal and Moh Huang of the Strong Motion Instrumentation Program (SMIP) for their assistance and advice during the project, and to the recommendations and comments provided by members of the SMIP Building Subcommittee of the Strong Motion Instrumentation Advisory Committee: Farzad Naeim (Chair), Lucie Fougner, Donald Jephcott, David Leung, Eduardo Miranda, John Robb, Dan Shapiro, Chris Tokas, and Chia-Ming Uang.

References

ASCE (American Society of Civil Engineers), 2006, ASCE/SEI 7-05, *Minimum Design Loads for Buildings and Other Structures*, including Supplement No. 1 and Errata.

ASCE (American Society of Civil Engineers), 2011, ASCE/SEI 7-10, *Minimum Design Loads for Buildings and Other Structures*.

ATC (Applied Technology Council), 1978, *ATC 3-06: Tentative Provisions for the Development of Seismic Regulations for Buildings*, Applied Technology Council, Redwood City, CA.

ATC (Applied Technology Council), 1984, *ATC 3-06 Amended: Tentative Provisions for the Development of Seismic Regulations for Buildings*, Applied Technology Council, Redwood City, CA. This reprint includes the 1982 “Amendments to ATC-3-06 Tentative Provisions for the Development of Seismic Regulations for Buildings for Use in Trial Designs” in Appendix B.

Bachman, R., and R. Drake, 1994, “1994 NEHRP Provisions for Architectural, Mechanical, and Electrical Components,” *Proceedings of the Fifth U.S. National Conference on Earthquake Engineering*, Earthquake Engineering Research Institute, Chicago, July 10-14.

Bachman, R., and R. Drake, 1995, “A Study to Empirically Validate the In-Structure Response Accelerations in the 1994 NEHRP Provisions Design Force Equations for Architectural, Mechanical and Electrical Components,” letter report submitted to the National Center for Earthquake Engineering Research per NSF Grant No. CMS-9416580, July.

Bachman, R., Drake, R. and P. Richter, 1993, “1994 Update to 1991 NEHRP Provisions for Architectural, Mechanical, Electrical Components and Systems,” letter report to the National Center for Earthquake Engineering Research, February 22.

BSSC (Building Seismic Safety Council), 1985, *NEHRP Recommended Provisions for the Development of Seismic Regulations for New Buildings, Part 1: Provisions*, 1985 Edition, Washington, D.C.

BSSC (Building Seismic Safety Council), 1992, *NEHRP Recommended Provisions for the Development of Seismic Regulations for New Buildings, Part 1: Provisions*, 1991 Edition, also referenced as FEMA 222, Washington, D.C.

BSSC (Building Seismic Safety Council), 1998, *NEHRP Recommended Provisions for Seismic Regulations for New Buildings and Other Structures, Part 1: Provisions*, 1997 Edition, also referenced as FEMA 302, Washington, D.C.

BSSC (Building Seismic Safety Council), 2004a, *NEHRP Recommended Provisions for Seismic Regulations for New Buildings and Other Structures, Part 1: Provisions*, 2003 Edition, also referenced as FEMA 450-1, Washington, D.C.

BSSC (Building Seismic Safety Council), 2004b, *NEHRP Recommended Provisions for Seismic Regulations for New Buildings and Other Structures, Part 2: Commentary*, 2003 Edition, also referenced as FEMA 450-2, Washington, D.C.

CBSC (California Building Standards Commission), 2010, *2010 California Building Code*, California Code of Regulations, Title 24, Part 2, Volume 2 of 2, Sacramento, CA.

Drake, R., and R. Bachman, 1995, "Interpretation of Instrumented Building Seismic Data and Implications for Building Codes," *Proceedings of the 64th Annual Convention of the Structural Engineers Association of California*, Structural Engineers Association of California, Indian Wells, CA, October 19-21.

Drake, R., and R. Bachman, 1996, "NEHRP Provisions for 1994 for Nonstructural Components," *Journal of Architectural Engineering*, American Society of Civil Engineers, Volume 2, No. 1, March.

Drake, R., and J. Gillengerten, 1994, "Examination of CDMG Ground Motion Data in Support of the 1994 NEHRP Provisions," *Proceedings of the Fifth U.S. National Conference on Earthquake Engineering*, Earthquake Engineering Research Institute, Chicago, July 10-14.

Fathali, S. and B. Lizundia, 2011a, *Evaluation of ASCE/SEI 7 Equations for Seismic Design of Nonstructural Components using Strong Motion Records*, prepared for the California Strong Motion Instrumentation Program California Geological Survey, Data Interpretation Project, Agreement 1008-921.

Fathali, S. and B. Lizundia, 2011b, "Evaluation of Current Seismic Design Equations for Nonstructural Components in Tall Buildings Using Strong Motion Records," *The Structural Design of Tall and Special Buildings*, John Wiley & Sons, Volume 20(S1), PP:40-36, December 2011.

Gillengerten, J. and R. Bachman, 2003, "Background on the Development of the NEHRP Seismic Provisions for Non-Structural Components and Their Application to Performance Based Seismic Engineering," *Proceedings of the 2003 ASCE Structures Congress and Exposition*, Seattle, WA, May 29-31.

Horne, J., and H. Burton, 2003, "Investigation of Code Seismic Force Levels for Hospital Equipment," *Proceedings of the Seminar on Seismic Design, Performance, and Retrofit of Nonstructural Components in Critical Facilities*, Applied Technology Council, ATC 29-2, San Francisco, October 23-24.

ICBO (International Conference of Building Officials), 1927, *1927 Uniform Building Code*, Whittier, CA.

ICBO (International Conference of Building Officials), 1935, *1935 Uniform Building Code*, Whittier, CA.

ICBO (International Conference of Building Officials), 1997, *1997 Uniform Building Code*, Whittier, CA.

ICC (International Code Council), 2009, *2009 International Building Code*, www.iccsafe.org.

ICC (International Code Council), 2012, *2012 International Building Code*, www.iccsafe.org.

Miranda, E., and S. Taghavi, 2009, "A Comprehensive Study of Floor Acceleration Demands in Multi-Story Buildings," ATC & SEI 2009 Conference on Improving the Seismic Performance of Existing Buildings and Other Structures, Applied Technology Council and Structural Engineering Institute of ASCE, San Francisco, December 9-11.

Singh, M., Moreschi, L., Suarez, L., and E. Matheu, 2006, "Seismic Design Forces I: Rigid Nonstructural Components," *Journal of Structural Engineering*, American Society of Civil Engineers, Volume 132, No. 10, October 1.

Singh, M., Moreschi, L., Suarez, L., and E. Matheu, 2006, "Seismic Design Forces II: Flexible Nonstructural Components," *Journal of Structural Engineering*, American Society of Civil Engineers, Volume 132, No. 10, October 1.

Schroeder, M., and R. Bachman, 1994, "Analytical Studies in Support of the 1994 NEHRP Provisions for Nonstructural Components," *Proceedings of the Fifth U.S. National Conference on Earthquake Engineering*, Earthquake Engineering Research Institute, Chicago, July 10-14.

Soong, T., Chen, G., Wu, Z., Zhang, R-H., and M. Grigoriu, 1993, *Assessment of the 1991 NEHRP Provisions for Nonstructural Components and Recommended Provisions*, National Center for Earthquake Engineering Research, Technical Report NCEER-93-0003, March 1.

EARTHQUAKE RECORD INTERPRETATION FOR SOIL-STRUCTURE INTERACTIONS EFFECTS OF TWO INSTRUMENTED BUILDINGS

Christine A. Goulet¹, Atsushi Mikami² and Jonathan Stewart³

¹Pacific Earthquake Engineering Research Center, University of California, Berkeley

²Department of Civil and Environmental Engineering, University of Tokushima,
Tokushima, Japan

³Civil & Environmental Engineering Dept., University of California, Los Angeles

Abstract

Kinematic soil-structure interaction (SSI) results from the incoherent nature of ground motions, which causes the motions of foundation slabs to generally be reduced from those in the free-field at high frequencies. We compare two models of kinematic SSI utilized in engineering practice: one based on finite element analysis and the second based on a semi-empirical approach. Predictions from both approaches are compared for two well-instrumented structures to observed transfer functions. The results show (1) the two models produce very similar transfer function estimates and (2) the model predictions are generally consistent with observations.

Introduction

It has long been recognized that foundation-level and free-field seismic ground motions have different characteristics as a result of the spatial variations in ground motions, even on sites with relatively uniform site conditions (e.g., Yamahara, 1970; Scanlan, 1976; Newmark et al., 1977). The spatial variation of ground motions in the horizontal plane causes foundation motions to be reduced in amplitude relative to free-field motions, an effect termed “base slab averaging”. Likewise, the spatial variation of ground motions vertically leads to an “embedment effect”. Both base slab averaging and embedment are kinematic soil-structure interaction (SSI) effects that influence foundation-level ground motions.

Two types of models have been independently developed over the years to predict kinematic SSI effects. The first is implemented in the computer program SASSI (a System for Analysis of Soil-Structure Interaction; Lysmer et al., 1981, 1999; Ostadan, 2005). SASSI computes the relative motion of the foundation to the free-field (input motion) in terms of a transfer function expressing the frequency-dependent ratio of foundation motion amplitude to free-field motion amplitude. Recent versions of SASSI (Ostadan, 2005; Ostadan and Dang, 2007) allow the free-field motion to have a specified level of coherency (producing spatial variation in phase angles). The second approach for prediction of transfer functions from base slab averaging is based on a theoretical solution by Veletsos and co-workers (1989, 1997) coupled with empirical calibration of an incoherence parameter by Kim and Stewart (2003). The Kim and Stewart approach includes both base slab averaging and embedment effects.

In this paper we compare predictions from the SASSI and semi-empirical models for the conditions present at two instrumented buildings: the Factor building in Los Angeles, California and the Atwood building in Anchorage, Alaska. Both buildings are well suited to these analyses for several reasons:

- i. The buildings have shallow foundations (mat, footing and grade beam) appropriate for use with the kinematic SSI models;
- ii. The buildings consist of moment-resisting steel frames that are not conducive to significant inertial SSI effects, thus simplifying data interpretation for kinematic effects;
- iii. The buildings are well instrumented, including foundation sensors and nearby reference arrays with both surface and downhole high resolution sensors; and
- iv. Data have been recorded during multiple events, allowing investigation of event-to-event variability.

A limitation of the data is that strong shaking has not been recorded. Hence, the structures' responses are essentially in their elastic range; the noise levels are also high, occasionally leading to low signal-to-noise ratios.

Our motivation for these comparisons is to (1) investigate the degree to which the results from the two kinematic SSI models differ from each other and from data and (2) to add new data points to the empirical data set available for the calibration of the semi-empirical model.

Site and Building Descriptions

Factor Building

The Doris and Louis Factor Health Science building is a 17-story special moment-resisting steel frame structure located on the University of California, Los Angeles campus (UCLA). As shown in Figure 1, the building has 15 stories above ground and two basement levels. The Factor building was constructed in the 1970s and was designed under the 1973 building code. It has a footprint of approximately 22.4 m by 38.6 m (73.5 ft by 126.5 ft) from the top basement floor to the 9th floor inclusively. The lower basement (level B) has a smaller footprint of 22.4 m by 29.7 m (73.5 by 97.5 ft). A diagonally-braced overhang at floors 10-15 increases the East-West dimension by 7.4 m (24.2 ft) on the west side and by 3.2 m (10.5 ft) on the east side. The ground surface has a gradient uphill towards the north side, making the first floor at the ground surface on the south side and the second floor at the ground surface on the north side. The building rests on shallow foundations. Figure 1 shows the underlying soil conditions, which consist of Pleistocene alluvium ranging from sands to clays having $V_s \approx 400$ -600 m/s beneath the foundation.

The Factor building was instrumented following the 1994 Northridge earthquake with a 72-channel sensor array configured as shown in Figure 1. The array includes vertical sensors on the foundation that enable evaluation of rocking in the east-west direction. A 100 m deep vertical array configured with triaxial accelerometers at 100m depth and at the ground surface is located 25 m from the edge of the building in a botanical garden. Additional details on the building and borehole arrays are provided in Goulet et al. (2011).

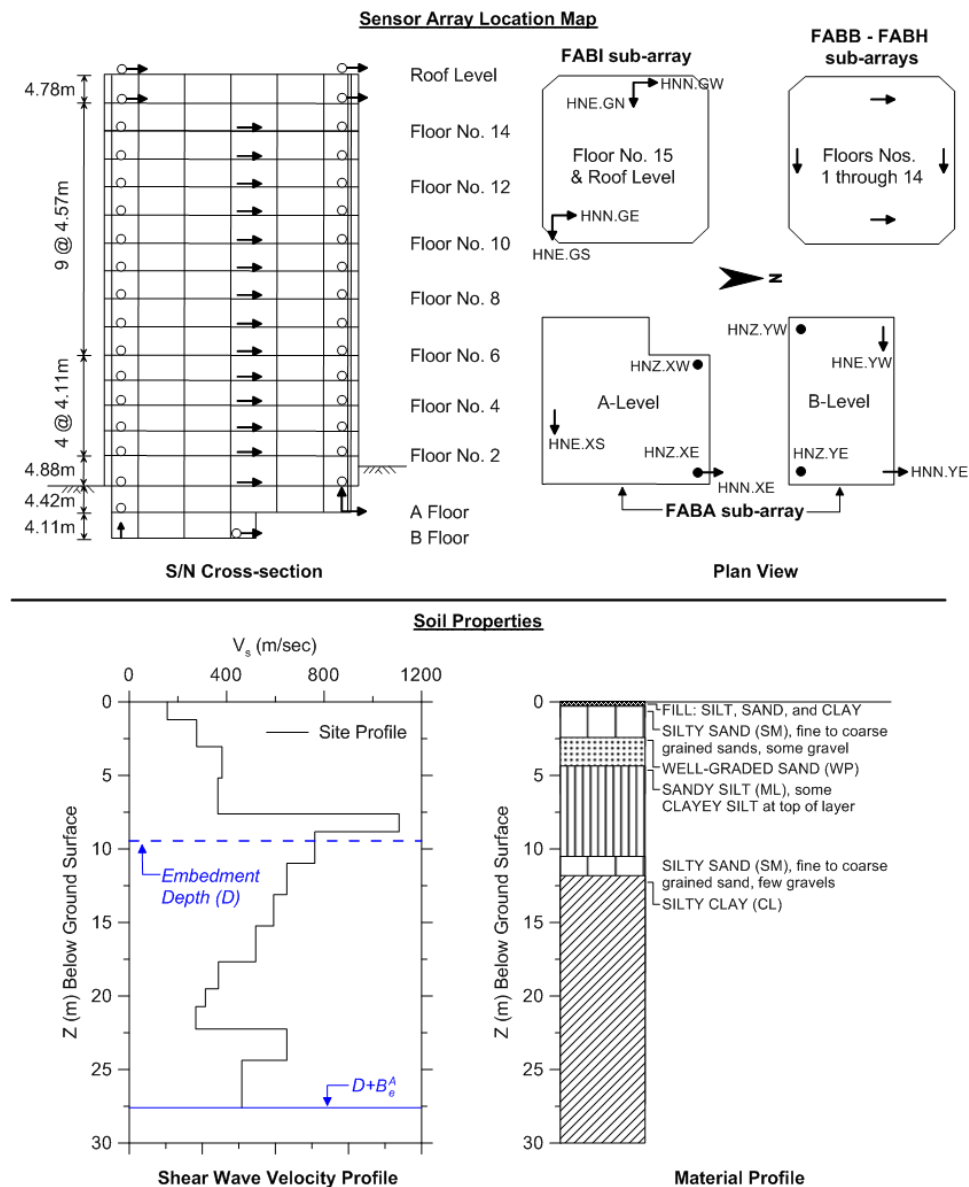


Figure 1. Schematic of the Factor building, showing the sensor array and the subsurface soil profile. Arrows indicate sensor orientation with empty circles pointing into the page and filled circles pointing out of the page. The depths shown on the velocity profile are presented in Table 1. Soil profile information after LeRoy Crandall and Associates, 1976.

Atwood Building

The Atwood building is a 21-story moment-resisting steel frame structure located in downtown Anchorage, Alaska. As shown in Figure 2, the building has 20 stories above ground and a single basement level. The Atwood building was built in 1980 under the 1979 Uniform Building Code. The Atwood building has a square footprint of 39.6 m (130 ft) with a square concrete core of 14.6 m (48 ft). As shown in Figure 2, the reinforced concrete shallow foundation system consists of a mat under the center core with a perimeter wall footing

connected with grade beams. The foundation is connected to that of the adjacent plaza by grade beams.

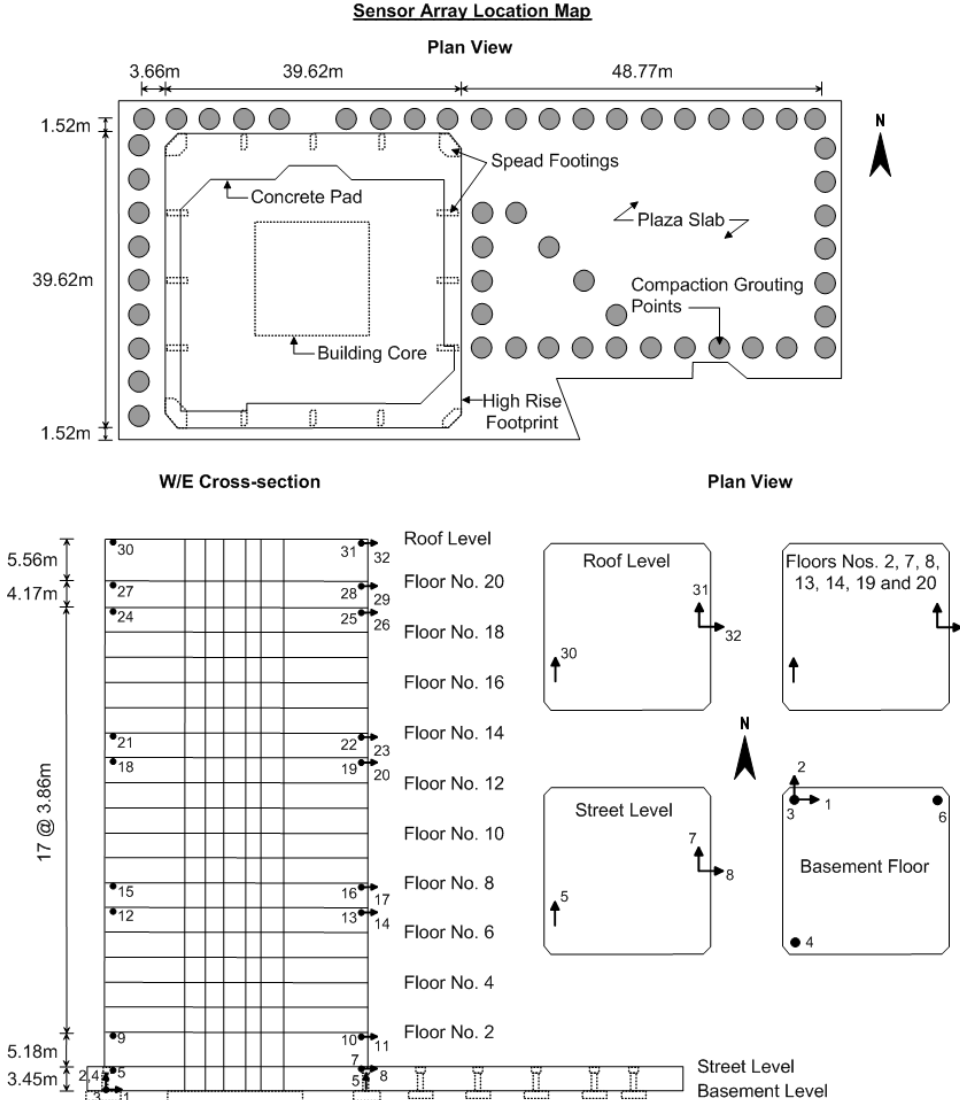


Figure 2. Schematic of the Atwood building, showing the sensor array. Arrows indicate sensor orientation with empty circles pointing into the page and filled circles pointing out of the page.

Figure 3 shows the underlying soil conditions, which consist of a thick soil layer of the Bootlegger Cove Formation with an average thickness of about 30 m in the vicinity of the site. This geologic formation is mostly composed of silty materials deposited in a late Pleistocene glaciomarine-glaciodeltaic environment (Ulery et al., 1983). We were unable to locate site-specific boreholes or geophysical logs for the Atwood building, and the site conditions are taken from a borehole at the Delaney Park site (the location of the free-field array) 165 m from the Atwood building. Even at the borehole location, there are no geophysical measurements, but V_s profiles have been estimated by Nath et al. (1997) and Yang et al. (2008) from inversion of array data, with the results shown in Figure 3.

The instrumentation system, consisting of structural and borehole arrays, was installed in 2003. As shown in Figure 2, the structural instrumentation is composed of 32 accelerometers distributed on 10 of the 21 floors of the structure. The two basement floors have three vertical sensors each that allow computation of rotation in both directions. A 30.5 m deep vertical array of six sensors distributed at depth plus one at the surface is located approximately 165 m from the Atwood building at Delaney Park. The surface sensor is used as the free-field motion. Further details on the instrumentation system are provided in Çelebi (2003; 2006).

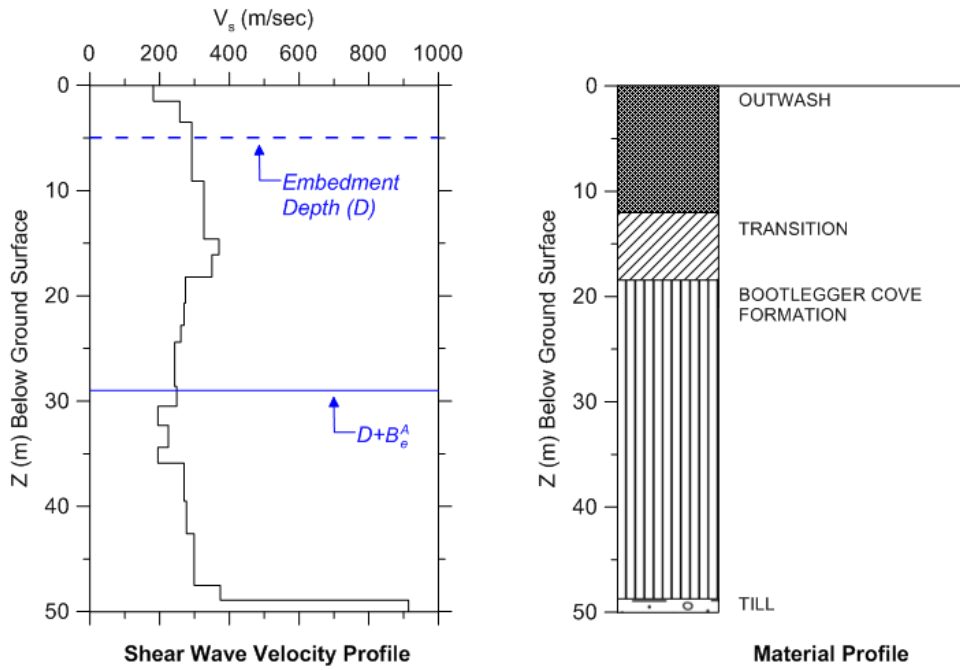


Figure 3. Shear wave velocity profile at the location of the borehole array in Delaney Park after Nath et al. 1997 and Yang et al., 2008. The depths shown on the velocity profile presented in Table 1. The borehole array is about 165 m (540 ft) away from the Atwood building.

Modal Properties

We performed system identification analyses similar to those described in Stewart and Fenves (1998) to identify fixed- and flexible-base modal parameters for the Factor and Atwood buildings. Modal parameters for the two base fixity conditions were nearly identical, indicating period lengthening near unity and practically zero foundation damping. This is expected, as the ratio of structure to soil stiffness $h / (V_s T)$ (where h = height to centroid of first mode shape, V_s = soil shear wave velocity, and T = structure fixed base period) is very small (0.10 for Factor, 0.07 for Atwood), so inertial SSI effects are expected to be minimal per classical method such as those in Veltos and Nair (1975). The details of these analyses are presented in Goulet et al. (2011). In the remainder of this article, we focus on kinematic interaction effects for the two buildings, which are expected to be more significant as a result of their embedment and large foundation area.

Model-Based Kinematic Transfer Functions

Semi-Empirical Model

Veletsos and co-workers (1989, 1997) developed models for theoretical base slab averaging that combine an analytical representation of the spatial variation of ground motion with rigorous treatment of foundation-soil contact. Kim and Stewart (2003) calibrated Veletsos' analysis procedure against observed foundation/free-field ground motion variations as quantified by frequency-dependent transfer functions. Two types of transfer functions can be computed from the models presented by Veletsos and co-workers:

$$H_u(\omega) = \frac{u_{FIM}}{u_g} \quad H_\theta(\omega) = \frac{\theta_{FIM} L}{u_g} \quad (1)$$

where u_{FIM} denotes foundation translation, u_g is the ground motion translation in the same direction, θ_{FIM} denotes kinematic rotation about an axis normal to the direction of u_{FIM} and u_g , and L is the foundation half dimension in the same direction as u_{FIM} and u_g . The acronym 'FIM' indicates Foundation Input Motion, which is the motion of the foundation for the hypothetical condition of no inertia (in the structure or foundation). Motions recorded on actual foundations, which naturally have inertia, represent an approximation of FIM. Similarly, the acronym FFM is used to represent the free-field motion.

The Kim and Stewart calibration considered the horizontal translation transfer function only (H_u), and resulted in apparent κ values (denoted κ_a) for each structure/data set combination. Those κ_a values reflect not only incoherence effects, but necessarily also include average foundation flexibility and wave inclination effects for the calibration data set. Kim and Stewart's analyses were for 29 sites having structure/free-field arrays similar to those for Atwood and Factor, although with lower quality sensors and data acquisition systems (e.g., much of the data were from analogue systems). The Kim and Stewart model is of particular interest because its recommendations form the basis of seismic guidelines for retrofit of existing buildings (e.g., ASCE 2007; updated in NIST CJV, 2012).

Table 1 lists the model input parameters required to apply the semi-empirical base slab averaging model and embedment model from Kim and Stewart (2003). Those parameters are based on the foundation dimensions and on the shear wave velocity profile over the embedment depth of the foundation and to a depth of $B_e^A = \sqrt{A_f/4}$ below the foundation.

Table 1. Input parameters to the Kim and Stewart (2003) semi-empirical model

<i>Parameter</i>	<i>Factor</i>	<i>Atwood</i>
Embedment Depth (D)* (m)	9.5	5.0
Area of Foundation (A_f) (m ²)	1034	1822
Effective Foundation Size (B_e^A) (m)	18.1	24.1
Average V_s to Embedment Depth, D * (m/s)	427	243
Average V_s from Base of Foundation D to $D + B_e^A$ * (m/s)	492	291

* The depths and the shear wave velocity profiles are shown in Figures 1 and 3 for the Factor and Atwood buildings, respectively.

Finite Element Model in SASSI

SASSI was originally developed by Lysmer et al. (1981, 1999) and utilized the substructure approach in which the linear SSI problem is divided into sub problems based on the principle of superposition using linear material properties. Soil is assumed to consist of horizontal layers overlying either a rigid base or an elastic half-space. The structure and foundation are modeled by finite elements. Foundations are modeled as massless slabs to exclude inertial effects, with a Youngs modulus appropriate for concrete. Ostadan and Dang (2007) extended SASSI to include incoherent ground motions that include stochastic phase variations as prescribed by the spatial coherency model of Abrahamson and co-workers (1991, 2005). We utilize this extended version of SASSI in the present analyses.

Figure 3(a) shows the foundation finite element model developed for the Factor building foundation system. Basements A and B were modeled as described in the previous section. Figure 3(b) shows the SASSI finite element model for the Atwood building foundation system.

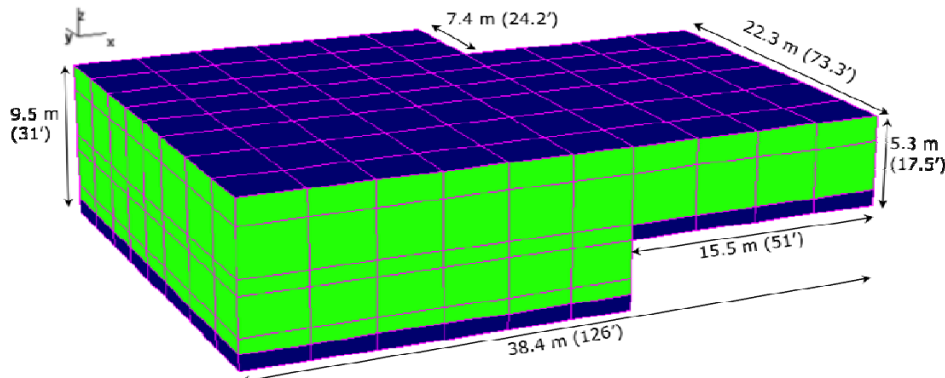


Figure 3(a). SASSI finite element model, Factor building. The positive x axis points to the North.

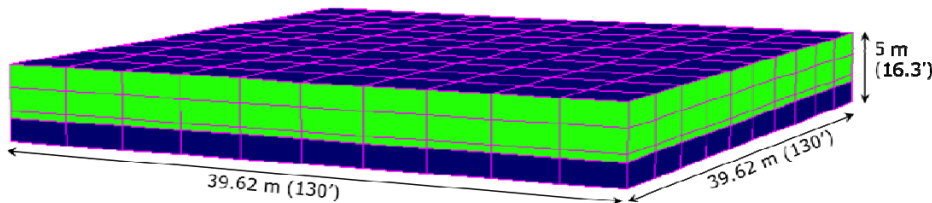


Figure 3(b). SASSI finite element model, Atwood building.

Model Comparisons for Subject Buildings

Figures 4(a) and (b) compare the transfer functions for the Factor and Atwood buildings as predicted using the semi-empirical and SASSI approaches. In the case of the semi-empirical approach, we show transfer functions for the base slab averaging and embedment effect alone and with the two combined. The combination is through simple multiplication at each respective frequency. Embedment effects are more important than base slab averaging effects for the subject buildings in the frequency ranges of interest (less than approximately 8 Hz). SASSI

results are nearly identical in the two horizontal directions, so only a single direction is shown in the figures.

The combined semi-empirical model (including base slab averaging and embedment effects) provides similar transfer functions to those from SASSI.

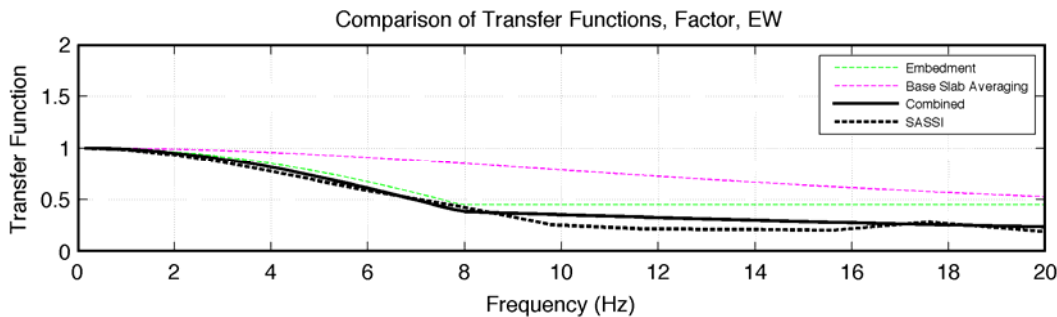


Figure 4(a). Comparison of kinematic transfer functions, Factor building. The EW-NS directions lead to slightly different shapes for the SASSI model (not shown), due to the asymmetry of the foundation plan.

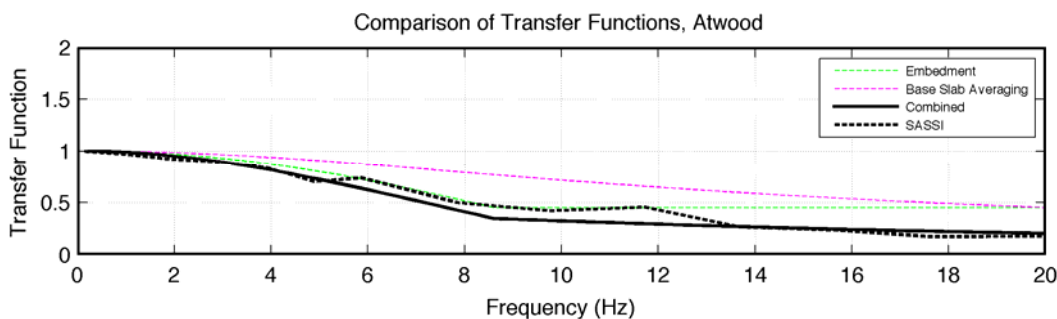


Figure 4(b) Simplified semi-empirical SSI model for kinematic transfer function, Atwood building. Due to the symmetric foundation, the SASSI transfer functions are exactly the same in both directions.

Kinematic Transfer Functions from Recordings

Selection of Recordings

A large number of events were recorded by both building arrays, but most of the accelerations were of very low amplitude. The event selection criteria used are:

1. Availability of array recordings for basement, roof and free-field.
2. Signal-to-noise ratio as large as possible (a trial of motions indicate satisfactory results generally for peak ground acceleration (PGA) stronger than about 2% g for the free-field records).

For the Factor building, many changes in instrumentation occurred in the 2003-2005 period making it difficult to correctly process the data. Therefore, events recorded after January 2006 were selected, which is a time period for which the instrumentation configuration and sensors naming scheme are best known.

Table 2 lists the selected earthquakes, and the PGA values for the free-field records. As described in Goulet et al. (2011), many more records were analyzed over the course of the project, mostly for system identification analysis of modal vibration properties and to define the usable signal to noise ratio; these results are not reported here for brevity.

Table 2. Selected records for both buildings

<i>Building</i>	<i>Earthquake ID</i>	<i>Date, Epicentral Location</i>	M_w	<i>Hypocentral Distance (km)</i>	<i>PGA, Free-Field EW (cm/s²)</i>	<i>PGA, Free-Field NS (cm/s²)</i>
Factor	2007/221	Aug. 9, 2007, Chatsworth	4.6	31	8.1	7.3
	2008/211	Jul. 29, 2008, Chino Hills	5.4	64	24.0	22.6
Atwood	20041108	Nov. 8, 2004, Denali National Park	4.9	222	2.1	1.7
	20050216	Feb. 16, 2008, Point McKenzie	4.7	14	11.8	10.1

Computation Procedures

The transfer functions in Eq. (1) are frequency-dependent and complex-valued. Typically the phase of the transfer function is not used and the analysis emphasizes transfer function amplitude. This convention is followed and subsequent references to “transfer function” imply the amplitude of the complex-valued ratios.

Recall that the FIM is the theoretical motion of the base slab if the foundation and structure had no mass. The recorded foundation motion has been shown to provide a good estimate of the FIM for frequencies distinct from the fundamental-mode frequencies of vibration of the structure (Kim and Stewart, 2003).

Transfer functions are evaluated from the recordings using procedures described in Mikami et al. (2008). Frequency domain smoothing is applied to spectral density functions for the ‘input’ (denominator in Eq. 1, denoted y) and ‘output’ (numerator in Eq. 1, denoted x), from which transfer functions are computed as follows:

$$|H(\omega)| = \sqrt{\frac{S_{yy}}{S_{xy}}} \quad (4)$$

where S_{yy} is the smoothed auto-spectral density functions for the output and S_{xy} is the cross-spectral density function of the input/output pair. This transfer function formulation represents an average that tends to minimize the impact of noise in the data (Goulet et al. 2011; Ljung, 1999 and Pandit, 1991). The method and degree of smoothing is described further below. In addition, the coherence (square of coherency) of the data is calculated as:

$$\gamma^2(\omega) = \frac{|S_{xy}(\omega)|^2}{S_{xx}(\omega)S_{yy}(\omega)} \quad (5)$$

The coherence varies between zero and one and is used to judge the effects of noise in the data. Frequency ranges in the transfer function that are dominated by noise (typically high frequencies) will have low coherence. Incoherence can be due to noise or to natural physical processes such as wave scattering in the soil.

As described by Mikami et al. (2008), the calculation of transfer and coherence functions for a given record pair is affected by the time windows analyzed (e.g., full record, shear-wave window, etc.) and the method and level of smoothing. Because the window selection is largely subjective, we attempted to make the selection more systematic and reproducible. The approach followed in the present work is as follows:

- The window of time considered in the analysis (time window) was selected using four alternate approaches: subjective selection of strong shaking (encompassing approximately the shear wave window, and sometimes, initial portion of surface waves), and three windows based on the 5-75%, 5-85% and 5-95% significant duration window from normalized Arias Intensity (Arias, 1970). An example of showing a window selection for a record is shown in Figure 5.
- We perform frequency domain smoothing using Hamming windows of width $2m+1$ applied directly to the power spectral values (larger m corresponds to more smoothing; we use $m = 3, 5, 7$, and 9). The appearance of the transfer function depends on the level of smoothing and the number of frequencies in the spectral density function (larger for longer duration time series). For a shorter array and a given level of smoothing, the transfer function will effectively be smoother, which affects the interpretation. Although we completed both time-domain and frequency domain smoothing, we focus here on frequency domain smoothing results. Because of the relatively short record durations, sub-dividing short duration records, as in time-domain smoothing, can produce results very sensitive to the level of smoothing.

Transfer functions were computed for the four window widths and four levels of smoothing defined above. Figure 6 shows an example of the transfer and coherence functions produced with this approach. We also show on the coherence plot the predicted median coherence for the FFM-FIM separation distance based on Abrahamson and co-workers (1991, 2005) empirical model (derived from dense arrays of ground stations). Points that correspond to coherence larger or equal to 0.8 are also marked with blue circles on the transfer functions. The shaded region in Figure 6 represents a general interpreted transfer function over the usable bandwidth, which is established by a polynomial regression on the transfer function points. Two regressions were performed: one using only the highly coherent data points (coherence > 0.8) and one using all the data points for the selected bandwidth.

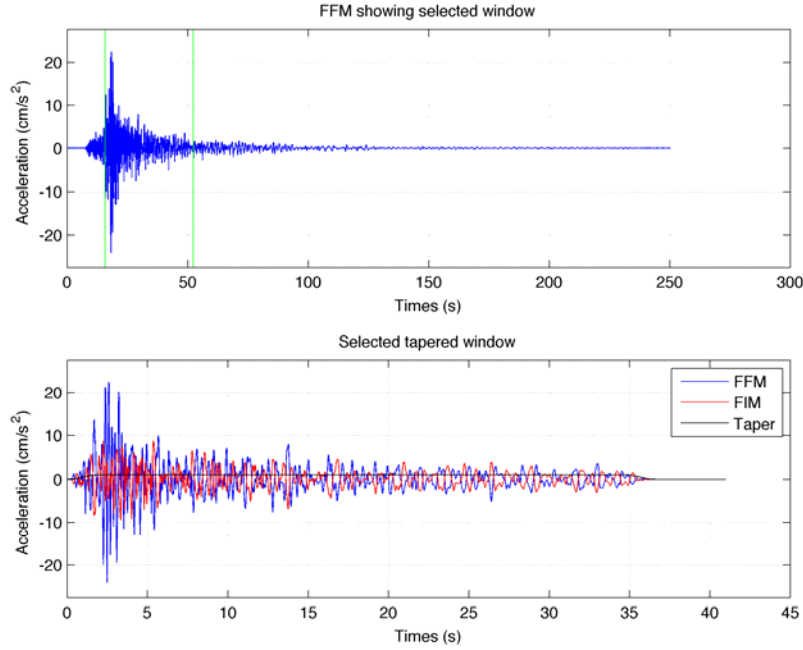


Figure 5. Example of time series window selection based on the FFM input, 2008/211 EW, Factor building. The bottom plot also shows the taper to zero at the beginning and end of the window.

The general transfer function shapes are similar for different window durations and smoothing levels, but the interpretation could be affected as a result of shifting locations of peaks and troughs. The approach adopted here is intended to provide more robust interpretations than would be obtained with strict adoption of a single widow duration and smoothing level or from subjective criteria that could vary substantially from record-to-record.

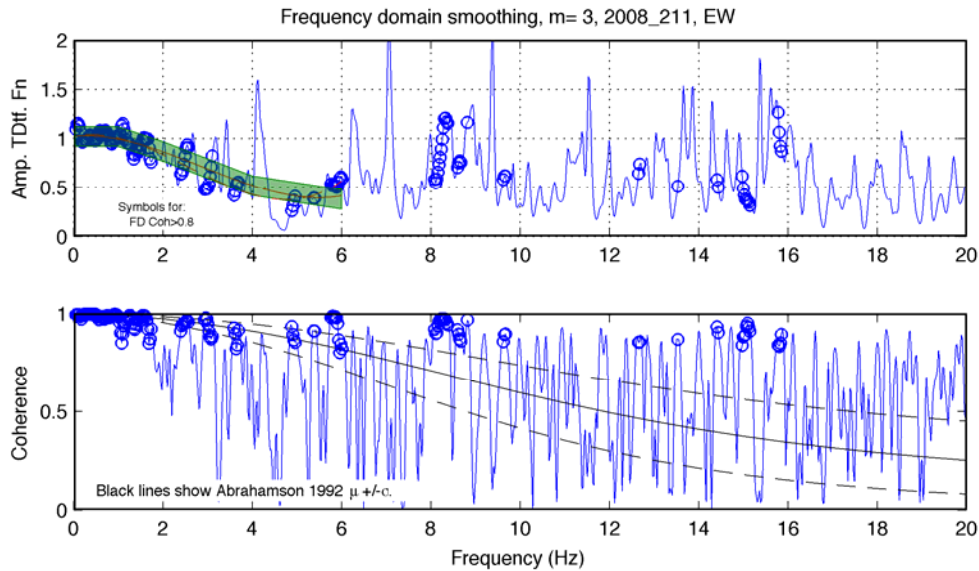


Figure 6. Transfer function and coherence for the 2008/211 EW data set, Factor building. Frequency domain smoothing with 7 points Hamming window.

As pointed out by Mikami et al. (2008), perhaps the most critical element of this procedure is identification of the usable frequency range of the transfer function. The reliability of the transfer function ordinates degrades as coherence falls. At the extreme where the coherence corresponds to that of white noise (frequencies $> \sim 11$ Hz in Figure 6), the transfer function essentially represents the ratio of two noise signals, and only sampling across very large numbers of records would produce meaningful results. At low frequencies coherence tends to be near unity, and transfer function ordinates are robust, so the practical issue is the maximum usable frequency of the transfer function. We identify the usable frequency range as the range having dense spacing of high coherence ordinates (typically greater than approximately 0.8). At high frequencies, occasional high coherence points can be found, but when widely spaced on the frequency axis, we argue that the transfer function is beyond its useful frequency range. Hence, the maximum usable frequency is that which separates the portion of the frequency spectrum having relatively closely spaced from relatively sparse high frequency ordinates. This judgment is admittedly subjective.

Results for the Factor and Atwood Buildings

Figures 6 and 7 show selected transfer and coherence functions for the Factor building computed for the two events listed in Table 2 in the EW and NS directions respectively. The jagged blue lines show the transfer function and coherence computed for a specified window and level of smoothing, as given in the caption, whereas the shaded green area is the best-fit interpretation over the usable frequency range derived from multiple computations with variable levels of smoothing as described above. The regression curves used to constrain the green shaded area are shown in Figure 6 by the red solid and dashed lines for all and only the high coherence data respectively. Blue circles are used to highlight ordinates for which the coherence is larger than 0.8. The Abrahamson and co-workers (1991, 2005) coherence model is shown for reference in the coherence plots.

The maximum usable frequency is taken as 6 Hz in the EW direction and 8 Hz in the NS direction based on the spacing of high coherence data points (narrow at lower frequencies, wide at higher frequencies). Note that the loss of coherence at 6-8 Hz is unrelated to the data acquisition system in this case, which has a wide bandwidth. The loss of coherence is a natural process that is fully expected for accelerometers at distinct locations, as reflected by the median coherence prediction (from Abrahamson and co-workers, 1991 and 2005) shown in the plots, which follows the same general trend as the data. Similar values of limiting frequencies have been encountered in previous work for other structures (Kim and Stewart 2003; Mikami et al. 2008).

A consistent peak and trough pair in the 4-5 Hz frequency range is visible for the 2008/211 EW earthquake dataset (Figure 6). This is not observed in the NS transfer functions for the same earthquake or in the 2007/221 dataset (Figure 7). It is unclear what causes this feature.

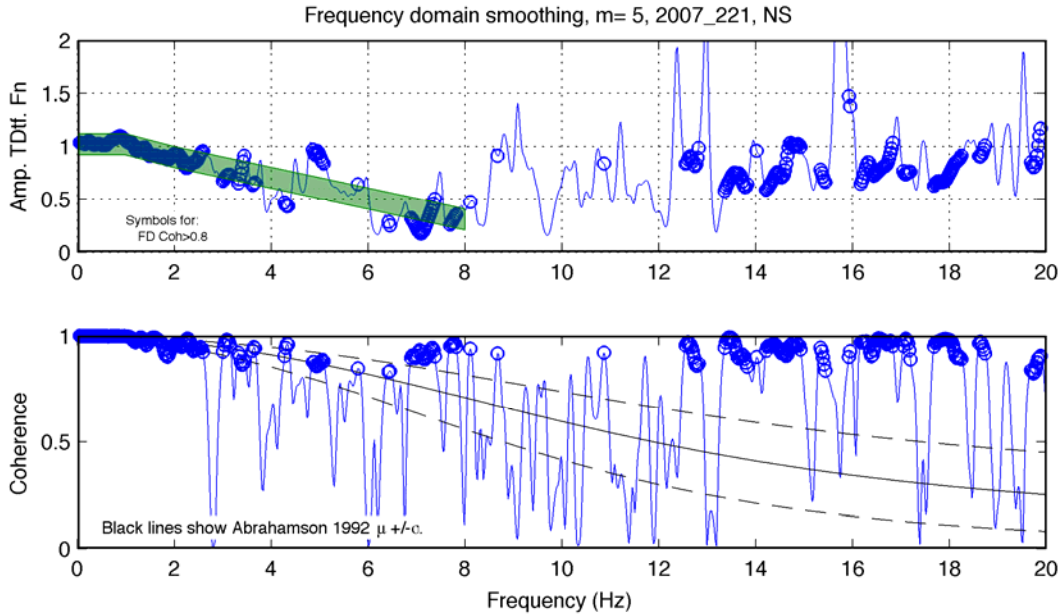


Figure 7. Transfer function and coherence for the 2007/221 NS data set, Factor building.

Sample results for the Atwood building are presented in Figures 8-9 in the same format. Using data from the two earthquakes listed in Table 2. The relatively large separation distance between the FFM and FIM (165 m) results in relatively rapid decay of coherence with frequency. If the transfer function interpretations were performed only with high coherence data, the maximum frequency would be in the range of 1-1.5 Hz. Nonetheless, transfer function ordinates at higher frequencies are stable under different levels of smoothing up to approximately 8 Hz or more and are reasonably consistent between components for the two events considered. Nonetheless, due to the large impact of noise, the transfer function ordinates should be viewed as few samples of an essentially random process, and it is unlikely that they accurately reflect the mean of the underlying physical process (i.e., the kinematic transfer function).

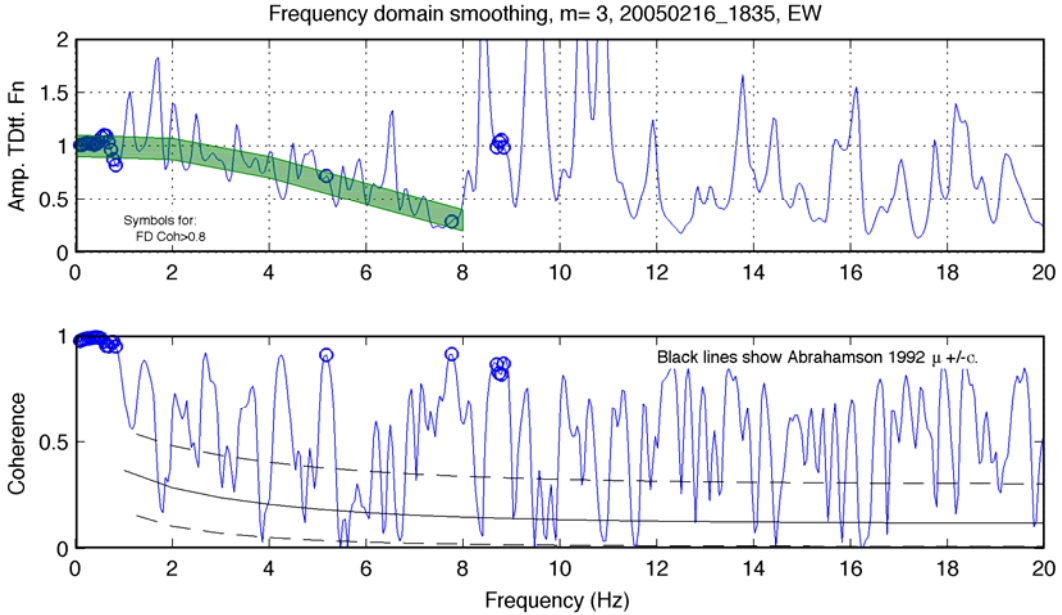


Figure 8. Transfer function and coherence for the 20050216 EW data set, Atwood building.

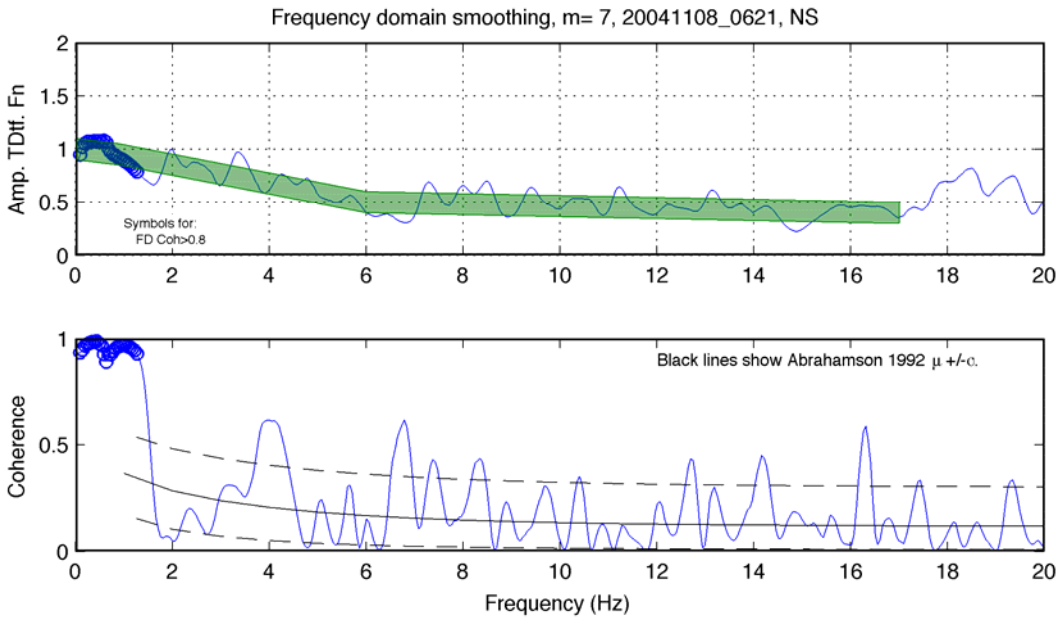


Figure 9. Transfer function and coherence for the 20041108 NS data set, Atwood building.

Interpretation and Discussion

As shown previously in Figure 4, the SASSI and semi-empirical models for kinematic SSI provide very similar estimates of transfer functions. Figures 10-13 compare those estimates to the transfer functions from data. We show transfer function bands for each earthquake at each site that envelop the component-specific bands presented previously. The data tend to agree, in a general sense, with the model predictions, keeping in mind that the data-based transfer functions are represented by bands rather than single lines.

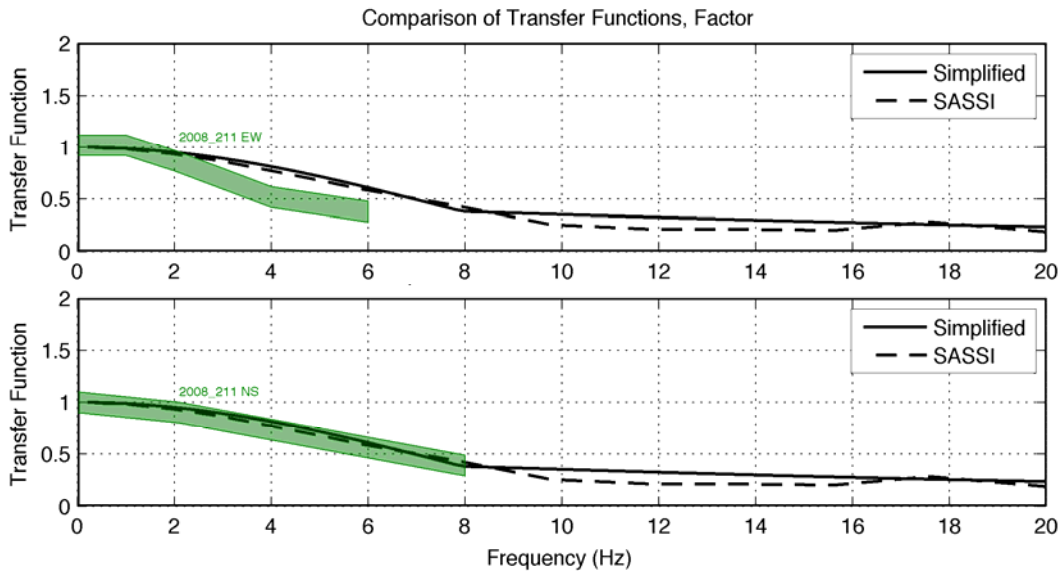


Figure 10. Comparison of transfer functions, 2008/211 earthquake data, Factor building. EW component on top, NS component on bottom.

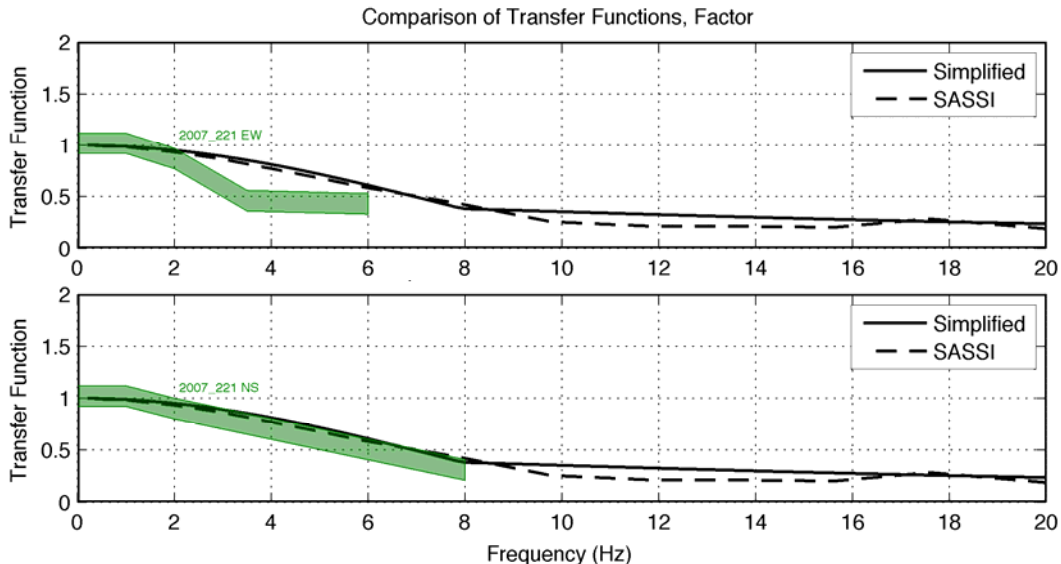


Figure 11. Comparison of transfer functions, 2007/221 earthquake data, Factor building. EW component on top, NS component on bottom.

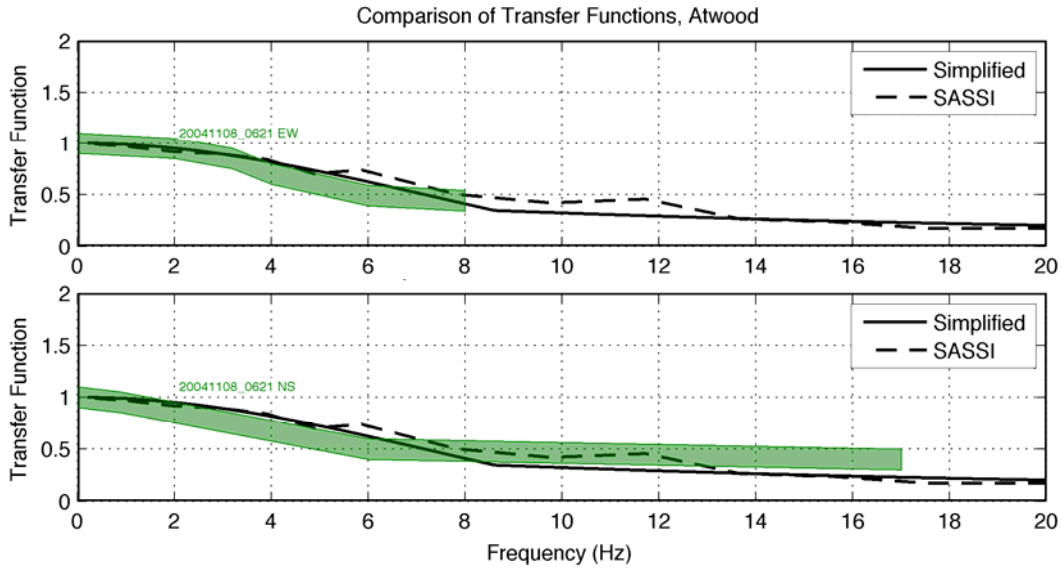


Figure 12. Comparison of transfer functions, 20041108 earthquake data, Atwood building. EW component on top, NS component on bottom.

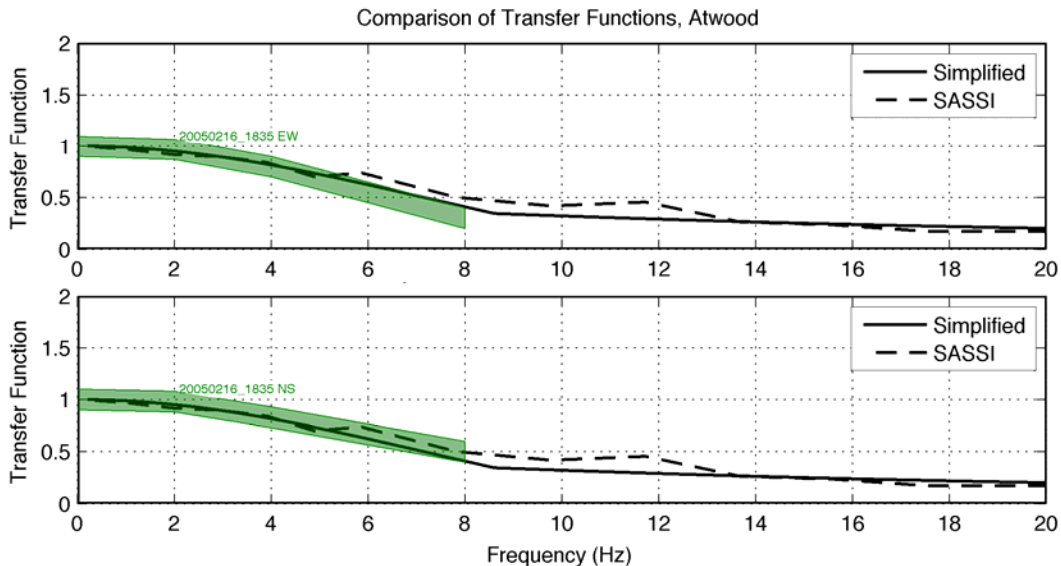


Figure 13. Comparison of transfer functions, 20050216 earthquake data, Atwood building. EW component on top, NS component on bottom.

A significant source of uncertainty affecting the data interpretation that could be reduced with further optimization of the array set are the geophysical data at the sites and the instrument spacings. As described previously, high quality geotechnical and geophysical data should ideally be present for both the building and free-field sites. One important issue encountered was the lack of information on the sub-surface geology, either at the building location or at the free field sensor location. This is important because both models considered here (Kim and Stewart, 2003 and SASSI) use the shear wave velocity as input. In order to allow a fair comparison of data and models, it would be important to have the detailed shear wave velocity profile around and under the buildings and at the free field station. The quantification of differences in shear wave velocity profiles at both locations would bring insight to the results interpretation, by allowing

the understanding of site response effects. For Factor, both shear wave velocity profiles were obtained (building and free-field station location), although accurate elevation datum was not available to relate the two profiles. For the Atwood building location, soil profile information was not available. The only profile available was derived from seismic wave inversion at the free-field array location. If site conditions at the two locations were significantly different, variable levels of site response could be mistakenly interpreted as a kinematic interaction effect. Reduced instrument spacing, especially for the Atwood building, would improve the coherence of the signals and improve the confidence in the transfer function ordinates. Further recommendations on instrument layout to improve the ability to infer SSI effects (both kinematic and inertial) are provided in Goulet et al. (2011). Nonetheless, we find that the data-based results obtained through this work are consistent with the two models considered.

Acknowledgments

Funding for this work was provided by the Data Interpretation Project of the California Strong Motion Instrumentation Program, California Geological Survey, Agreement No. 1008-920. The authors would like to thank the Strong Motion Instrumentation Program and the Ground Response Subcommittee panel who provided insightful comments throughout the project.

Strong motion recordings for the project were provided by Chris Stephens from the U.S. Geological Survey and by Monica Koehler from Caltech. We would also like to acknowledge Drs. Robert Nigbor, Derek Skolnik, Mehmet Çelebi and Jamie Steidl for their help and guidance regarding the available data for this study.

References

- Abrahamson, N.A., Schneider, J.F., and Stepp, J.C. (1991). "Empirical spatial coherency functions for application to soil-structure interaction analyses", *Earthquake Spectra*, 7, 1-26.
- Abrahamson, N. A., (2005). "Updated coherency model", Report prepared for Bechtel Corporation.
- American Society of Civil Engineers (2007). "ASCE 41-06: Seismic Rehabilitation of Existing Buildings", American Society of Civil Engineers, 416 p.
- Arias, A. (1970). "A Measure of Earthquake Intensity", R.J. Hansen, ed. Seismic Design for Nuclear Power Plants, MIT Press, Cambridge, Massachusetts, pp. 438-483.
- Çelebi, M. (2006). "Recorded earthquake responses from the integrated seismic monitoring network of the Atwood Building, Anchorage, Alaska", *Earthquake Spectra*, v. 22, no. 4, p. 847-864.
- Çelebi, M. (2003). "Seismic Instrumentation Plan for Robert B. Atwood Building, Anchorage, AK 99501", Administrative Report, U.S. Geological Survey.

Goulet, C.A., Stewart, J.S. and Mikami, A. (2011). "Earthquake Record Interpretation and Soil-Foundation Structure Interaction Effects for the Atwood and Factor Buildings", California Strong Motion Instrumentation Program, Sacramento, Final Report, 60 pp.

Kim, S. and Stewart, J.P. (2003). "Kinematic soil-structure interaction from strong motion recordings," J. Geotech. & Geoenv. Engrg., ASCE, 129 (4), 323-335.

LeRoy Crandall and Associates Consulting Geotechnical Engineers (1976). "Report of Foundation Investigation and Site Response Study, Proposed Cancer Center/School of Nursing, Tiverton and South Circle Drives, Los Angeles, California for the University of California, Los Angeles", Campus Capital Programs building archives, University of California, Los Angeles.

Ljung, L. (1999). "System identification: Theory for the user", 2nd Ed., Prentice Hall, Englewood Cliffs, NJ.

Lysmer, J., M. Tabatabaie-Raissi, F. Tajirian, S. Vahdani, and Ostadan F. (1981), "SASSI-A System for Analysis of Soil-Structure Interaction," Report no. UCB/GT/81-02, Department of Civil Engineering, University of California, Berkeley.

Lysmer, J., Ostadan F. and Chin, C. (1999). "SASSI2000 Theoretical Manual."

Mikami, A., Stewart, J.P., and Kamiyama, M. (2008). "Effects of time series analysis protocols on transfer functions calculated from earthquake accelerograms", Soil Dynamics and Earthquake Engineering, 28 (9), 695-706.

Nath, S. K., Chatterjee, D., Biswas, N. N., Dravinski, M., Cole, D.A., Papageorgiou, A., Rodriguez, J.A., and Poran, C.J. (1997). "Correlation study of shear wave velocity in near surface geological formations in Anchorage, Alaska", Earthquake Spectra 13(1) 55-75.

NEHRP Consultants Joint Venture, 2012. Soil-Structure Interaction for Building Structures, Report NIST/GCR 11-917-14, National Institute of Standards and Technology, Washington, D.C

Newmark, N.M., Hall, W.J., and Morgan, J.R. (1977). "Comparison of building response and free field motion in earthquake," Proc. 6th World Conf. Earthquake Engrg., New Delhi, India, Vol. II, 972-978.

Ostadan, F, (2005). Soil-structure interaction analysis including ground motion incoherency effects, 18th International Conference on Structural Mechanics in Reactor Technology (SMiRT 18), Beijing, China.

Ostadan, F. and Dang, N. (2007), "SASSI-SRSS Approach for SSI Analysis with Incoherent Ground Motions", Bechtel National, San Francisco, California.

Pandit, S.M. (1991). "Modal and Spectrum Analysis", John Wiley, New York, NY.

Scanlan, R.H. (1976). "Seismic wave effects on soil-structure interaction," J. Earthquake Engrg. Struct. Dynamics, 4, 379-388.

Stewart, J. P., and Fenves, G. L. (1998). "System identification for evaluating soil-structure interaction effects in buildings from strong motion recordings", J. Earthquake Engrg. Struct. Dyn., 27, 869–885.

Ulery, C.A., Updike, R.G., and USGS Office of Earthquakes (1983). "Subsurface structure of the cohesive facies of the Bootlegger Cove formation, southwest Anchorage: Alaska", Division of Geological & Geophysical Surveys Professional Report 84, 5 p., 3 sheets, scale 1:15,840.

Veletsos, A. S., and Nair, V. V. (1975). "Seismic interaction of structures on hysteretic foundations", J. Struct. Eng., 101, 109–129.

Veletsos, A.S. and Prasad, A.M. (1989). Seismic Interaction of Structures and Soils: Stochastic Approach, ASCE Journal of Structural Engineering, Vol. 115, pp. 935-956.

Yamahara, H. (1970). "Ground motions during earthquakes and the input loss of earthquake power to an excitation of buildings," Soils and Foundations, 10(2), 145-161.

Yang, Z., Dutta, U., Xiong, F., Biswas, N and Benz, H. (2008). "Seasonal frost effects on the dynamic behavior of a twenty-story office building", Cold Regions Sc. & Techn. 51, 76-84.

DAMPING IDENTIFICATION IN BUILDINGS FROM EARTHQUAKE RECORDS

Dionisio Bernal, Salma Mozaffari Kojidi, Kenny Kwan and Michael Döhler

Civil and Environmental Engineering Department, Center for Digital Signal Processing,
Northeastern University, Boston, MA

Abstract

Seismic response records from the CSMIP database are used to formulate expressions for the expected value of damping ratios as a function of available regressors. The paper discusses the source of the high variance in the identification of damping and proposes mechanisms for the correlation between fundamental building frequency and damping as well as for the observation that damping increases with the mode number. The data analyzed is restricted to cases where the ground accelerations exceed 0.05g and the values obtained, not surprisingly, prove notably larger than those of previous studies, where very small amplitude vibrations were used. Reduced to the most basic observation the results show that the damping ratio of steel buildings (for linear but not ambient level vibration) is typically larger than the widely used 2%, while 5% is reasonable for concrete.

Introduction

The term damping is used to refer to the collection of mechanisms by which systems dissipate energy. Although the inherent damping of structural systems is not viscous, velocity proportional dissipation is widely used because it leads to mathematical simplicity and because, at least for small damping, it can be calibrated to mimic the actual dissipation well. In practice it is customary to specify damping through modal damping ratios, defined as the quotient of the damping constant of the mode to the minimum value for which the response to arbitrary initial conditions does not have harmonic terms. The problem of extracting damping of viscously damped linear systems from input-output data is a standard problem in identification and exact results are obtained by all consistent algorithms when the data generating system satisfies the assumptions (Juang 1994, Verhaegen and Verdult 2007, Van Overschee and De Moor 1996, Heylen et al. 1997).

Notwithstanding the availability of theory, estimation of consistent damping values from measured response is difficult in structures subjected broadband excitation. The reason for this will be discussed in some detail in the body of the paper but at this point we note that the result is essentially a consequence of the fact that the information (more precisely the Fisher information) encoded in the response data about damping is low. Low information implies that the estimated damping is a random variable with high variance and thus that realizations can differ substantially, either because the data set changes (even though the structure is the same) or because, for a given data set, details of the identification approach vary. One early example of discrepancies in damping estimates obtained for the same data set is that of the 12 high rise buildings subjected to the San Fernando earthquake, considered initially by Hart et al., (1975) and a few years later by McVerry (1979, 1980).

Notwithstanding the high variance, predictors for damping have been derived from the examination of data sets by various researchers. For example, Zhang and Cho (2009) extracted damping ratios from ambient vibration data for 82 buildings in Xi'an, China and proposed an expression for the first mode damping. Other studies include those by Jeary (1986), Lagomarsino (1993), Tamura et al. (1996), Sasaki (1998) and Satake et al. (2003). In most previous studies where large data sets have been considered the vibration amplitudes have been very small and, as a consequence, the damping values obtained can be considered a lower bound. In this study we limited examination to responses where the peak ground acceleration was no less than 0.05g. The cases that satisfied this limit were 69 concrete buildings, 44 steel, 14 masonry and 5 wood structures. Since the response accelerations considered here are significantly larger than in most of the previous studies, we expected the damping values to be larger and the results obtained confirmed this expectation.

In addition to the results of the identification and the regression the paper presents an examination of the variability in damping identification and offers some discussion on the observed trends. The theoretical base of the identification approach is summarized in Appendix A and the numerical values of the identified damping and the regressors for each considered case are presented in Appendix B.

Background and Relations

Equations of Motion

Let the subscript 1 stand for coordinates that are not prescribed and 2 for those that are. The equations of motion of a viscously damped linear system without external excitations can then be written as

$$\begin{bmatrix} M_{11} & M_{12} \\ M_{21} & M_{22} \end{bmatrix} \begin{Bmatrix} \ddot{y}_1 \\ \ddot{y}_2 \end{Bmatrix} + \begin{bmatrix} C_{11} & C_{12} \\ C_{21} & C_{22} \end{bmatrix} \begin{Bmatrix} \dot{y}_1 \\ \dot{y}_2 \end{Bmatrix} + \begin{bmatrix} K_{11} & K_{12} \\ K_{21} & K_{22} \end{bmatrix} \begin{Bmatrix} y_1 \\ y_2 \end{Bmatrix} = \begin{Bmatrix} 0 \\ 0 \end{Bmatrix} \quad (1)$$

The displacements that are not prescribed can be expressed as a linear combination of the prescribed ones plus a residual, namely

$$y_1 = r y_2 + u \quad (2)$$

which, when substituted into the top partition of eq.1 gives

$$M_{11}\ddot{u} + C_{11}\dot{u} + K_{11}u = -(M_{12} + M_{11}r)\ddot{y}_2 - (C_{12} + C_{11}r)\dot{y}_2 - (K_{12} + K_{11}r)y_2 \quad (3)$$

Since the matrix r is arbitrary, it can be selected to cancel any of the terms on the *rhs* of eq.3, taking r as

$$r = -K_{11}^{-1}K_{12} \quad (4)$$

neglecting the damping contribution to the *rhs* term, and recognizing that for lumped mass models one has $M_{12} = 0$, one gets

$$M_{11}\ddot{u} + C_{11}\dot{u} + K_{11}u = -M_{11}r \ddot{y}_2 \quad (5)$$

which is the conventional expression used to represent earthquake excitation. The point to note here is that the properties on the matrices on the *lhs* of eq.5 are those of the system with restraints at the prescribed coordinates. This means that if only horizontal motion is used to define the input, the properties that a system identification algorithm obtains include the flexibility and dissipation at the soil structure interface in all DOF, other than horizontal translation. For familiarity in the subsequent treatment we drop the subscripts in eq.5 and replace \ddot{y}_2 by the more commonly used \ddot{x}_g , namely, we use

$$M \ddot{u} + C \dot{u} + K u = -M r \ddot{x}_g \quad (6)$$

where, for 2D single component input r is a vector of ones.

Damping Ratio

Let the *rhs* of eq.6 equal zero, namely

$$M\ddot{u} + C\dot{u} + Ku = 0 \quad (7)$$

the solution to eq.7 is of the form $u(t) = \sum \alpha_i \psi_i e^{s_i t}$ and one finds, by substitution that

$$\left[M s_i^2 + C s_i + K \right] \psi_i = 0 \quad (8)$$

where α_i 's are scalars. The values of s_i 's that satisfy the equation are complex and come in complex conjugate pairs. Writing the solution in terms of its real and its imaginary part, calling on Euler's identity, and replacing s by the value at the solution, λ , one finds that

$$u(t) = \sum \alpha_i \psi_i e^{\lambda_{ir}t} (\cos(\lambda_{ii}t) + i \sin(\lambda_{ii}t)) \quad (9)$$

which shows that the rate of decay of the free vibration is determined by the real part of the eigenvalue and the vibration frequency by the imaginary. The definition of damping ratio, which does not require that the damping be classically distributed, is

$$\xi = \frac{-\lambda_R}{|\lambda|} \quad (10)$$

Eq.10 allows for a simple appreciation of why it is difficult to identify damping ratios with low variance. Namely, let the true pole for a given mode be a point in the complex plane and let there be a region around the pole where, due to noise, the identification algorithm places the pole. Assume the region of uncertainty around the pole is a circle of radius r , where r is a fraction of

the pole magnitude, say $r = \alpha|\lambda|$. Noting that the magnitude of the pole is an estimate of the undamped frequency (exact for classical damping) and recognizing that α is small, one concludes that the variability in frequency is small. The estimation of damping, however, which is given by eq.10, can experience much larger variations. In fact, examination of the geometry shows that the percent error in the frequency is essentially equal to α while the damping ratio, within the uncertainty circle, ranges from the true value to plus or minus α . Let α be 0.02, for example, in this case the frequency error is no more than 2% but the damping ratio can be over or under estimated by 0.02. If the true damping is 5%, one gets values as large as 7% and as low as 3%. To determine if the circular assumption for the uncertainty region is reasonable, we carried out a Monte Carlo study where a system was identified 1000 times using random realizations of the noise. As can be seen from fig.1, which shows results for the first and the second pole, the circular premise is not unreasonable.

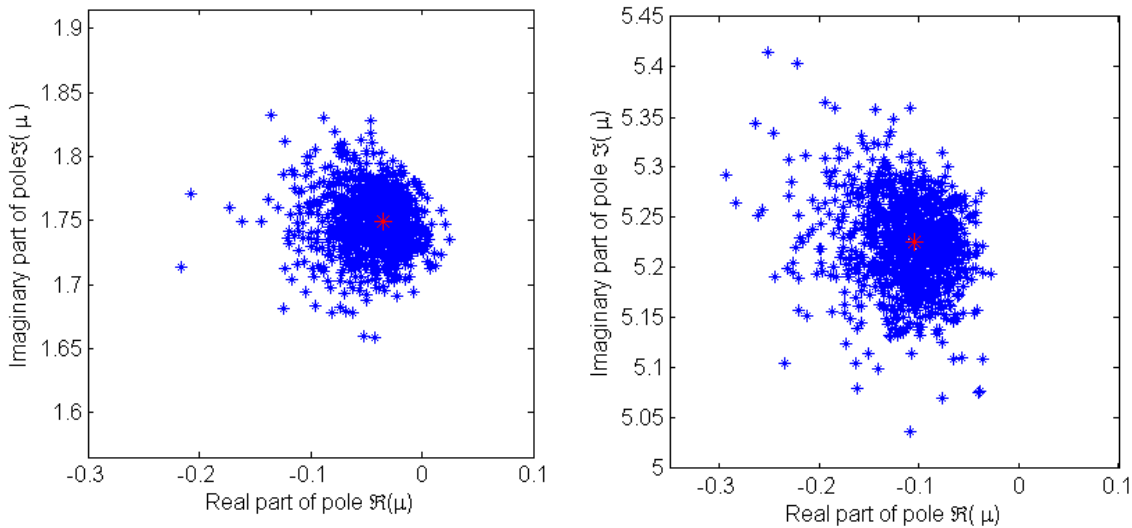


Figure 1. Uncertainty of the real part vs. the imaginary part of the 1st pole and 2nd pole in a 10-DOF system identified using white excitation and 5% additive noise.

Some Proposed Damping Predictors

Predictors for damping in buildings have been proposed through the years and some are summarized next:

Table 1. Damping Predictors

Expression	Source
$\zeta_1 = 0.01f_1 + 10^{\sqrt{D}/2} x / H$	Jeary (1986)
$\zeta_1 = 0.013f_1$ (Steel) $\zeta_1 = 0.014f_1$ (RC)	Satake et al. (2003)
$\zeta_1 = 1.945 + 0.195T_1^{-3.779}$	Zhang and Cho (2009)
$\zeta_1 = 0.013f_1 + 0.0029$ (Steel)	Sasaki (1998)
$\zeta_1 = 0.014f_1 + 470 \frac{x}{H} - 0.0018$ (Steel) $\zeta_1 = 0.013f_1 + 470 \frac{x}{H} + 0.0029$ (RC)	Satake (2003)
$\zeta_1 = \frac{\alpha}{f_1} + \beta f_1 + \gamma \left(\frac{x}{H} \right)$ $\alpha = 0.0072, \beta = 0.0070$ (RC) $\alpha = 0.0032, \beta = 0.0078$ (Steel)	Lagomarsino (1993)
For higher modes damping ratios: $\zeta_n = (1.3 \sim 1.4)h_{n-1}$ (Steel) $\zeta_n = 1.4h_{n-1}$ (RC) $\zeta_n = (1.7 \sim 1.8)h_{n-1}$ (SRC)	Satake et al. (2003)

Discussion

Inspection of the expressions in Table 1 shows that the damping ratio tends to increase with frequency and, although only noted in some of the expressions, that it also tends to increase with amplitude. Justification for correlation with amplitude is evident, since some energy dissipating mechanisms “turn on” only when the amplitude crosses some threshold, but the rational for the correlation with frequency is less apparent. We contend here that the causal connection may not be with frequency but with some measure of the size of the interface between the structure and the ground. Another item worth commenting on is the issue of how the damping ratios in higher modes compare to that of the first mode. In this regard Satake (2003) has postulated, based on a trend observed in the first few modes, that the expected value of the damping ratio is higher in the modes above the fundamental. The assertion is consistent with the idea that damping increases with frequency but our contention is that the observation derives from the effectiveness of the mode shape in activating the dissipation mechanism. To illustrate, we formulated a 6-story one bay model where the damping is assumed to come from dashpots of equal magnitude located at each of the connections between beams and columns and computed the equivalent modal damping for the six modes. Results for the case where the behavior is dominated by frame action (relatively rigid beams) and where flexure dominates (relatively flexible beams) are depicted in fig.2. As can be seen, the damping increases in the early modes (magnitude depending on the relative beam-column stiffness) but eventually decreases, as the joint rotations for sufficiently high modes (due to the wavy nature of the mode) are small. It is interesting that the results for the shear type behavior are (in this case at least) in qualitative agreement with the empirical result proposed by Satake for increases from the 1st to 2nd and the 2nd to 3rd mode.

Sensitivity of Identified Damping to Nonlinear Response

While an increase in damping is expected when the amplitude grows, the effect is not as large as one may anticipate. Support for the contention is found in the short duration over which the nonlinearity is activated for earthquake input. To illustrate, the identified frequencies and equivalent damping of a SDOF with a frequency of 1 Hz and 5% viscous damping were obtained from identification for three different response levels using the Whittier ground motion. The first level is linear and is used to confirm that the ID is able to identify the correct model. The other two correspond to nominal displacement ductility levels of 2 and 4. The identified damping values are {5, 5.82, and 8.4} percent and the identified frequencies are {1, 0.99, and 0.98} hertz respectively. The increase in damping, especially at ductility 2 is very modest. Plots of the resulting force vs. drift are depicted in fig.3.

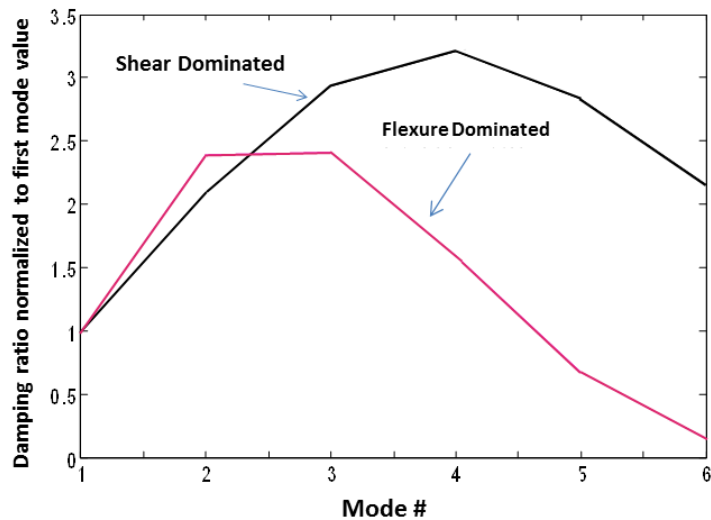


Figure 2. Ratio of damping between various modes in a 6-story model with dissipation simulated with dashpots at the beam-column joints.

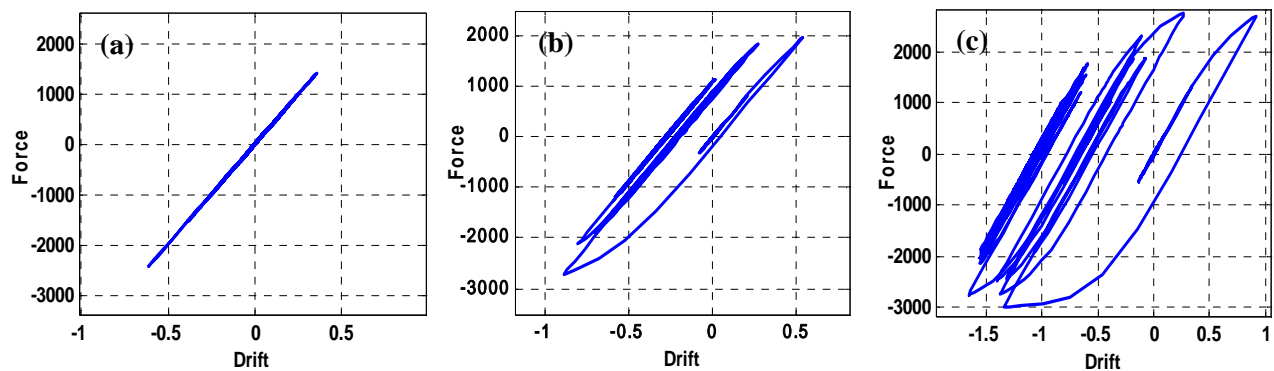


Figure 3. Force vs. drift for three response levels (a)-(c)

Uncertainty in Damping Estimation

This section presents some discussion on the estimation of damping from the perspective of the “information content” of a parameter in available data. It is shown that for conditions that are typical the coefficient of variation of damping ratios can be more than 50 times higher than that of frequencies. Similar results on the identification of ARMA models have been reported in Gersch (1974).

The Cramér-Rao Lower Bound and the Fisher Information

The accuracy with which any parameter can be estimated from noisy data is limited by the amount of information on the parameter that is contained in the data. For any distribution of the noise affecting the input and the output, the lower bound to the covariance Σ that a parameter estimator can have is known as the *Cramér-Rao Lower Bound* (CRLB). The CLRB depends only on the statistical distribution of the noise and on the sensitivity of the data to the parameter. The inverse of the CRLB is known as the *Fisher Information* (FI), which indicates “how much information” on the parameter is contained in the data set. Technically, the FI is defined as

$$I(\theta) = \mathbf{E} \left(\frac{\partial}{\partial \theta} \log f(Y | \theta) \right)^2 \quad (11)$$

where $f(Y | \theta)$ is the probability density function of the observed data Y given the parameter θ . If the sensitivity of the likelihood of the noisy data to changes in the parameter is high, then the derivative in eq.11 is large and so is $I(\theta)$. In practice, the likelihood function $f(Y | \theta)$ is in general unknown so other quantities derived from the data are used. For example, if the data can be used to generate a vector X that is normally distributed having a mean that depends on the parameters, $\gamma(\theta)$, and a covariance Σ , the FI of the parameter θ contained in X can be obtained as

$$I(\theta) = \mathbf{J}(\theta)^T \Sigma^{-1} \mathbf{J}(\theta) \quad \text{where} \quad \mathbf{J}(\theta) = \frac{\partial \gamma}{\partial \theta}. \quad (12)$$

Denoting Σ_λ as the covariance of the real and imaginary part of a pole, the FI of the frequency and the damping follows from eq.12 as

$$I(\xi, f) = \mathbf{J}_{\xi, f}^T \Sigma_\lambda^{-1} \mathbf{J}_{\xi, f} \quad (13)$$

where the sensitivity of the pole with respect to damping ratio and frequency is given by

$$\mathbf{J}_{\xi, f} = \frac{\partial(\Re(\lambda), \Im(\lambda))}{\partial(\xi, f)} = 2\pi \begin{bmatrix} -f & -\xi \\ -f\xi(1-\xi^2)^{-\frac{1}{2}} & \sqrt{1-\xi^2} \end{bmatrix}. \quad (14)$$

Due to the relation between the FI and the CRLB, an analytical relationship between the coefficients of variation of damping and frequency can be obtained from eq.14. This relation shows that the ratio depends only on the damping ratio. Assuming that the uncertainty region around the complex poles is circular, as depicted in the Monte-Carlo simulation in fig.1, the ratios between the coefficients of variation are shown in fig.4. As can be seen, the uncertainty on the damping ratios is around 50 times higher than that for the frequencies at $\xi = 0.02$, and the ratio is near 25 for $\xi = 0.05$.

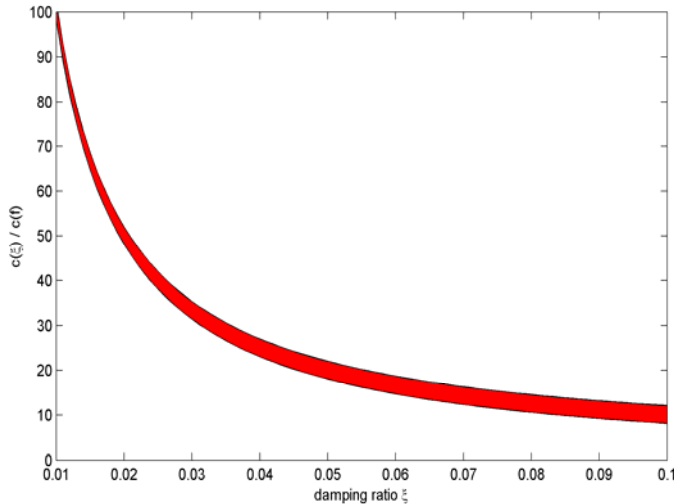


Figure 4. Range of the ratio of the coefficient of variation of damping and frequency when the uncertainty region around the pole is circular

Regression Analysis

Linear Regression

In a first step we considered fitting the damping values to a linear expression using a single regressor, x, namely

$$\xi = \alpha_0 + \alpha_1 x \quad (15)$$

where x is taken as either: a) identified frequency (f), b) building height (H), c) spectral acceleration (SA), d) spectral velocity (SV), e) spectral displacement (SD), f) peak ground acceleration (PGA), g) peak ground velocity (PGV) or h) peak ground displacement (PGD) or their inverses. For each regression, the coefficient of determination was computed. This coefficient is defined as

$$R^2 = 1 - \frac{\sum_i (y_i - \bar{y})^2}{\sum_i (y_i - f_i)^2} \quad (16)$$

where y_i is the identified value, \bar{y} is the mean of the identified results and f_i is the prediction given by the regression equation. The regression was carried out for the first mode damping ratio ζ_1 for steel, concrete, masonry, and wood buildings. When the mode considered is dominated by translation in one direction, the ground motion in this direction was used to compute the ground motion parameters. When the mode is strongly coupled, or torsional, we used the average of the ground motion parameters for the two directions. In the case of steel buildings the best correlation was found with building height and the results are depicted in fig.5. The results for concrete, masonry and wood, showing the correlation with height and the correlation that led to the highest R value are shown in fig.6 (a)-(f).

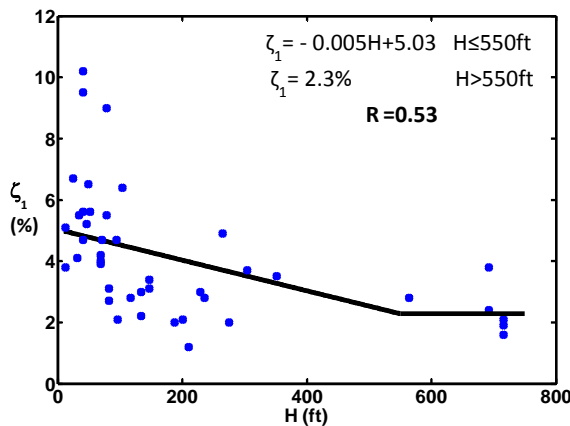


Figure 5. Linear regression for first mode damping ratio vs. building height - Steel buildings

Multivariate Regression

To investigate whether using more than one regressor could lead to major improvements, we looked at the use Artificial Neural Networks (ANN). The idea was not to propose an ANN to predict damping values but, if a simple network gave a notable improvement in the correlations, then it should be possible to extract the nonlinear relation of the network and a simplified expression perhaps could be formulated. To gain some appreciation of how the ANN performed and to gain some confidence in the extraction of the function, we first applied the methodology using a network having one input plus one hidden layer with two neurons. The results for concrete buildings is shown in fig.7, where the equation identified by the network proved to be

$$\zeta_1 = -0.37 \tanh\left(\frac{-3.7}{H} - 0.39\right) - 1.07 \tanh\left(\frac{-8.25}{H} - 9.09\right) - 1.04 \quad (17)$$

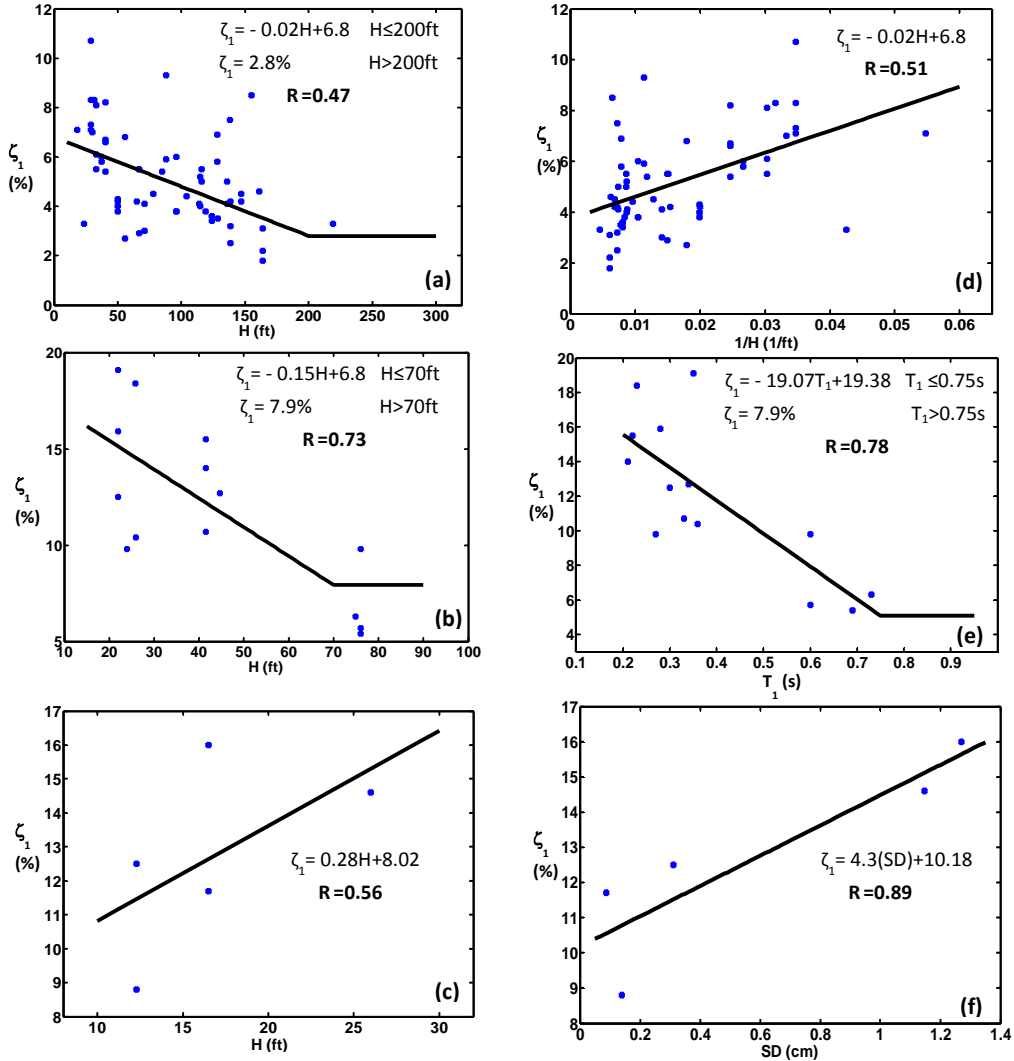


Figure 6. Linear regression for first mode damping ratio vs. building height and best linear regression for concrete (a) & (d), masonry (b) & (e), and wood (c) & (f) buildings respectively.

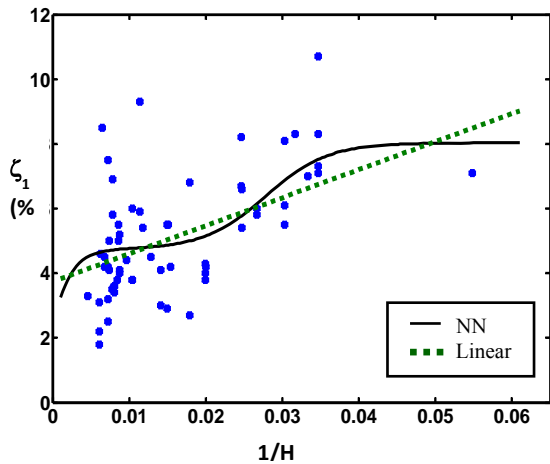


Figure 7. Non-linear regression using ANN for concrete buildings

Needless to say, there is no justification for recommending the complicated expression in eq.17, since the result is entirely dependent of the particular data set considered. Having established that the ANN was working properly we tried it with the same configuration but using two inputs. Table 2 shows the best R values obtained for each building type using one and two regressors as well as the linear regression result. In the two regressor case, the first regressor is either frequency or height or its reciprocal and the second regressor is any of the ground motion related parameters. Although the two-input ANN offered the highest R values, as expected, the improvements over the single input ANN are modest and it was concluded that there was no good reason to pursue it, given the available data.

Table 2. Summary of R values for the regression analysis

	R ANN 2 par	R ANN 1 par	R Linear
Steel	0.79	0.72	0.53
Concrete	0.68	0.64	0.51
Masonry	0.93	0.81	0.78

Conclusions

The analytical investigations show that damping ratios identified from earthquake records are realizations from a distribution with high variance. The reason for the high variance can be traced to the low sensitivity of the transient response to the damping but it can also be visualized from the pole location in the complex plane and the distribution of the uncertainty. In this regard the paper shows that the coefficient of variation of damping estimates are 25 to 50 times larger than the coefficient of variation of frequency estimates. The results of the present study are in agreement with previous results which indicate that the damping ratio increases with frequency. It is speculated here, however, that the causal relationship may be with the relative importance of dissipation through the soil-structure interface and not with frequency per se. The paper suggests that the relation between the damping of higher modes and the first one is likely governed by the efficiency with which the mode shape activates the dissipation mechanism. It was found that predictive equations more complex than linear regression with a single parameter could not be justified, given the data. All and all the results show that damping in steel buildings is larger than the 2% that is typically assigned while the widely used 5% is reasonable for concrete, if a single value is to be used.

Acknowledgements

The research reported in this paper was carried out with support from the California Strong Motion Instrumentation Program (CSMIP) through standard agreement 1010-934. This support is gratefully acknowledged.

Appendix A – Identification

Time domain algorithms are typically based on an indirect approach. Namely, a model mapping the sampled input and the sampled output is obtained and then it is converted to continuous time. The postulated model in sampled time has the form

$$x(k+1) = A_d x(k) + B_d \ddot{x}_g(k) \quad (a.1)$$

where the measurements are given by

$$\ddot{y}(k) = C x(k) \quad (a.2)$$

The procedure begins by noting that for the model in eq.a.1 the output is related to the input as

$$y(k) = \sum_{j=1}^k Y_j \ddot{x}_g(k-j) \quad (a.3)$$

where Y_j , known as a Markov Parameter (MP) is given by

$$Y_j = C A_d^{j-1} B_d \quad (a.4)$$

Once the MP are obtained from eq.a.3, the next task is to untangle the matrices $\{A_d, B_d, C\}$ from the triple product. This is done by defining the Hankel matrix H_k as

$$H_k = \begin{bmatrix} Y_{k+1} & Y_{k+2} & \cdots & Y_{k+\beta} \\ Y_{k+2} & Y_{k+3} & \cdots & Y_{k+\beta} \\ \vdots & \vdots & \vdots & \vdots \\ Y_{k+\alpha} & . & \cdots & Y_{k+\beta+\alpha-1} \end{bmatrix} \quad (a.5)$$

where α and β are user defined parameters and noting that with

$$P_\alpha = \begin{bmatrix} C_d \\ C_d A_d \\ \vdots \\ C_d A_d^{\alpha-1} \end{bmatrix} \quad (a.6)$$

and

$$Q_\beta = [B_d \quad A_d B_d \quad A_d^2 B_d \quad \cdots \quad A_d^{\beta-1} B_d] \quad (a.7)$$

$$H_k = P_\alpha A_d^k Q_\beta \quad (a.8)$$

so it follows that H_0

$$H_0 = P_\alpha Q_\beta \quad (a.9)$$

one then performs a singular value decomposition of H_0 , namely

$$H_0 = R \Sigma S^T \quad (\text{a.10})$$

and after retaining only the N most important singular values, has

$$H_0 = R_N \Sigma_N S_N^T \quad (\text{a.11})$$

where R_N contains the first N columns of R, S_N the first N columns of S and Σ_N is the diagonal matrix having the N significant singular values. Splitting the diagonal singular value matrix into the product of two matrices (E_1 and E_2)

$$E_1 E_2 = \Sigma_N \quad (\text{a.12})$$

gives

$$H_0 = (R_N E_1)(E_2 S_N^T) \quad (\text{a.13})$$

and one can then take

$$P_\alpha = R_N E_1 \quad (\text{a.14})$$

$$Q_\beta = E_2 S_N^T \quad (\text{a.15})$$

from where, given the definitions in eq.'s a.6 and a.7 one has that

- The first m rows of P_α provide a realization for C.
- The first r columns of Q_β provide a realization for B_d .

The matrix A_d can be obtained from the block Hankel matrix for $k = 1$, namely, given that

$$H_1 = P_\alpha A_d Q_\beta = R_N E_1 A_d E_2 S_N^T \quad (\text{a.16})$$

and the fact that R_N and S_N are orthonormal one gets

$$A_d = E_1^{-1} R_N^T H_1 S_N E_2^{-1} \quad (\text{a.17})$$

Discrete to Continuous Transfer

Once the sampled time model is available its conversion to continuous time follows as (Bernal 2006)

$$A_c = \frac{1}{\Delta t} \ln(A_d) \quad (\text{a.18})$$

$$B_c = \frac{1}{\Delta t} A_d^{-1} B_d \quad (\text{a.19})$$

$$C_c = C \quad (\text{a.20})$$

The damping ratios are obtained as the real part of the eigenvalues of A_c divided by their magnitude.

Appendix B - Data

Table B.1. Data for regression analysis

Station #	Earthquake	$\zeta_1(\%)$	T _{1(s)}	H(ft)	SA(g)	SV(cm/s)	SD(cm)	PGA(g)	PGV(cm/s)	PGD(cm)
58262	Loma Prieta	3.3	0.27	23.5	0.195	8.33	0.362	0.108	12.77	2.38
47391	Morgan Hill 84	7	0.59	30	0.129	11.87	1.111	0.066	6.52	3.05
57502	LomaPrieta	8.3	0.23	31.6	0.299	10.95	0.409	0.109	27.96	19.67
58334	Loma Prieta	6.4	0.20	NA*	0.161	5.05	0.161	0.075	8.29	1.40
58334	Berkeley 71667366	5.5	0.18	NA	0.133	3.78	0.109	0.040	1.17	0.06
58334	Piedmont	4.9	0.18	NA	0.135	3.80	0.109	0.068	2.75	0.22
58348	Loma Prieta	8.2	0.45	40.6	0.222	15.60	1.119	0.117	19.98	5.85
58348	Lafayette	6.7	0.42	40.6	0.063	4.11	0.272	0.055	2.12	0.17
23511	Whittier	5.4	0.29	40.5	0.110	4.89	0.222	0.046	2.04	0.14
23511	Chinohills	6.6	0.34	40.5	0.232	12.17	0.650	0.130	11.94	2.30
23495	Big Bear	7.3	0.52	28.8	0.369	29.72	2.438	0.174	12.40	1.92
23495	Landers	10.7	0.45	28.8	0.272	19.14	1.372	0.105	11.29	3.21
23495	Palm Springs	7.1	0.40	28.8	0.137	8.54	0.544	0.042	3.62	0.55
23495	SanBernardino	8.3	0.43	28.8	0.048	3.25	0.225	0.059	2.30	0.16
58263	Loma Prieta	4	0.15	NA	0.139	3.17	0.074	0.071	10.85	4.39
58503	Loma Prieta	6	0.29	37.5	0.204	9.17	0.419	0.102	14.51	2.25
58503	Elcerrito	5.8	0.25	37.5	0.103	4.06	0.164	0.059	2.01	0.09
23622	Landers	7.1	0.24	18.25	0.164	6.16	0.235	0.090	14.40	8.09
25213	Santa Barbara	5.5	0.32	33	1.043	52.15	2.660	0.378	34.26	5.47
58235	Morgan Hill 84	6.1	0.25	33	0.201	7.73	0.302	0.060	4.23	0.89
58235	Loma Prieta	8.1	0.30	33	0.728	33.71	1.592	0.315	36.57	7.34
58196	Lafayette	6.8	0.33	55.8	0.115	6.01	0.319	0.056	2.40	0.13
58196	Piedmont	2.7	0.33	55.8	0.128	6.66	0.353	0.061	2.42	0.23
89770	Ferndale 2007	4.1	0.37	NA	0.664	38.69	2.298	0.231	21.29	4.86
58488	Loma Prieta	4.2	0.25	50	0.136	5.31	0.211	0.052	4.21	0.85
58462	Loma Prieta	5.4	0.96	84.8	0.106	15.86	2.427	0.103	10.41	2.01
14311	Whittier	3	0.34	71	0.243	12.90	0.699	0.094	6.15	0.72
14311	Chinohills	4.1	0.32	71	0.087	4.38	0.225	0.066	7.66	1.43
24463	Whittier	3.8	1.43	119	0.091	20.24	4.602	0.131	12.73	1.95
12284	Borrego Springs Jul2010	4.3	0.68	50.2	0.044	4.67	0.503	0.053	2.18	0.31
12284	Calexico Apr2010	4	0.69	50.2	0.104	11.22	1.231	0.052	4.29	3.16
12284	Palm Springs	3.8	0.60	50.2	0.082	7.71	0.739	0.090	8.06	2.40
23285	San Bernardino	2.9	0.52	67	0.012	1.01	0.084	0.059	1.35	0.07
24468	Northridge	4	1.59	114.8	0.082	20.29	5.126	0.117	8.69	1.42
24468	Whittier	5.2	1.54	114.8	0.113	27.05	6.624	0.324	20.07	2.37
24579	Landers	5.8	1.43	128	0.053	11.80	2.683	0.038	6.76	4.15
24579	Northridge	6.9	1.52	128	0.092	21.67	5.225	0.150	13.43	2.90

SMIP12 Seminar Proceedings

Station #	Earthquake	$\zeta_1(\%)$	T _{1(s)}	H(ft)	SA(g)	SV(cm/s)	SD(cm)	PGA(g)	PGV(cm/s)	PGD(cm)
47459	Loma Prieta	5.5	0.35	66.3	0.953	52.58	2.957	0.359	54.87	18.23
58479	Loma Prieta	4.2	0.34	65	0.164	8.65	0.465	0.070	15.10	4.21
58490	Loma Prieta	4.5	1.00	78	0.216	33.63	5.353	0.114	16.16	2.66
24655	Northridge	5.5	0.52	67	0.441	35.48	2.911	0.286	19.08	4.44
24571	Landers	4.1	2.00	136	0.044	13.80	4.392	0.036	6.37	2.03
24571	Northridge	4.1	2.13	136	0.024	8.08	2.736	0.156	8.92	1.28
24571	Sierra Madre	5	1.96	136	0.030	9.03	2.819	0.104	7.54	0.75
58394	Loma Prieta	4.4	1.72	104	0.136	36.50	10.017	0.125	14.95	3.31
24385	Sierra Madre	5.9	0.54	88	0.103	8.66	0.741	0.074	4.62	0.67
24385	Whittier	9.3	0.55	88	0.241	20.67	1.807	0.209	10.97	1.00
57355	Morgan Hill 84	3.6	0.91	124	0.144	20.48	2.963	0.058	12.28	3.38
57355	Alum Rock	3.4	1.04	124	0.063	10.26	1.700	0.071	5.81	1.14
57355	Loma Prieta	3.6	1.01	124	0.133	20.92	3.363	0.086	18.11	9.93
57356	Morgan Hill 84	3.8	0.61	96	0.139	13.17	1.270	0.054	12.10	2.84
57356	Loma Prieta	6	0.67	96	0.185	19.40	2.072	0.093	16.55	7.26
57356	Alum Rock	3.8	0.73	96	0.088	10.05	1.167	0.114	7.98	1.12
24322	Northridge	1.8	3.13	164	0.064	31.41	15.622	0.832	60.65	13.55
24322	Whittier	3.1	2.50	164	0.008	3.31	1.315	0.257	8.11	0.49
24322	Chinohills	2.2	1.54	164	0.015	3.66	0.896	0.073	3.39	0.29
58364	Loma Prieta	3.5	0.80	128.5	0.103	12.92	1.645	0.047	7.57	1.35
14578	Chinohills	5.5	1.25	116	0.050	9.73	1.936	0.100	9.11	1.04
14578	Northridge	5	1.19	116	0.034	6.29	1.192	0.069	5.47	1.36
24601	Northridge	4.2	1.16	138.7	0.029	5.24	0.970	0.021	1.66	0.58
24601	Sierra Madre	2.5	1.01	138.7	0.068	10.67	1.715	0.068	5.24	0.71
24601	Landers	3.2	1.06	138.7	0.102	16.94	2.868	0.043	7.29	6.53
24581	Chinohills	8.5	1.79	155	0.010	2.68	0.763	0.059	4.09	0.35
24236	Whittier	7.5	1.85	138.3	0.041	11.98	3.532	0.118	9.46	1.37
58483	Loma Prieta	3.3	2.44	219	0.057	21.67	8.414	0.123	17.09	4.31
13589	Landers	4.5	0.82	146.9	0.124	15.86	2.069	0.041	6.31	2.84
13589	Northridge	4.2	0.85	146.9	0.092	12.16	1.640	0.076	5.56	1.74
58639	Piedmont	4.1	0.81	114	0.012	1.52	0.195	0.031	1.55	0.11
24680	Chinohills	4.6	1.47	161	0.011	2.62	0.613	0.027	2.01	0.25
58496	Loma Prieta	6.7	0.33	25.2	0.228	11.67	0.609	0.102	6.41	0.919
24198	Chinohills	5.5	0.68	34	0.077	8.28	0.903	0.074	5.76	0.628
01699	Calexico May2010	5.1	0.16	12.4	0.149	3.62	0.090	0.059	2.54	0.216
01699	Ocotillo Jun2010	3.8	0.15	12.4	0.142	3.39	0.082	0.062	3.95	1.351
54331	Mammoth Lakes	4.1	0.17	31.9	0.171	4.59	0.126	0.124	3.85	0.215

SMIP12 Seminar Proceedings

Station #	Earthquake	$\zeta_1(\%)$	T _{1(s)}	H(ft)	SA(g)	SV(cm/s)	SD(cm)	PGA(g)	PGV(cm/s)	PGD(cm)
58506	Loma Prieta	5.2	0.71	46.2	0.282	31.22	3.524	0.110	20.35	4.730
23516	Landers	10.2	0.56	41.3	0.205	17.74	1.568	0.082	15.07	7.640
23516	Chinohills	9.5	0.49	41.3	0.161	12.28	0.958	0.069	4.78	0.419
23516	San Bernardino	4.7	0.56	41.3	0.125	10.85	0.959	0.102	7.30	0.467
57562	Loma Prieta	6.5	0.74	49.5	0.320	36.72	4.297	0.177	18.47	6.665
24104	Chatsworth	5.6	0.46	41	0.161	11.64	0.858	0.084	6.12	0.365
24370	Whittier	2.7	1.28	82.5	0.088	17.66	3.604	0.226	12.51	1.270
24370	Sierra Madre	3.1	1.28	82.5	0.052	10.38	2.118	0.124	5.84	0.782
24609	Landers	9	0.74	78.5	0.153	17.57	2.057	0.083	10.40	5.070
24609	Northridge	5.5	0.75	78.5	0.083	9.75	1.167	0.056	9.29	2.720
14323	Whittier	6.4	1.39	104	0.035	7.63	1.688	0.073	8.53	1.163
24652	Northridge	4.7	0.26	71.5	0.344	13.89	0.573	0.205	14.04	3.069
23481	Landers	4.7	1.59	94.4	0.038	9.29	2.347	0.059	5.86	2.279
23515	Landers	2.8	2.00	117.6	0.091	28.47	9.063	0.088	14.95	7.451
23634	BigBear	4.2	0.50	69	0.104	8.01	0.631	0.062	5.04	1.471
23634	Landers	3.9	0.49	69	0.175	13.45	1.055	0.080	12.35	6.510
23634	Northridge	4	0.49	69	0.103	7.87	0.611	0.049	4.28	0.724
24248	Chinohills	3.1	0.69	147	0.048	5.19	0.569	0.052	3.16	0.521
24248	Whittier Narrows	3.4	0.65	147	0.010	0.98	0.101	0.051	1.27	0.064
24249	Chinohills	3	0.71	134	0.065	7.16	0.808	0.059	2.91	0.326
24249	Whittier Narrows	2.2	0.68	134	0.010	1.05	0.113	0.045	1.31	0.070
24514	Whittier	2.1	0.34	96	0.184	9.89	0.541	0.057	3.68	0.561
58261	Loma Prieta	5.6	0.69	52.5	0.229	24.62	2.702	0.061	8.61	1.938
14533	Whittier	4.9	1.19	265	0.067	12.48	2.365	0.048	5.73	1.244
14654	Northridge	2	2.08	188	0.046	15.10	5.007	0.128	11.39	3.149
24288	Chinohills	3.5	1.16	351.2	0.045	8.25	1.527	0.067	6.47	1.021
24569	Northridge	2.8	1.18	236	0.119	21.86	4.092	0.137	12.56	3.104
24602	Chinohills	1.9	1.79	716	0.013	3.67	1.044	0.078	6.59	0.925
24602	Landers	2.1	5.88	716	0.017	15.94	14.927	0.121	7.73	4.005
24602	Northridge	1.6	1.85	716	0.071	20.39	6.009	0.159	12.71	2.955
24602	Sierra Madre	1.6	1.72	716	0.027	7.38	2.026	0.113	8.05	0.935
24629	Chinohills	3.8	1.92	692.5	0.010	3.07	0.939	0.065	4.97	0.642
24629	Northridge	2.4	1.85	692.5	0.060	17.38	5.124	0.099	8.42	3.061
24643	Northridge	3.7	0.82	304	0.443	56.66	7.392	0.260	16.18	4.880
57318	Alum Rock	2	2.17	275	0.020	6.95	2.404	0.063	6.09	1.184
57357	Loma Prieta	1.2	2.22	210.6	0.218	75.58	26.730	0.090	21.23	8.584
58354	Loma Prieta	2.1	1.33	201	0.039	8.12	1.724	0.079	6.85	0.795

SMIP12 Seminar Proceedings

Station #	Earthquake	$\zeta_1(\%)$	T _{1(s)}	H(ft)	SA(g)	SV(cm/s)	SD(cm)	PGA(g)	PGV(cm/s)	PGD(cm)
58480	Loma Prieta	3	2.27	229.3	0.034	11.94	4.317	0.161	15.81	2.649
58532	Loma Prieta	2.8	2.17	564	0.159	54.07	18.709	0.203	26.39	7.879
12266	Anza	18.4	0.05	25.8	0.197	1.67	0.014	0.0750	2.510	0.148
14606	Northridge	5.4	0.19	76	0.093	2.70	0.079	0.1100	8.626	1.571
14606	Chinohills	9.8	0.10	76	0.263	4.19	0.068	0.1290	11.922	1.824
14606	Whittier Narrows	5.7	0.18	76	0.023	0.63	0.018	0.2196	6.053	0.221
24517	Landers	10.7	0.09	41.5	0.139	2.03	0.030	0.0536	7.119	3.158
24517	Northridge	15.5	0.06	41.5	0.119	1.20	0.012	0.0555	9.274	2.530
24517	Whittier	14	0.07	41.5	0.133	1.48	0.017	0.0510	2.806	0.176
57476	Loma Prieta	10.4	0.10	26	0.630	9.46	0.145	0.2647	3.599	0.189
58264	Loma Prieta	9.8	0.10	24	0.477	7.60	0.123	0.2081	33.690	14.157
58492	Loma Prieta	6.3	0.16	74.9	0.195	4.82	0.122	0.0582	7.827	2.118
89473	Petrolia	19.1	0.05	22	0.216	1.77	0.015	0.1263	17.767	4.415
89473	Ferndale Jan2010	12.5	0.08	22	0.366	4.57	0.058	0.1414	11.807	2.137
89473	Petrolia Aftershock	15.9	0.06	22	0.482	4.74	0.047	0.1599	12.489	2.330
89494	Ferndale Jan2010	12.7	0.08	44.7	0.565	6.94	0.087	0.2161	22.426	5.183
12759	Anza	12.5	0.08	12.3	0.4334	5.41	0.069	0.2247	10.858	0.923
12759	Borrego Springs Jul2010	8.8	0.11	12.3	0.1933	3.43	0.062	0.0657	4.441	0.785
36695	San Simeon	16	0.06	16.5	1.2786	12.47	0.124	0.4484	30.092	7.341
36695	Atascadero	11.7	0.09	16.5	0.1095	1.46	0.020	0.0562	1.426	0.049
89687	Ferndale Jan2010	14.6	0.07	26	0.5131	5.48	0.060	0.2462	26.074	5.340

*NA: Information is not available on CSMIP website

References

- Bernal, D. (2007) Optimal Discrete to Continuous Transfer for Band Limited Inputs. *Journal of Engineering Mechanics*, 133(12), 1370-1377.
- Gersch, W. (1974). On the achievable accuracy of structural system parameter estimates, *Journal of Sound and Vibration*, 34(1) 63–79.
- Hart, G.C. & Vasudevan R. (1975) Earthquake design of buildings: damping. *Journal of the Structural Division, ASCE 1975*;101(1):11–29.
- Heylen, W., Lammens, S. & Sas, P. (1997) Modal Analysis Theory and Testing. *KUL Press, Leuven*.
- Jeary, A. P. (1986). Damping in tall buildings—A mechanism and a predictor. *Earthquake Eng. Struct. Dyn.*, 14, 733–750.
- Juang, J. (1994) Applied system identification. *Englewood Cliffs, NJ: PTR Prentice Hall, Inc* , 1994.
- Lagomarsino, S. (1993). Forecast models for damping and vibration periods of buildings. *J. Wind. Eng. Ind. Aerodyn.*, 48, 221–239.
- McVerry, G.H. (1979). Frequency Domain Identification of Structural Models from Earthquake Records. *Ph.D. thesis, California Institute of Technology*.
- McVerry, G.H. (1980) Structural identification in the frequency domain from earthquake records. *Earthquake Engineering and Structural Dynamics*, 8:161–80.
- Sasaki, A., Suganuma, S., Suda, K. & Tamura, Y. (1998). “Full-scale database on dynamic properties of buildings—Frequency and amplitude dependencies of buildings.” *Proc., Annual Meeting of the Architectural Institute of Japan (AIJ), Fukuoka, AIJ Japan*, B-2, 379–380.
- Tamura, Y. & Suganuma, S. (1996). Evaluation of amplitude dependent damping and natural frequency of buildings during strong winds. *J. Wind. Eng. Ind. Aerodyn.*, 59, 115–130.
- Van Overschee, P., & De Moor, B. (1996) Subspace identification for linear systems: Theory, implementation, applications. *Kluwer Academic, Boston*.
- Verhaegen & Verdult (2007) Filtering and system identification: An introduction. *Cambridge University Press*.
- Zhang, Z. & Cho, C. (2009) Experimental Study on Damping Ratios of in-situ Buildings. *World Academy of Science, Engineering and Technology*, 26, 614-618.

**CALIBRATING COMPUTER MODELS FOR SEISMIC ANALYSIS:
CASE STUDIES USING INSTRUMENTED BUILDING RECORDS**

Daniel Swensen and Sashi Kunnath

Department of Civil and Environmental Engineering
University of California, Davis

Abstract

Modern performance-based seismic evaluation of buildings calls for nonlinear analysis of the structural system to estimate seismic demands and assess building performance. The availability of new software with expanded capabilities is gradually making it more feasible to conduct fully nonlinear simulations of building systems. However, at present, there are no readily available guidelines to aid a structural engineer in the process of building an appropriate nonlinear model of the system. As an initial step towards developing such guidelines, the suitability of three widely used computer programs (SAP2000, Perform-3D and OpenSEES) for seismic evaluation of buildings is investigated in this project by utilizing response data recorded from instrumented buildings and comparing the performance of different nonlinear models and methods in terms of their predictive abilities and response sensitivity to modeling choices. Preliminary findings from a preliminary set of simulations on a 9-story steel moment frame building are reported in this paper.

Introduction

The development and application of performance-based seismic design and evaluation of buildings has been hindered by the lack of general guidelines for the practicing engineer regarding the effective use of nonlinear analysis in structural design. There are various nonlinear analysis programs in use today, and an even greater number of modeling choices within and between computer programs. It is essential for engineers to understand the nuances of nonlinear modeling so as to construct a reliable simulation model and analyze its seismic behavior.

Recorded motions from building structures provide engineers and researchers with invaluable data to calibrate simulation models of complex three-dimensional structures. The suitability of existing nonlinear tools for seismic evaluation of buildings is investigated in this project by utilizing response data recorded from instrumented buildings and comparing the performance of different nonlinear models and methods in terms of their predictive abilities. The results presented in this paper represent preliminary findings from the first phase of a more comprehensive study involving several steel frame buildings of varying height.

Case Study: 9-Story Steel Moment Frame Building

The building considered in the evaluation is the Aliso Viejo 9-story office building (CSMIP Station No. 13364). This 9-story office building located in Aliso Viejo, California was

designed in 2006 according to the 2001 California Building Code, and constructed in 2008. The building is rectangular in plan with dimensions of approximately 220 ft. x 120 ft. The first floor story height is 17 ft. while the remaining story heights are 13.5 ft. for a total building height of 125 ft. There is a helistop located near the center of the building about 11 ft. above the roof level.



Figure 1: 9-Story office building considered in evaluation (courtesy of CSMIP)

The framing system consists of 3.25" of lightweight concrete over 3" steel deck at the second through the ninth floor levels, and 2.5" of lightweight concrete over 3" steel deck at the roof level. The helistop is 3.5" of normal weight concrete over 3" steel deck. Each level is supported by steel beams and columns. The ASTM designation for the steel beams and columns is A992. Steel columns are supported at ground level by 14" square prestressed precast concrete piles in groups of five or seven piles at each pile cap. The pile caps at the perimeter are tied together by reinforced concrete grade beams, while those at the interior are isolated. Lateral forces are resisted in each direction by steel special moment resisting frames located at the perimeter of the building. The connection used in the moment frames is SSDA's proprietary slotted beam connection. Braced frames resist lateral loading at the helistop level only.

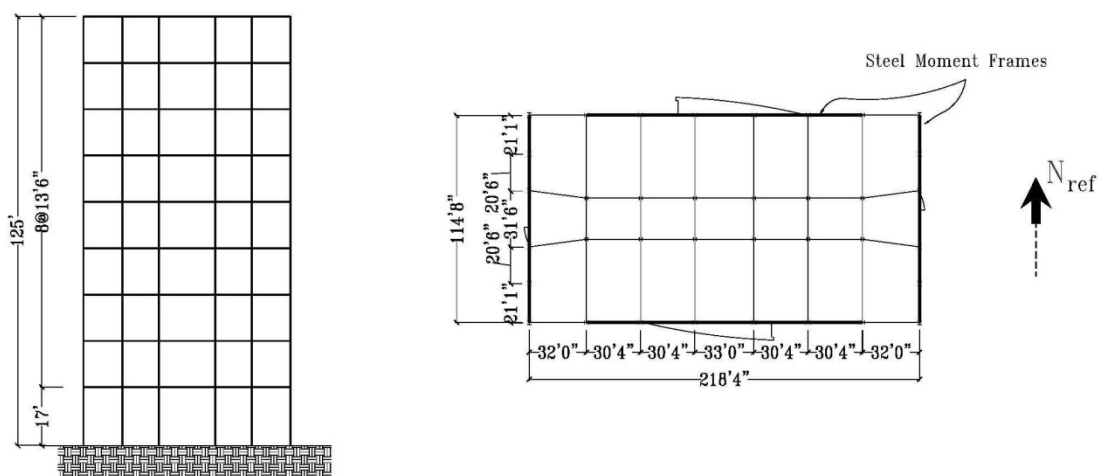


Figure 2: Elevation of typical steel moment frame (N-S Direction) and floor plan of the building

Instrumentation and Recorded Data

This office building was instrumented in 2007 with a total of 15 accelerometers. There are 4 accelerometers located at the ground floor level, 2 accelerometers at the second and fifth floors, 3 accelerometers at the sixth floor and roof, and 1 accelerometer at the ninth floor, as can be seen in Figure 3. The instrumentation of this structure allows for the measurement of the following motions:

1. Ground Floor (foundation): vertical, horizontal in two directions and torsional
2. Second Floor: horizontal in two directions
3. Fifth Floor: horizontal in two directions
4. Sixth Floor: horizontal in two directions and torsional
5. Ninth Floor: horizontal in one direction
6. Roof: horizontal in two directions and torsional

This station has recorded data from two earthquakes: the Chino Hills earthquake of 2008 with a PGA of 0.026g and the Laguna Niguel earthquake of 2012 with a PGA of 0.029g. The noted PGAs are based on the recorded motion at the base of the building.

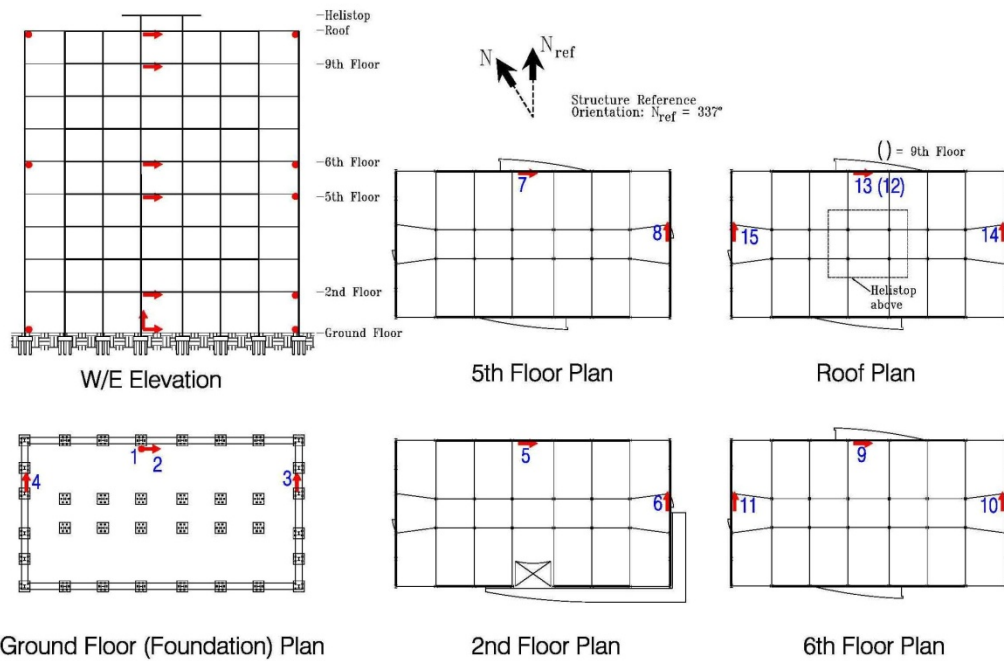


Figure 3: Layout of accelerometers in the building (courtesy of CSMIP)

System Identification Studies

The acceleration time histories recorded during the Chino Hills event were used to generate Fourier amplitude spectra for each instrumented level. At the Ground Floor, Sixth Floor, and Roof levels the average of the transverse accelerometers was used in the generation of the spectra. In this way the torsional modes of vibration were suppressed. The Fourier amplitude spectra were then used to develop the transfer functions which can be seen in Figure 4.

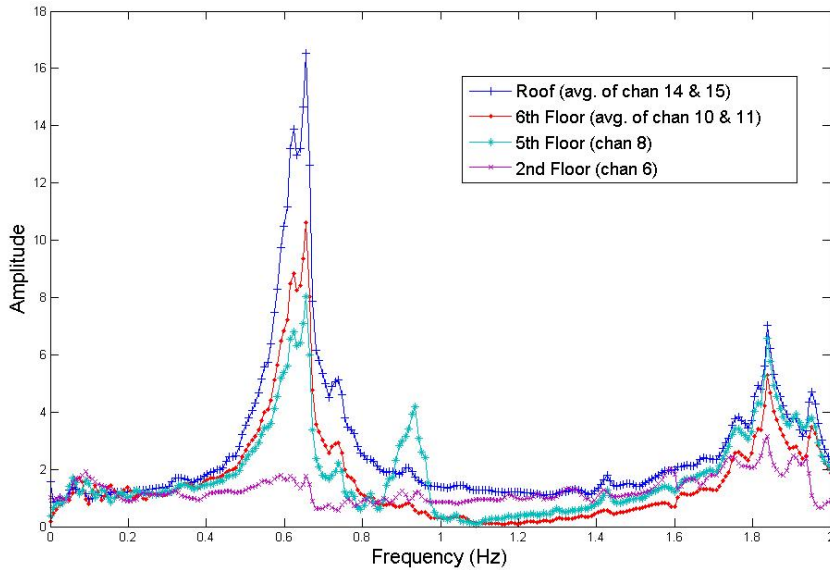


Figure 4: Transfer functions at instrumented levels of the building

The peak marking the first lateral mode of vibration can be seen at approximately 0.63 Hz, corresponding to a fundamental period of vibration of 1.59 seconds. Likewise, the second mode of lateral vibration can be seen at approximately 1.84 Hz, corresponding to a period of 0.54 seconds. In the Fifth Floor transfer function a peak can be seen at approximately 0.94 Hz. This peak corresponds to the first torsional mode of vibration. A similar peak would be seen in the Sixth Floor and Roof level transfer functions if the torsional response had not been suppressed by taking the average of the transverse channels.

Simulation Model of Building and Calibration

Two-dimensional linear models of the building were developed using the following software: SAP2000, Perform-3D, and OpenSEES. A three-dimensional linear model was developed using only the SAP2000 software. The two-dimensional models represent framing for the north-south reference direction of the structure. The details of the development of the models and relevant assumptions are summarized below:

- Centerline dimensions were used (i.e. panel zone were not modeled explicitly)
- All frame elements and connections are linear elastic
- Diaphragms were assumed to be rigid in plane
- Columns were assumed to be fixed at the base
- Moment connections were modeled as rigid, while gravity frame shear tab connections were modeled as partially rigid with rotational stiffness proportional to beam bolt group depth as outlined in Liu and Astaneh-Asl (2000).
- The stiffness resulting from composite action between the beam-slab system was included in the model. A composite moment of inertia was calculated based on the cross-sectional properties of the beam and slab and the moment of inertia of the beam was modified to reflect the increased stiffness. The composite moment of inertia was determined to be approximately three times that of the moment of inertia of the beam.

Only the moment frame beams were modified in this way; the stiffness of the gravity frame beams was left unaltered.

- The mass assigned at each level was estimated based upon the drawings and Table C3-1 (Minimum Design Dead Loads) of ASCE7-05. As there are two identical moment frames at the perimeter in the north-south direction of the building, only one-half of the total mass at each level was assumed to be tributary to the frame model. The seismic mass at the roof level was comprised simply of dead load, whereas at the floor levels additional mass was included to reflect the presence of partitions and some live load.
- The helistop framing was not explicitly modeled but the associated mass was assigned to the roof level nodes.

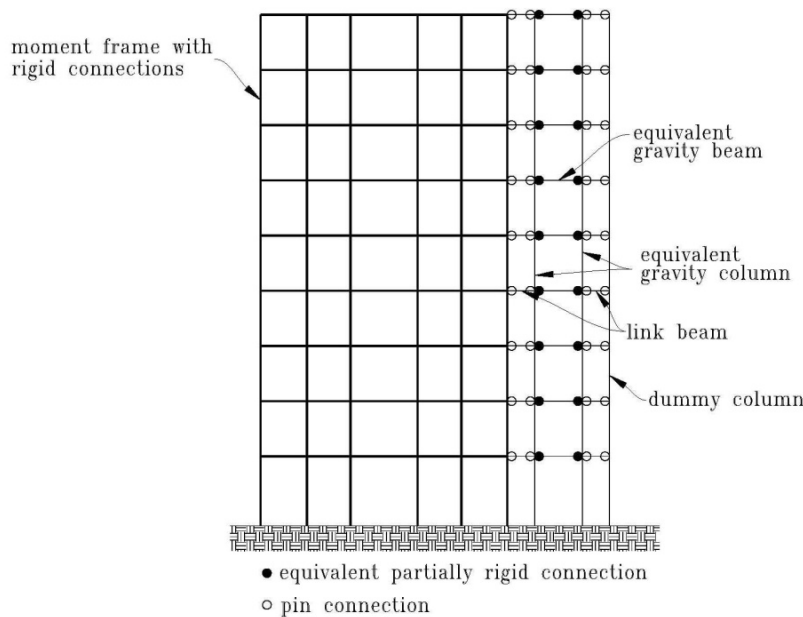


Figure 5: Elevation of two-dimensional model of building with equivalent gravity framing and dummy columns

- An equivalent gravity frame was included in the models in order to capture the stiffness contribution of the gravity framing, as well as to be able to account for any lateral force induced by P-delta effects within the gravity frame system. The cross-sectional area, shear area, and bending stiffness (EI/L) of the modeled gravity columns was made equivalent to that of one-half of the total of the gravity columns at each level. The shear area and bending stiffness of the gravity beams was modeled in a similar manner. The rotational stiffness of the modeled partially rigid beam-to-column connections was made proportional to one-half of the combined rotational stiffness of the gravity frame shear tab connections at each level. The equivalent gravity frame is tied to the moment frame by rigid links with pinned ends at each level.
- Dummy columns were included to account for the additional stiffness required at each level in order to calibrate the model, which additional stiffness represents the combined stiffening effect of those elements of the building not explicitly included in the model (e.g. non-structural components, partition walls, etc.). In order to adjust the stiffness of the dummy columns the moment of inertia of the elements was simply increased or

decreased as required. The dummy columns are tied to the gravity frame by rigid links with pinned ends at each level.

- Gravity loads were applied to the moment frame at each level based upon tributary area of the dead and live load estimates. The gravity loads applied at each level to the equivalent gravity columns are proportional to one-half of the total gravity load minus that which is tributary to the moment frame at each level.
- The models were calibrated to the motions recorded during the Chino Hills earthquake. In order to best match the acceleration and displacement amplitudes the damping was set at 5% of critical for all modes in SAP2000 and Perform-3D. In OpenSEES, Rayleigh damping was used with 5% damping assigned to modes 1 and 3.

Model Validation

The first and second modal periods resulting from the two-dimensional models in SAP2000, Perform-3D, and OpenSEES are shown in Table 2 below. The table also shows the effect of the inclusion of the gravity frame and dummy columns on the modal periods. It can be seen that a significant stiffness contribution was required of the dummy columns in order to lower the periods to the approximate 1.59 seconds for T_1 and 0.54 seconds for T_2 , which were estimated from the transfer functions as described previously.

Table 2: Comparison of modal periods from different computer programs

	Moment Frame Only		Moment Frame + Gravity Frame		Moment Frame + Gravity Frame + Dummy Columns	
	T_1	T_2	T_1	T_2	T_1	T_2
SAP2000	2.08	0.72	2.00	0.69	1.58	0.50
Perform-3D	2.08	0.72	2.00	0.69	1.58	0.50
OpenSEES	2.08	0.72	1.97	0.69	1.56	0.50

Note: All period values are shown in seconds

Using the ratio of the amplitude of the transfer function at each level with the amplitude of the transfer function at the Roof level (at 0.63 Hz and 1.84 Hz), mode shapes can be estimated for the first and second modes of lateral vibration. The estimated mode shapes using the three computer programs is displayed in Figure 6. It can be seen from the figure that the mode shapes computed by each of the three programs match one another almost identically, and that the match to the estimated shapes is very close.

The average of the acceleration time histories recorded in the transverse direction during the Chino Hills earthquake at the Ground Floor level of the building was used as input motion for response history analyses of the two-dimensional linear models constructed in SAP2000, Perform-3D, and OpenSEES. A comparison of the computed acceleration time history response of each model with the actual acceleration response of the building to the Chino Hills earthquake can be seen in Figures 7-9.

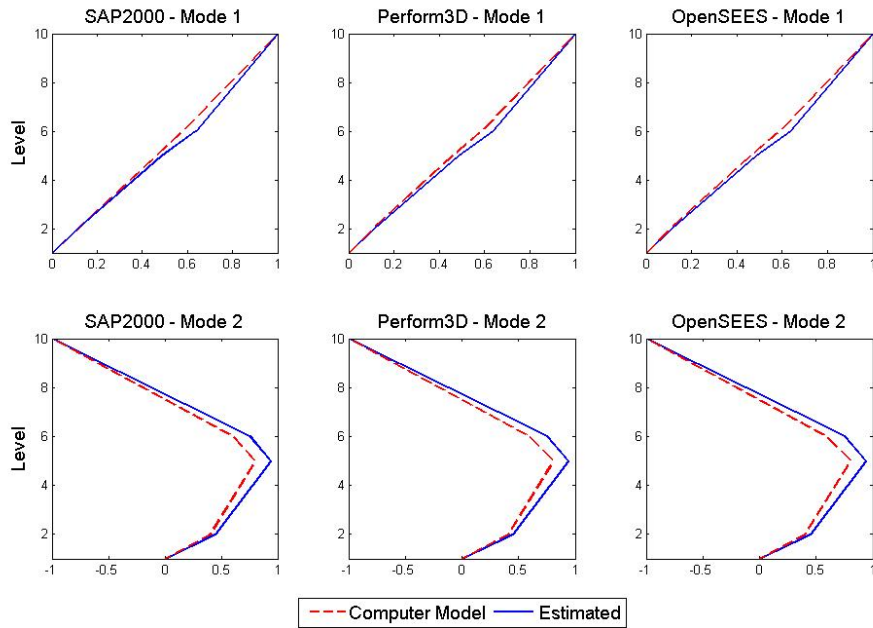


Figure 6: Comparison of computed vs. estimated shapes of first and second modes of vibration of the Aliso Viejo 9-story office building

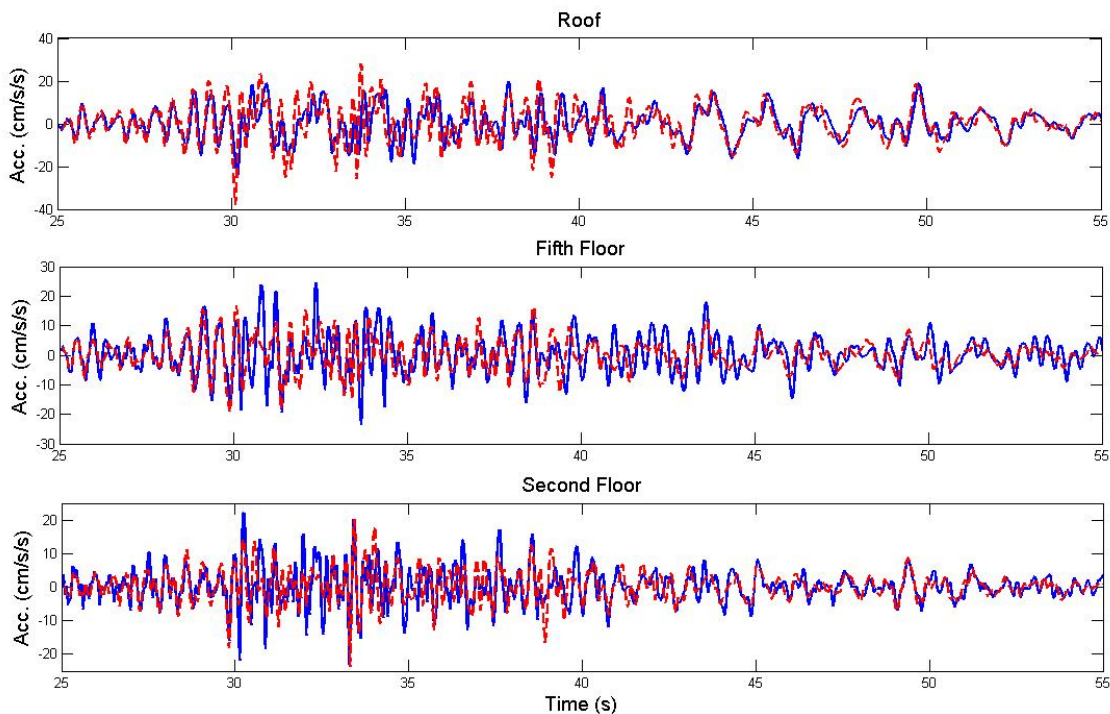


Figure 7: Comparison of computed (SAP2000) vs. actual acceleration time histories at selected instrumented levels of the building

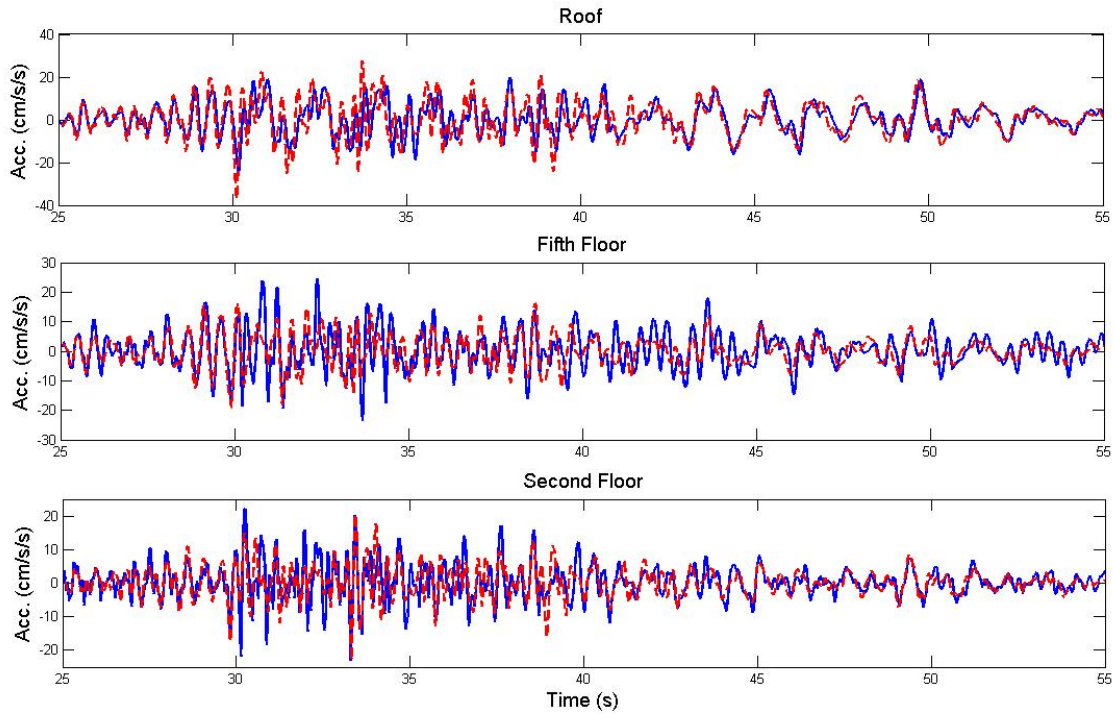


Figure 8: Comparison of computed (Perform-3D) vs. actual acceleration time histories at selected instrumented levels of the building

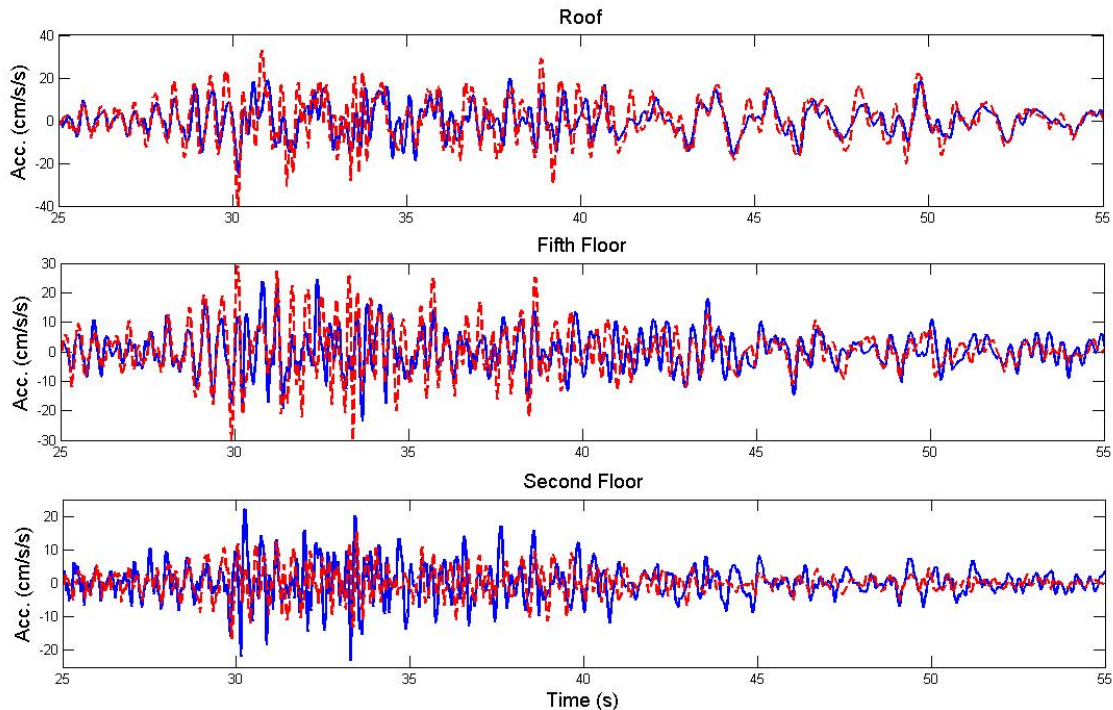


Figure 9: Comparison of computed (OpenSEES) vs. actual acceleration time histories at selected instrumented levels of the building

A comparison of the computed relative displacement time history response of each model with the computed relative displacement response of the building to the Chino Hills earthquake can be seen in Figures 10-12.

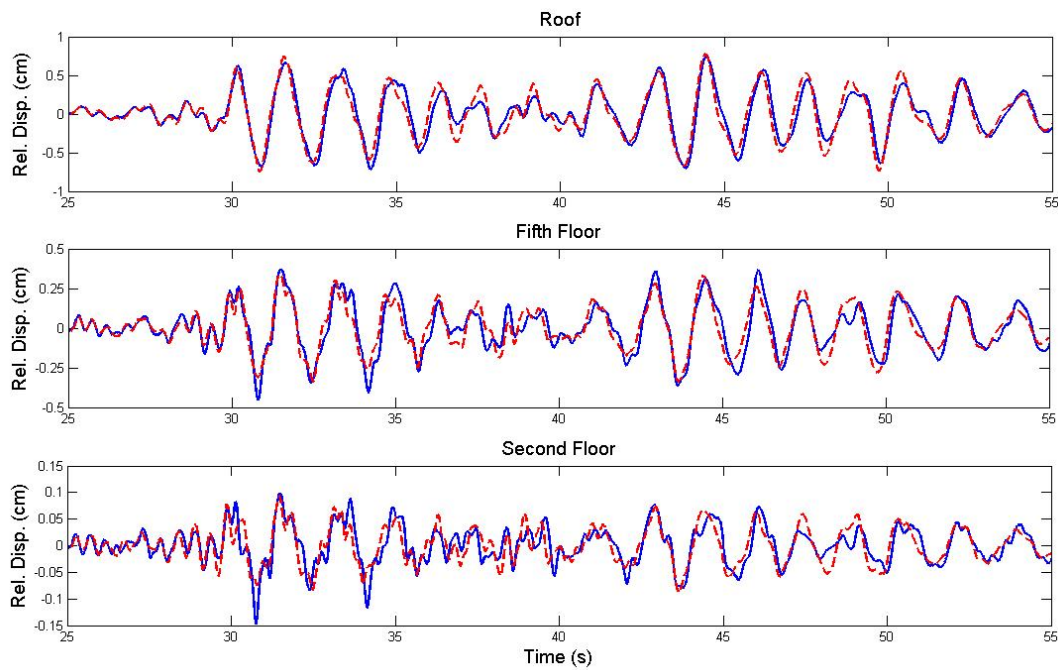


Figure 10: Comparison of computed (SAP2000) vs. recorded relative displacement time histories at selected instrumented levels of the building

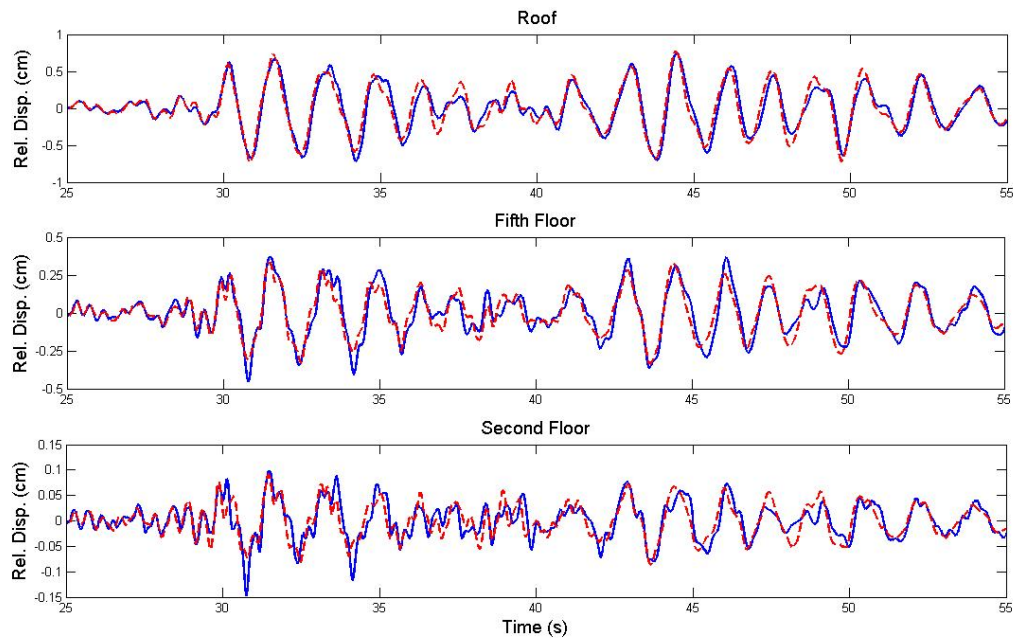


Figure 11: Comparison of computed (Perform-3D) vs. recorded relative displacement time histories at selected instrumented levels of the building

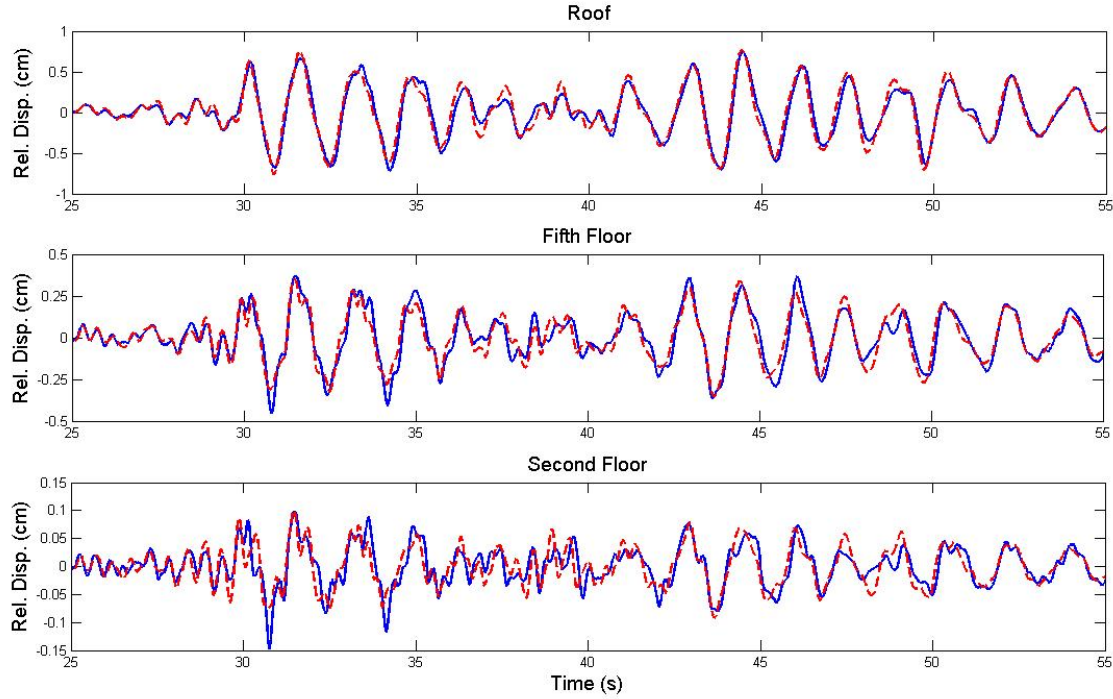


Figure 12: Comparison of computed (OpenSEES) vs. recorded relative displacement time histories at selected instrumented levels of the building

At the Roof, the average of the actual response recorded in the transverse direction was used for comparison in all cases. Overall, based on the assumptions previously noted, the computed roof accelerations compare well with observed responses for all three computer programs. The predictions of accelerations at the 5th and 2nd level are generally not as good as the estimates at the roof. In the case of displacements (relative to the ground), the predicted responses are quite good for both the roof and the 5th floor level. Some discrepancies are obvious in the computed responses at the 2nd floor level.

A direct comparison of the computed acceleration and relative displacement time history responses at the roof and second floor levels of each model to the Chino Hills earthquake can be seen in Figure 13. The relative displacement time history responses of the three different models match almost exactly. The SAP2000 and Perform-3D models match almost identically in acceleration as well, while the model developed in OpenSEES varies slightly from the other models in its acceleration response.

Nonlinear Sensitivity Analysis

Four different nonlinear models were generated from the elastic models in SAP2000, Perform-3D and OpenSEES. In SAP2000, concentrated hinges located at moment frame beam and column ends were used. The moment-rotation relationship of the hinges was assumed to be bilinear with 3% post-yield stiffness in one case, and elastic-perfectly plastic in another. The nonlinear model generated in Perform-3D used fiber hinges located at moment frame beam and column ends. The hinge length was assumed to be one-half of the member depth, and the stress-strain relationship assigned to each steel fiber was assumed to be elastic-perfectly plastic.

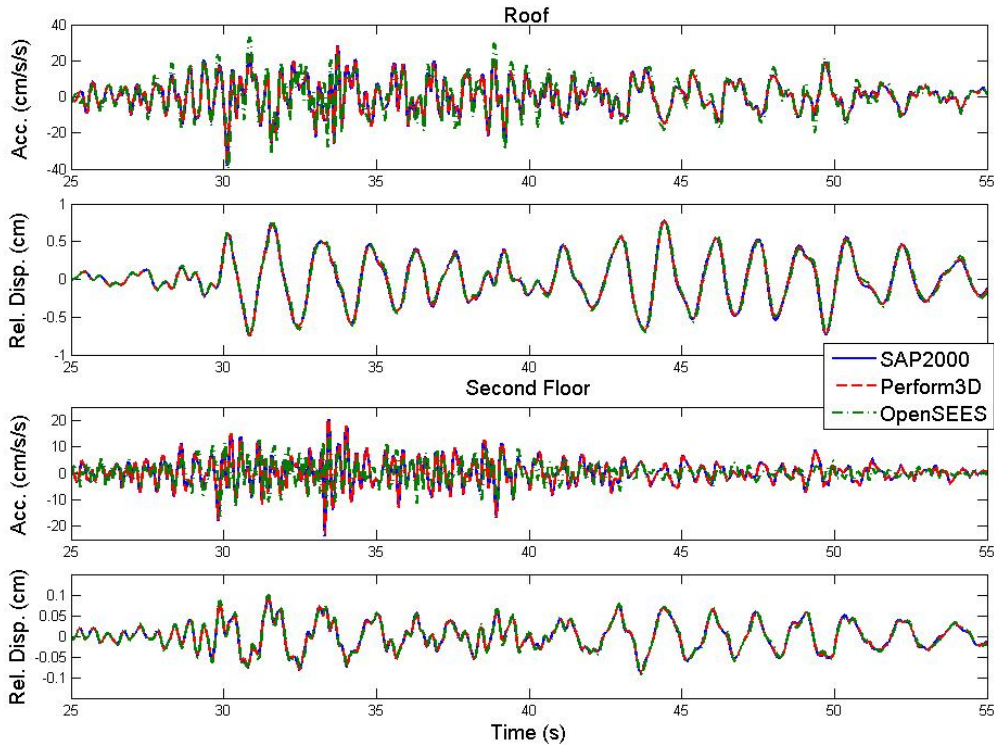


Figure 13: Comparison of computed acceleration and relative displacement time histories at roof and second floor levels using different computer programs.

In OpenSEES, two different nonlinear models were generated. The first used distributed plasticity elements for each moment frame beam and column. Five integration points were used for each distributed plasticity element. The second OpenSEES model used fiber hinges located at moment frame beam and column ends. Three different hinge lengths were assumed: one-half of the member depth, three-quarters of the member depth, and the full member depth. The stress-strain relationship assigned to each steel fiber in both models was assumed to be elastic-perfectly plastic.

For each of the four nonlinear models the expected yield stress of the steel wide flange framing (55 ksi) was used instead of the design yield stress (50 ksi) for establishing the associated strengths of the force-deformation or stress-strain relationships. In the equivalent gravity frames for each of these models, moment-rotation hinges were used at each end of the gravity beams with an assumed elastic-perfectly plastic force-deformation relationship. The plastic moment capacities for these partially-rigid connections were determined as outlined in Fouch and Yun (2002). Also, the dummy columns were not included in these models for the nonlinear response history analyses.

Figure 14 compares the inter-story drift ratios resulting from the nonlinear response history analyses which were performed by scaling the original ground motions by a factor of 10 to induce inelastic behavior in the building. The results from the SAP2000 model diverged quite significantly from the other programs, which were all based on models using elements with fiber

sections. The results from the Perform-3D and OpenSEES models varied from one another, but only slightly.

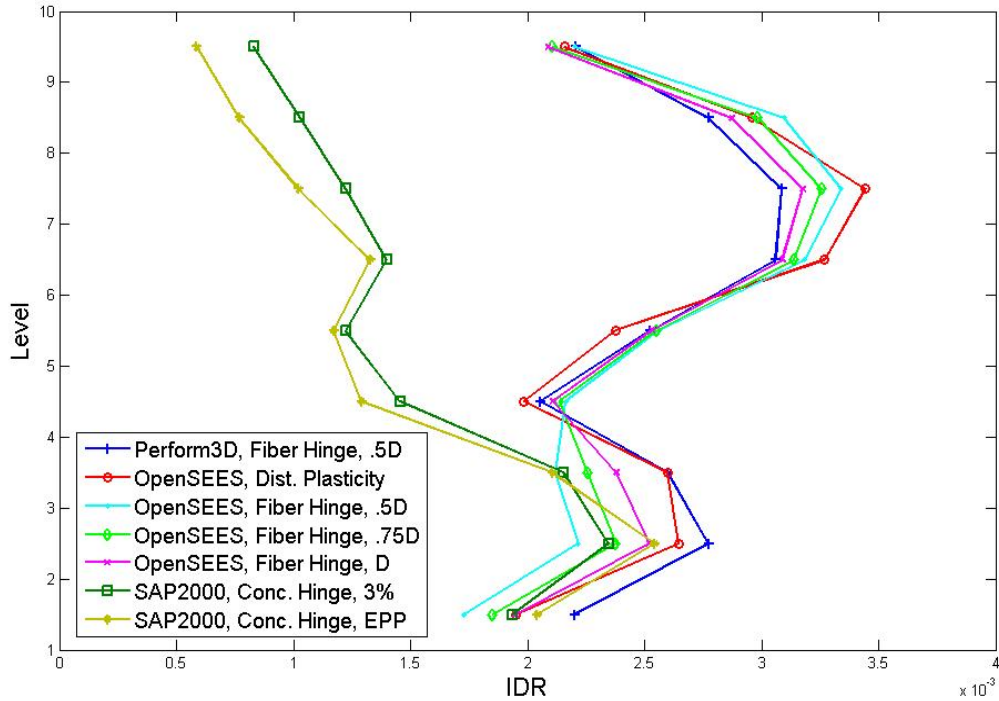


Figure 14: Comparison of computed peak inter-story drift ratios using the three computer programs and different nonlinear modeling assumptions

Concluding Remarks

For the case of purely elastic behavior, all three computer programs, under generally similar modeling assumptions, produce comparable results for the displacement response of the building compared to the actual recorded response. Some discrepancies in the acceleration response at the lower levels of the building are evident even at these low levels of ground shaking. At increased ground shaking intensities (achieved in this study by scaling the original recorded motion), the results from SAP2000 are seen to deviate from OpenSEES and Perform-3D given the modeling options used in the study. Further investigation is needed to characterize the noted differences in the three computer programs due to inherent modeling assumptions.

References

- Foutch, D.A. and Yun, S. (2002). "Modeling of steel moment frames for seismic loads," *Journal of Constructional Steel Research*, 58 (2002), 529-564.
- Liu, J. and Astaneh-Asl, A. (2000). "Cyclic Tests on Simple Connections Including Effects of the Slab," *Report SAC/BD-00/03*, SAC Joint Venture.

**3D WAVE PROPAGATION AND SITE EFFECTS IN THE HUMBOLDT BAY AREA
USING STRONG GROUND MOTION RECORDS FROM
THE M6.5 2010 FERNDALE EARTHQUAKE.**

Arben Pitarka¹, Hong Kie Thio² and Paul Somerville²

¹Lawrence Livermore National Laboratory, Livermore

²URS Corporation, Los Angeles

Abstract

In this study we simulated and analyzed strong ground motion data recorded in the Humboldt Bay and Eureka areas during the M6.5 Ferndale area earthquake of January 2010. The scope of the presented work was two-fold. First, we investigated the main aspects of seismic wave generation and propagation, including kinematic rupture process and 3D wave propagation scattering. Our goal is to analyze their potential effects on seismic motion recorded at free field stations across Humboldt Bay and Eureka, and test the performance of a standard broadband strong ground motion simulation technique. Second, using non-linear site response analysis, we investigated the effects of shallow sedimentary layers on strong ground motion recorded by the Humboldt Bay geotechnical array. Our study provides insight into the composition of the wave field during the earthquake and an improved understanding of how the wave field is affected by the local 3D structure and the non-linear response of the shallow sediments of the Humboldt Bay.

Introduction

The M6.5 Ferndale earthquake occurred north of the Mendocino Triple junction, in a region with complex structure caused by subducting plates. This strike-slip earthquake occurred at a depth of about 29 km within the subducting Gorda plate, with a preliminary estimate of the depth extent of faulting ranging between about 10 and 20 km (U.C. Berkeley). Damage was concentrated along the coast from Ferndale to Eureka. Areas founded on deep estuary and river deposits had higher damage compared with areas located on shallower soils and rock (Storesund, 2010). In Figure 1, we compare the recorded ground motions with the ground motions predicted by the NGA ground motion prediction equations for crustal earthquakes (Abrahamson et al., 2008) and the ground motion model for intraslab earthquakes of Zhao et al. (2006). The NGA ground motion prediction equations have more gradual attenuation with distance than the recorded ground motions, and do not provide a good fit to their amplitudes. This is not surprising, because the earthquake was clearly a mantle earthquake, not a shallow crustal earthquake of the kind modeled by the NGA ground motion prediction equation used here. Its location below the oceanic Moho in a region that is expected to have a low velocity gradient apparently resulted in rapid attenuation, because there is no strong velocity gradient such as the Moho to cause the gradual attenuation of ground motions from crustal earthquakes (e.g. Somerville *et al.*, 1984). In general the peak amplitude of ground motion acceleration recorded

along the coast (distances between 40km and 55km) is much higher than predicted by both ground motion prediction equations. The largest recorded ground acceleration and velocity were about 44% g and 47 cm/s respectively at Ferndale, about 43 km east of the epicenter.

The Zhao et al. (2006) model is derived from normal and thrust faulting mantle earthquakes at depth within subducted slabs, whereas the 2010 Ferndale earthquake was a strike-slip earthquake that occurred within the shallow part of the slab that lies oceanward of the subduction zone. It nevertheless provides a better fit to the recorded ground motions, having a rate of attenuation similar to that of the data.

The complexity of the source process, and the three-dimensional underground structure need to be considered when analyzing the strong ground motions recorded during the earthquake. Their potential contributions to the double pulse-like motion and large variability of peak acceleration recorded at stations with similar source distance is the focus of our investigation.

Strong Motion Records

In our investigation we used ground motion data recorded by over 20 free-field strong-motion stations of the California Geological Survey (CGS) and U.S. Geological Survey, and the vertical geotechnical array, posted at the Center of Engineering Strong Motion Data web site. The corrected three component accelerograms were downloaded from the website of the CGS strong motion center (<http://www.strongmotioncenter.org>). This data set provides an excellent resource to analyze wave propagation and local site effects.

The location of the strong motion sites, and the location of four selected sites that were used in our preliminary data analysis, are shown in Figure 2. A photo of the bridges in the Humboldt Bay area, where the geotechnical array is located, is shown in Figure 3.

Three-Dimensional Velocity Model

We used geotechnical data for the area (e.g. Clarke, 1992) and available geophysical and geological profiles to extend the 3D velocity model of the Eel River basin developed by the URS group (Graves, 1994). The URS velocity model was originally developed to study ground motion and rupture process of the 1992 Cape Mendocino earthquake (Graves, 1994). Our model extended to the north and includes the Humboldt Bay and Eureka areas. The map of the basin depth is shown in Figure 4. The offshore basin structure is not well resolved by the available data. Therefore we assumed a rather flat geometry that extends east of the fault. The background crustal model is based on GIL7, a 1D regional velocity model (Dreger, 2011, personal communication). In our model, the basin sediments are represented by two layers with a minimum velocity of 620 m/s. In our long period ground motion simulation we used a 200 m grid spacing which allow for accurate finite-difference computation of the wave field up to 0.8 Hz. A map view and a vertical cross-section of the 3D velocity model are shown in Figure 5.

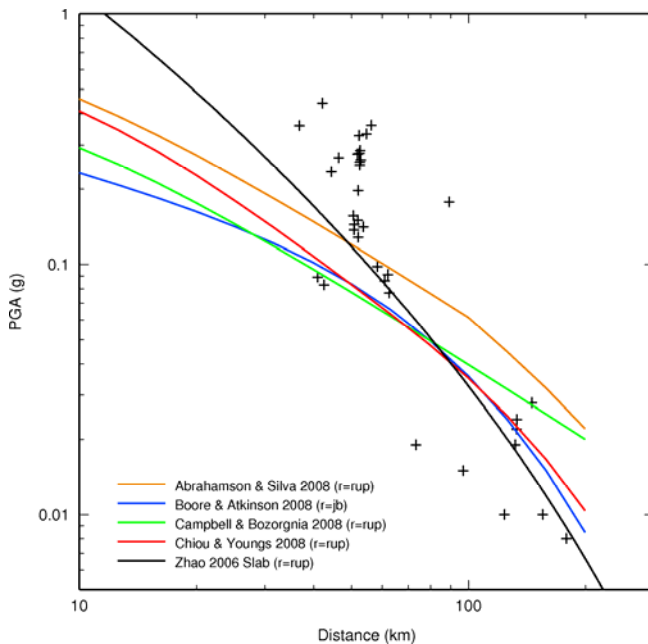


Figure 1. Comparison of recorded peak acceleration of the 2010 Ferndale earthquake with the predictions of the NGA (Abrahamson et al., 2008) ground motion models for shallow crustal earthquakes and the Zhao et al. (2006) ground motion prediction model for intraslab earthquakes

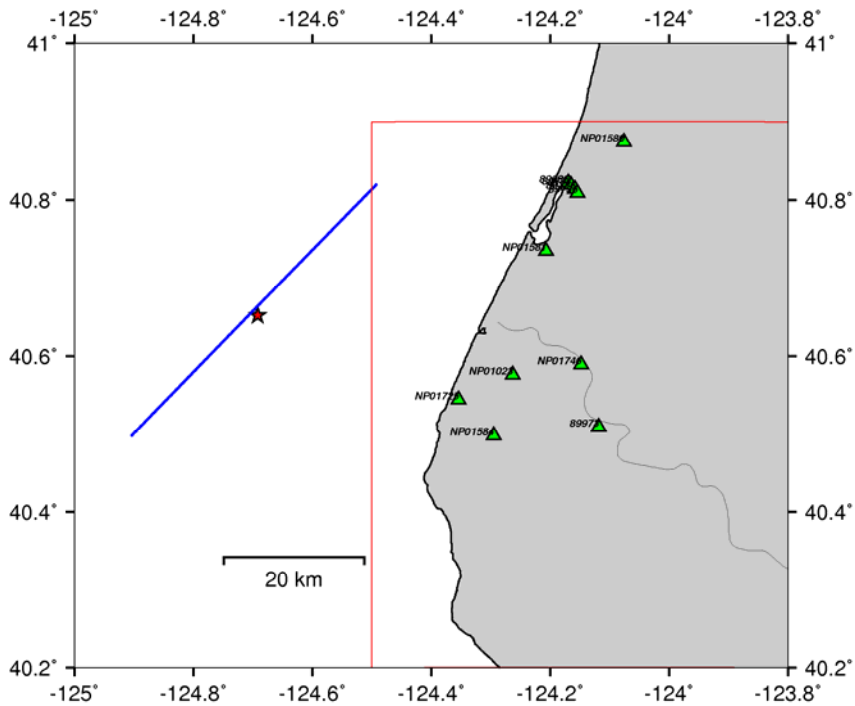


Figure 2. Map of the study area showing the stations location (triangles), ocean-bottom fault projection (blue line), and epicenter location (star). Red square indicates the area for which a 3D model for the shallow sediments was developed.



Figure 3. Humboldt Bay Middle Channel Bridge (courtesy of Caltrans)

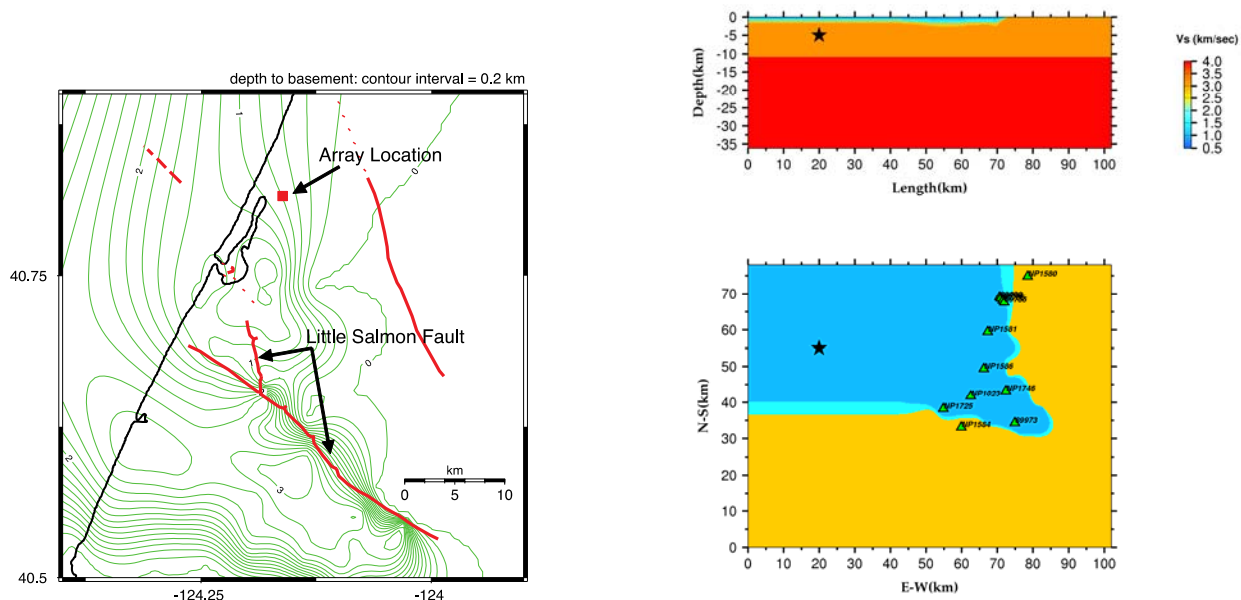


Figure 4. Left panel: Map of the basin depth. Green contour lines show depth to the basement, and red lines indicate location of major faults. The array location is shown by the red square. Right panel: The three-dimensional velocity model. Top Panel: E-W vertical section crossing the epicenter. Bottom Panel: Map view of the basin showing the strong motion stations location (triangles), and earthquake epicenter (star).

Broad-Band Strong Ground Motion Modeling

Kinematic Slip Model

Analysis of the earthquake indicates that slip occurred on a near-vertical, left-lateral fault oriented about N47E. Large strike-slip earthquakes like this one are common in the interior of the Gorda plate. The hypocenter was located at a depth of 29 km, but accuracy is relatively poor owing to the earthquake occurring about 40 km offshore and 56 km from the nearest seismic station. Preliminary inversion of long period ground motion displacement by the UC Berkeley Seismological Laboratory (Dreger, 2010, personal communication) estimated a fault length of about 25 km; rupture proceeded unilaterally to the southwest. The peak estimated slip between the two sides of the fault was 2.4 meters.

We started the investigation of the source process by simulating ground motion velocity at 11 stations located along the coast. Our simulation using 3D Green's functions (Pitarka, 1999) indicates that the original kinematic slip model does a poor job at explaining the recorded data. Based on trial and error analysis we produced a refined kinematic rupture model that explains the overall characteristics of recorded strong ground motion in a broad frequency range. The slip model is shown in Figure 5. The fault geometry is the same and the mechanism is similar to UC Berkeley's model. We use a strike angle of 230 degrees, dip angle of 86 degrees, rake angle of 11 degrees, maximum rupture velocity of 2.8 km/s, and a maximum rise time of 1.7s. The local slip is represented by two time-windows with a 0.3 s overlapping. The subfault dimensions are 1 by 1km. The details of the rupture kinematics are not well resolved due to poor station distribution and limited knowledge of underground structure in the source region. Our kinematic model suggests that the rupture was bilateral, and a zone of large slip was located north of hypocenter, with a maximum slip of 1.2 m.

Ground Motion

We used the broad-band simulation procedure of Graves and Pitarka (2010) to simulate strong ground motion at 11 stations shown in Figure 2. The broadband ground-motion simulation procedure is a hybrid technique that computes the low-frequency and high-frequency ranges separately and then combines the two to produce a single time history. At frequencies below 1 Hz, the methodology is deterministic and contains a theoretically rigorous representation of fault rupture and wave propagation effects, and attempts to reproduce recorded ground-motion waveforms and amplitudes. At frequencies above 1 Hz, it uses a stochastic representation of source radiation, which is combined with a simplified theoretical representation of wave propagation and scattering effects. The simulation uses site corrections proposed by Campbell and Bozorgnia (2008) using Vs30.

The comparison between recorded and simulated time histories and response spectra of acceleration, and velocity at 11 sites located along the coast is shown in Figure 6 and Figure 7, respectively. Due to primarily bilateral rupture initiating at the center of the fault, the Ferndale event produced strong rupture directivity effects toward the northeast and southwest. Due to their relative location with respect to the fault most of the sites are affected by the rupture

directivity toward the north. The large velocity pulse observed on the N-S component at stations north-east of epicenter is well reproduced by the simulation. This pulse is controlled by the rupture directivity to the north. The large pulse observed on the E-W component at sites south-east of epicenter is not well reproduced by the simulation. This could indicate that the second asperity located south of the rupture initiation has a much larger slip.

We compute the model bias and standard error for 5% damped spectral acceleration over a suite of periods from 0.05 to 8 s for the simulation using 11 sites. The results are displayed in Figure 7 for the fault-parallel, fault-normal, and average horizontal (geometric mean) components. The model bias is near zero for all components across the entire bandwidth indicating that, on average, the simulation is accurately reproducing the main characteristics of the observed ground motions. The largest standard error for these comparisons is about 0.2 natural log units for periods less than about 0.8 s. For periods longer than 0.8 s, the standard error increases to about 0.4 natural log units. The increased standard error at the longer periods is probably due to deficiencies in our assumed rupture model, which have a relatively stronger impact on the deterministic aspects of the simulation.

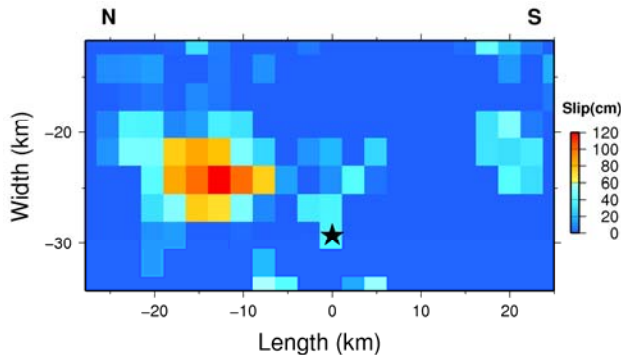


Figure 5. Kinematic slip model developed in this study

Nonlinear Soil Response Analysis

The ground motions from the 2010 Ferndale earthquake recorded at the Humboldt Bay geotechnical array provide another opportunity for testing the efficiency of current nonlinear techniques for predicting soil response under moderate shaking. The array is located about 0.25 mile north-west of the west abutment of the Middle Channel Bridge (see Figure 3). It contains four borehole instruments installed at the free surface and at depths of 19m, 33m, 56m, and 136m. The corrected three component accelerograms were downloaded from the website of the CGS strong motion center (<http://www.strongmotioncenter.org>).

We used the computer program NOAH_SH based on the nonlinear soil response technique of Bonilla et al. (2005) to analyze the recorded response at borehole instruments. NOAH_SH is based on the staggered-grid finite-difference method and Iwan's (1967) nonlinear soil model.

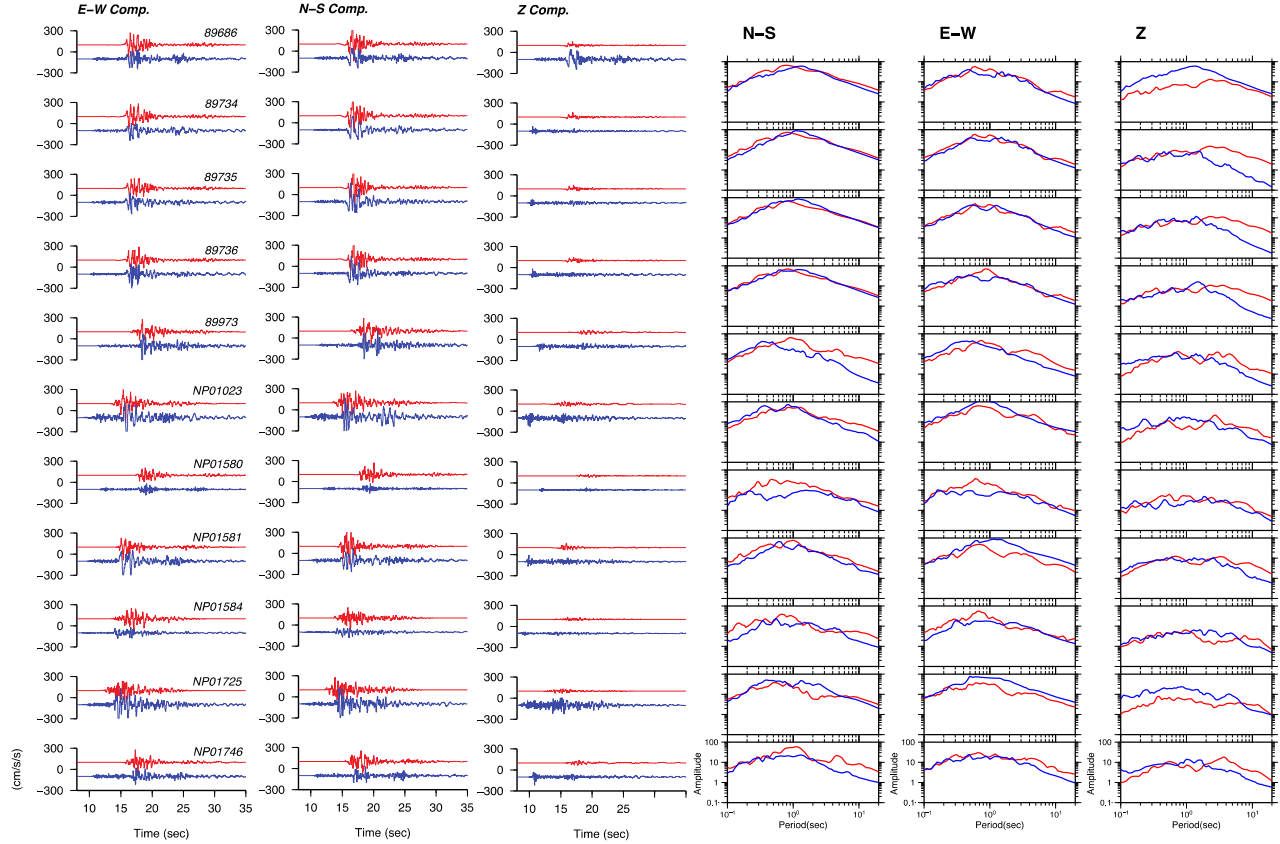


Figure 6. Comparison of simulated (red traces) and recorded (blue traces) ground motion acceleration. Left panel: acceleration time histories. Right panel: acceleration response spectra.

The technique operates in the time domain by tracking the earthquake load through stress-strain space. It allows the direct use of G/Gmax laboratory data that can be assigned to each layer. Typically it uses the Masing rule for unloading and re-loading that may result in an over-prediction of hysteretic damping at large strains. Reviews of the methodology can be found in the work of Joyner and Chen (1975) and Bardet (2001). Recent applications of the NOAH_SH computer program as well as comparisons with other traditional methods such as the equivalent linear method are shown in the study of Hartzell *et al.* (2004). Our choice of a fully nonlinear technique is based on the fact that nonlinear finite-difference techniques have several advantages over the classical equivalent nonlinear method. First, with a finite difference method one can easily obtain the strain from the node displacement gradient that is then introduced into the constitutive equation to compute the stress. Second, the constant damping, independent of frequency, used in the equivalent nonlinear methods causes the over-attenuation of high frequencies. This unrealistic feature becomes more pronounced at high levels of strain.

In our site response analysis we used the Peninsular Range (PR) modulus reduction, G/G_{max} , and damping curves as a function of shear strain for cohesionless soil developed by Silva *et al.* (1997, 1999) and the Vucetic and Dobry (1991) curves for a plasticity index of 30 for the top clay layers. The PR curves are a subset of the EPRI (1993) curves developed by modeling recorded motion. We used them for soils below 7 m.

The 1D velocity model used in the non-linear simulations is based on borehole shear-wave speeds provided by Caltrans. The shear wave velocity increases from about 180 m/sec at the free surface to 630 m/s in hard rock at 220 m depth. The shear wave velocity profile is shown in Figure 8.

Figure 9 compares time histories and amplitude spectra of recorded and computed acceleration at the geotechnical array. The recorded E-W component of the acceleration at a depth of 136 m was used as input motion to compute the non-linear response of the shallow sedimentary layers. The synthetic accelerograms compare well with the recorded accelerograms at all depths. Similarly Figure 10 compares the recorded and simulated time histories of acceleration assuming a linear soil response. The simulation results clearly shows that in comparison with linear response the non-linear response of soils suppresses much of the high frequency energy as the waves propagate through the soil column. Significant non-linear response is observed even at a depth of 56 m.

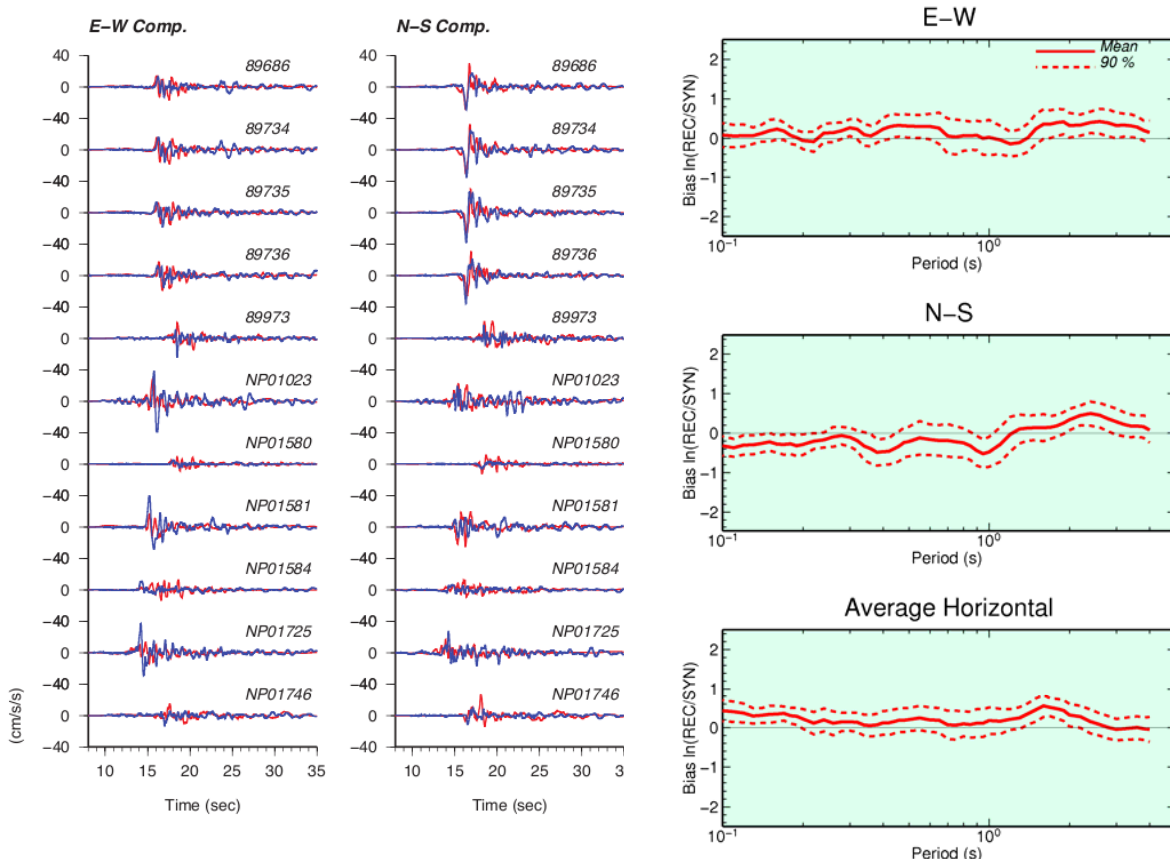


Figure 7. Left panel: Comparison of simulated (red) and recorded (blue) ground motion velocity time histories. Right panels: Model bias (heavy line) and standard error (shaded between dotted lines) for 5% damped spectral acceleration using 11 sites. Top panel shows the fault-parallel component, middle panel shows the fault-normal component and bottom panel shows the average horizontal (geometric mean) component.

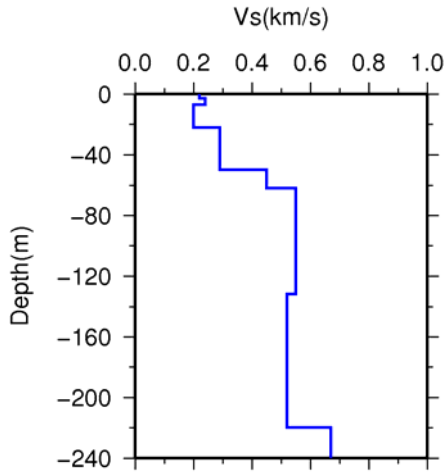


Figure 8. Shear-wave velocity profile used in the 1D non-linear analysis

Conclusion

In order to reproduce the recorded peak amplitude of ground motion, the stress drop used in our broad-band simulations is about 25% higher than the one we use in typical simulations of strike-slip faults for crustal earthquakes. This indicates that the stress drop of the Ferndale earthquake was relatively high. Our finding is in agreement with observations made for deep earthquakes of similar type.

Our wave propagation modeling demonstrates that the fault rupture was bilateral, and that rupture directivity was strong on both rupture directions. Basin induced waves caused a second large pulse, and amplified ground motion at basin sites. This is illustrated in Figure 11 which compares recorded acceleration decomposed into empirical modes (Huang et al., 1998) at two free-field basin sites (NP01581, geotechnical array 89734) and site NP01580, located outside the basin. The second large pulse is strong at all sites inside the basin. In contrast, such pulse is not observed at rock sites. Based on analysis of simulated ground motion using 3D models with and without the basin structure we concluded that the second large pulse observed at basin sites is a basin induced wave. The basin and local site effects contributed to large amplification of ground motion at soils sites along the coast.

1D wave propagation analysis at the geotechnical array, using a fully non-linear numerical technique, show that the seismic response of soft sedimentary layers in the Humboldt Bay can be well modeled by a fully non-linear technique. The next step in our study will be the investigation of the sensitivity of the computed waveforms to velocity variation in the approximate 1D velocity models used in the non-linear soil response analysis. The effect of input motion characteristics on the non-linear response at the geotechnical array will be finally investigated by using broad-band synthetic accelerograms from the 2010 Ferndale earthquake, simulated during this study.

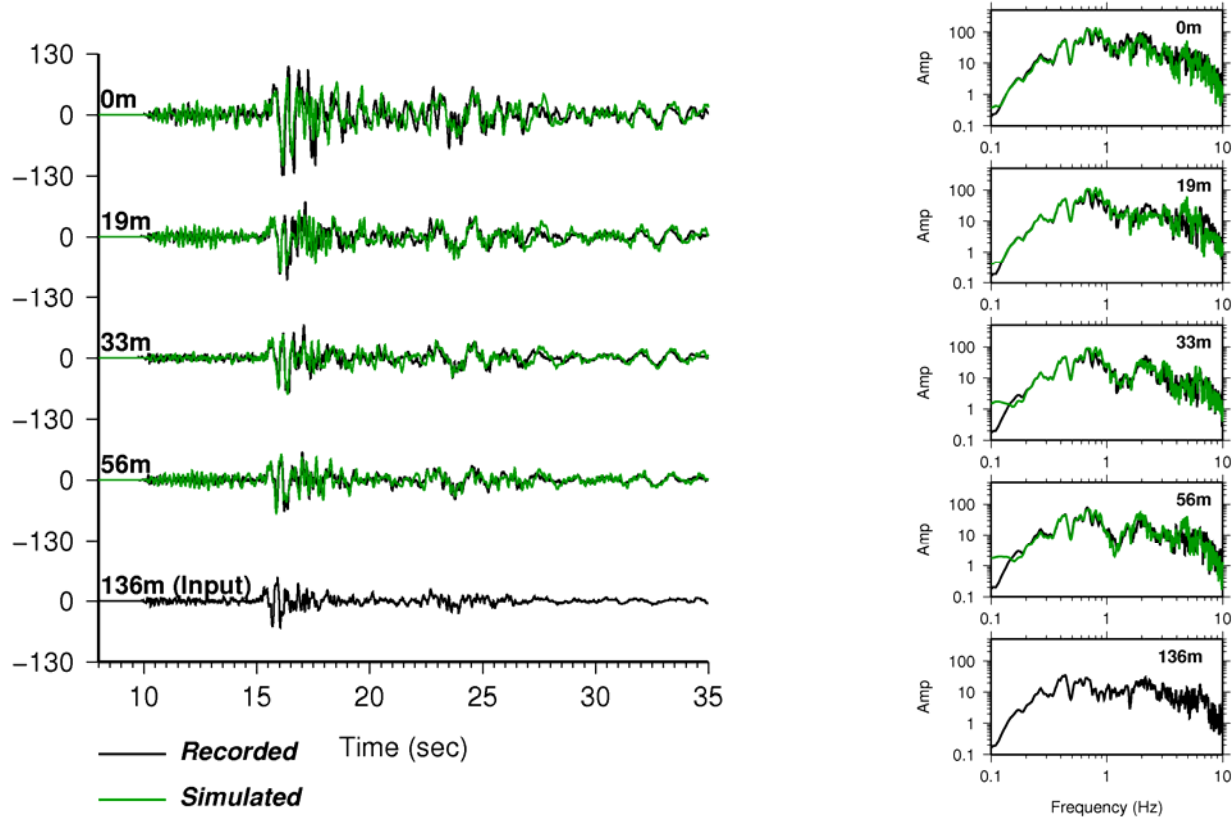


Figure 9. Comparison between recorded (black traces) and synthetic (green traces) acceleration calculated at borehole stations using the non-linear technique. The input motion is applied at a depth of 136 m.

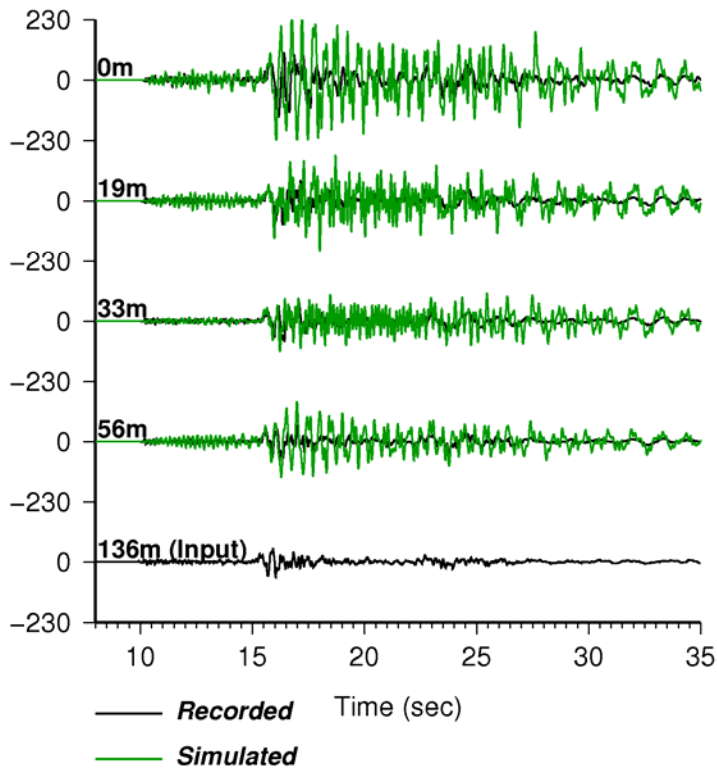


Figure 10. Comparison between recorded (black traces) and synthetic (green traces) acceleration calculated at borehole stations using linear response of soils.

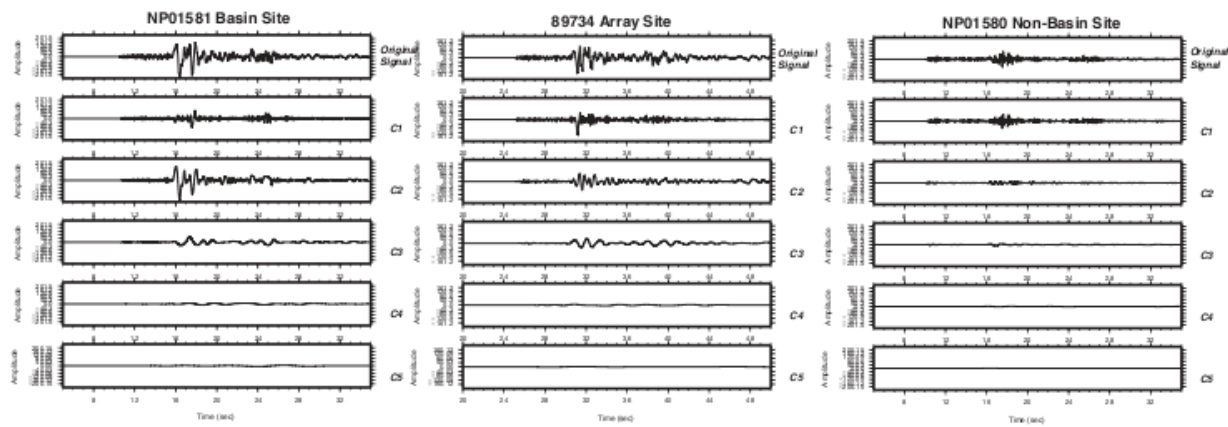


Figure 11. Empirical mode decomposition (C_i) of the horizontal acceleration recorded at free-field stations NP01581, geotechnical array 89734, and NP01580. The second large pulse that dominates the second mode. This pulse of relatively low frequency is only visible in basin sites.

References

- Abrahamson, N.A., G.M. Atkinson, D.M. Boore, Y. Bozorgnia, K.C. Campbell, B. Chiou, I. M. Idriss, W.J. Silva, and R.R. Youngs (2008). Comparisons of the NGA Ground-Motion Relations. *Earthquake Spectra* 24, 45-66.
- Bardet, J.P. and T. Tobita (2001). NERA a computer program for Nonlinear Earthquake site Response Analyses of Layered Soil Deposits, Department of Civil Engineering, University of Southern California, 46 pp.
- Bonilla, L. F. (2000). Computation of linear and nonlinear site response for near field ground motion, *Ph.D. Thesis*, University of California, Santa Barbara.
- Bonilla, L., F., R. Archuleta, and D. Lavallee (2005). Hysteretic and dilatant behavior of cohesionless soils and their effects on nonlinear site response: field data, observations and modeling, *Bull. Seism. Soc. Am.*, 95, 2373-2395.
- Clarke, S. H. (1992). Geology of the Eel River basin and adjacent region: Implications for late Cenozoic tectonics of the southern Cascadia Subduction Zone and Mendocino Triple Junction, *AAPG Bulletin*, 76, 199-224.
- Graves R. W. (1994). Rupture history and strong ground motion modeling of the 1992 Cape Mendocino earthquake. Report to USGS, award # 1434-93-G-0237.
- Graves, R. W. and A. Pitarka (2010). Broadband ground-motion simulation using a hybrid approach. *Bull. Seism. Soc. Am.*, 100, 5A, 2095-2123.
- Hartzell, S.H., L.F. Bonilla, and R.A. Williams (2004). Prediction of nonlinear soil effects, *Bull. Seism. Soc. Am.*, 94, 1609-1629.

Huang, N. E., Shen, Z., Long, S. R., Wu, M. C., Shih, E. H., Zheng, Q., Tung, C. C. & Liu, H. H. (1998). The empirical mode decomposition method and the Hilbert spectrum for non-stationary time series analysis. *Proc. R. Soc. Lond. A* **454**, 903–995.

Iwan, W.D. (1967). On a class of models for the yielding behavior of continuous and composite systems, *J. of App. Mech.*, 34, 612-617.

Joyner, W., and A.T. Chen (1975). Calculation of nonlinear ground response in earthquakes, *Bull. Seism. Soc. Am.*, 65, 1315-1336.

Pitarka, A. (1999). 3D elastic finite-difference modeling of seismic motion using staggered grids with nonuniform spacing. *Bull. Seism. Soc. Am.* 89, 54-68.

Silva, W., N. Abrahamson, G. Toro, and C. Costantino (1997). Description and validation of the stochastic ground motion model, Report submitted to Brookhaven National Laboratory, Associated Universities, Inc., Upton, New York 11973, Contract No. 770573.

Silva, W., Li, S., B. Darragh, and N. Gregor (1999). Surface geology based strong motion amplification factors for the San Francisco Bay and Los Angeles areas. Pearl Report to PG&E/CEC/Caltrans. (<http://www.pacificengineering.org>).

Somerville, P.G., N.F. Smith, and R.W. Graves (1994). The effect of critical Moho reflections on the attenuation of strong motion from the 1989 Loma Prieta earthquake, in "The Loma Prieta, California, Earthquake of October 17, 1989 - Strong Ground Motion," U.S. Geological Survey Professional Paper 1551-A, A67-A75.

Storesund, R., L. Dengler, S. Mahin, B.D. Collins, M. Hanshaw, F. Turner, K. Welsh (2010). M6.5 Earthquake Offshore Northern California January 9, 2010. GEER Field Reconnaissance Summary.

Vucetic, M., and R. Dobry (1991). Effect of soil plasticity on cyclic response, *J. Geotech. Eng. ASCE* 117, 89–107.

Zhao J.X., Zhang J., Asano A., Ohno Y., Oouchi T., Takahashi T., Ogawa H., Irikura K., Thio, H.K., Somerville P.G., Fukushima Y. (2006). Attenuation relations of strong ground motion in Japan using site classification based on predominant period. *Bull. Seism. Soc. Am.* 96, 914–925.

**STRONG MOTION INSTRUMENTATION OF A 62-STORY CONCRETE CORE
RESIDENTIAL BUILDING IN SAN FRANCISCO**

Moh Huang¹, Anthony Shakal¹, Carl Petersen¹, Mehmet Celebi²,
John Hooper³, and Ron Klemencic³

¹ Strong Motion Instrumentation Program, California Geological Survey, Sacramento, California

² Earthquake Science Center, U.S. Geological Survey, Menlo Park, California

³ Magnusson Klemencic Associates, Seattle, Washington

Abstract

The One Rincon Hill Tower in San Francisco is the tallest concrete core shear wall structure in California. After completion of the construction, the building was extensively instrumented in 2012 with 72 sensors in a joint effort by the California Strong Motion Instrumentation Program of the California Geological Survey and the National Strong Motion Program of the U.S. Geological Survey. This paper describes the sensor locations in the building and the instrumentation objectives. Data of the building ambient vibration obtained by the instrumentation system and results of preliminary analysis are also presented and discussed.

Introduction

The One Rincon Hill Tower (south tower of a complex including two towers and pavilion) is a 62-story concrete core shear wall structure located in downtown San Francisco. The tower with 376 condominium homes was designed in 2004 and the construction was completed in 2008 (Figure 1). The building height from the foundation to the roof is about 618 feet which exceeds the 240 feet limit specified in the code for a typical concrete shear wall structure. The structural and architectural systems of the building were designed according to the 2001 San Francisco Building Code and based on performance-based seismic design (Klemencic et al., 2006 and Klemencic, 2008). However, the design was also peer-reviewed because of its uniqueness.

A special feature in the structural design is the use of outrigger columns connected to core shear walls with steel buckling-restrained braces (BRBs). In addition, the building is equipped with two water tanks (about 5' tall) located between Level 62 and 63 (Post, 2008 and 2012). These water tanks are designed to act as liquid tuned mass damper in order to reduce the sway from strong winds. These are predominately used to enhance human comfort from frequent wind storms with return periods of 1 to 10 years. One Rincon Tower is the first building in California to have a liquid tuned mass damper.



Figure 1. Views of the One Rincon Hill Tower from the street and from a neighboring high-rise building in downtown San Francisco. (photos by M. Huang)

Building Structure System

Vertical Load Carrying System

The vertical load carrying system of the building consists of concrete flat slabs supported by concrete columns and core shear walls. Typical residential floors are 8" thick post-tensioned slabs spanning between the center core and perimeter concrete columns. Post-tensioned tendons used in the concrete slabs are 0.5" in diameter (7-wire strand) with an ultimate tensile strength of 270 ksi. The floor slab at the center core is typically 12" thick.

The floor plan is rectangular at the Base Level with a footprint of about 113' by 137'. A curved outer facade is located on the west side between the 7th Level and upper levels. Below the 7th Level, concrete shear walls surround the building.

The maximum size of the outrigger columns is 2'-8" by 7'-6" at the Base Level. All reinforcement used in seismic resisting elements is in conformity with the ASTM A-706, Grade 60 standards. The minimum ultimate compressive strength of the concrete at 28 days is 5000 psi for the basement walls and foundation walls. The concrete strength at 56 days is 5500 psi for post-tensioned floor slabs and varying between 6000 and 8000 psi for columns and shear walls.

Lateral Force Resisting System

The lateral force resisting system of the building is comprised of a concrete ductile core wall system with added concrete outrigger columns in the transverse direction. An isometric view of the lateral force resisting system is shown in Figure 2. The core wall system is arranged in the form of perforated structural tube. The outrigger columns are connected to the core with steel buckling-restrained braces at two locations and terminate at Level 55. Lateral forces are carried by the floor diaphragms to the shear walls. Moments and shear forces are delivered to the foundation by the shear walls.

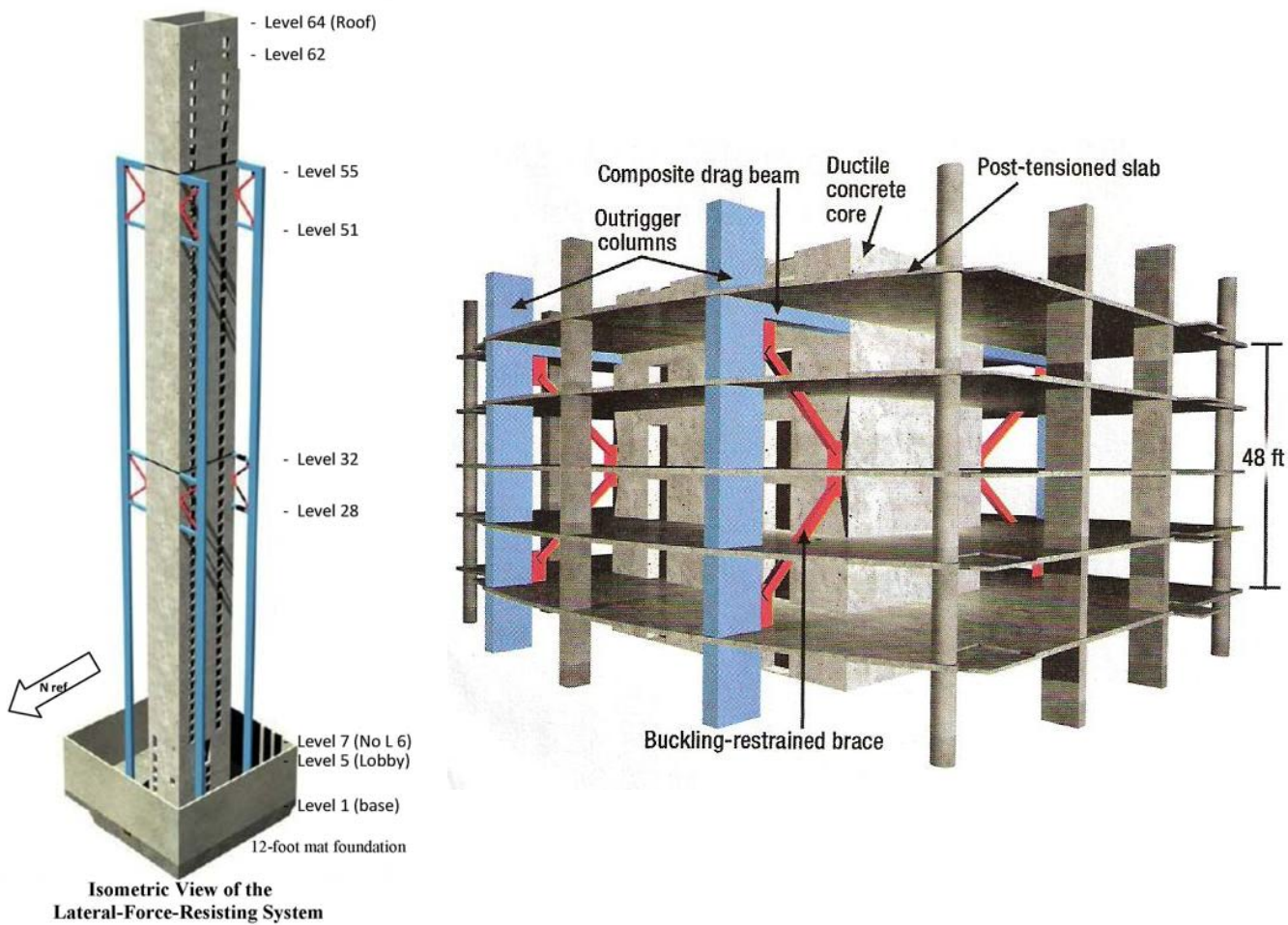


Figure 2. Lateral force resisting system of One Rincon Hill Tower and the outrigger systems.
(from Klemencic et al., 2006)

In addition, the building has two water tanks located on the very top of the building. These tanks were designed to reduce sway from powerful Pacific winds by acting as tuned mass dampers. Conceptually, the presence of a tuned liquid damper allows the inertia of a great mass to be balanced by a comparatively lightweight tank of liquid in such a way that the liquid moves in one direction as the structure moves in the other, thus damping the structure's oscillation.

The seismic design methodologies for the One Rincon Hill Tower follow a path similar to previous performance-based design lateral systems in San Francisco. The goal of the seismic design is to ensure that the overall building behavior meets stated performance objectives at two different levels of anticipated seismic demand (DBE and MCE). The design of the lateral force resisting system follows a two-step process. First is the elastic analysis and design considering the wind loads and the DBE level earthquake forces. The second stage is comprised of nonlinear response analysis using strong-motion records scaled to the MCE ground shaking.

According to the structural plans, key design parameters of the building are as follows:

- Live loads for typical floors were taken as 40 psf and 25 psf for the roof, while partition dead load was assumed as 20 psf.
- Equivalent static force analysis was conducted based on Site Class B soil condition with the following lateral load coefficients: Zone 4; $I = 1.0$; $N_a = 1.0$; $N_v = 1.04$. The response reduction factor was taken as 4.5 for the structural system composed of shear wall/bearing wall.
- Wind loads were computed based on wind tunnel testing conducted at the University of Western Ontario, Canada. Peak building wind acceleration was limited to 20 mg considering a 10-year return period for the input wind forcing function.
- Site specific response spectra were developed for both the DBE and MCE earthquake levels. The code-based elastic design was only performed for the DBE earthquake level.
- The time history records were selected and scaled to be consistent with the site-specific MCE response spectrum. Seven pairs of ground motions were used in the nonlinear response analysis.

The building meets the code-specified drift limits for the nonlinear analysis. The nonlinear seismic behavior of the structure is governed by coupling beam flexural behavior and flexural yielding of the wall near the Ground Level. Other potential mechanisms and actions are verified to remain elastic under the forces corresponding to the nonlinear time history analysis. These actions include wall shear, wall flexure outside of the intended hinge zone, foundation and diaphragms (Klemencic et al., 2006).

Foundation

The site of the One Rincon Hill Tower is underlain by Franciscan rock. According to the soil report (Treadwell & Rollo, 2004), the allowable bearing pressure is 30 ksf. The foundation of the building consists of a 12' thick massive mat foundation embedded into deep serpentine rock. Foundation design and analysis were carried out using a finite element method (Winkler-Foundation method). Demands on the mat foundation were determined through the nonlinear analysis.

Strong-Motion Instrumentation

The planning for the instrumentation of the One Rincon Hill Tower began in 2007. The permission of instrumentation was successfully obtained by CGS/CSMIP from the construction project manager and the developer in 2007. In general, instrumentation of a building involves the installation of accelerometers or other sensors at key locations throughout the structure. The number and location of sensors determines the amount of information that may be recovered about the response of the building after an earthquake. Sensors installed at key structural members allow the important modes of vibration to be recorded and specific measurement objectives to be achieved.

Target locations for 36 accelerometers in the One Rincon Hill Tower were initially developed by CSMIP engineering staff after studying the lateral force resisting systems from the structural plans. At the request of the Developer and the Project Manager, the sensors could not be installed inside any residential units. Therefore, the sensors could only be installed in the central core. The sensor locations developed were then reviewed by the structural engineer of record and representative members of the CSMIP Strong Motion Instrumentation Advisory Committee. CSMIP staff marked these sensor locations and started field installation in May 2008. However, the field installation was stalled due to electrical union requirements. Furthermore, the sensors in the stair wells of the center core had to be re-located by requirement of the City Fire Department.

In 2011, USGS/NSMP expressed interest in joining in the instrumentation of the building. Through the efforts and cooperation of upper management of CGS and USGS, the permission for joint instrumentation by CGS and USGS was secured from the Home Owner Association. The original 36 sensors and their locations were augmented with additional sensors from the USGS/NSMP. The instrumentation of the building was completed in May 2012.

The final instrumentation plan includes 72 accelerometers in the One Rincon Hill Tower. The locations of these 72 sensors are shown in Figure 3. Each of the 72 sensors is connected via cabling to one of three central recorders. The digital recorders coupled with a communication system allow the recording system to immediately send the data to the CSMIP office in Sacramento after the system is triggered by an earthquake. In addition, continuous, real-time data transmission to the USGS/NSMP office in Menlo Park is under development. Due to the congested built environment around the Tower, no instrument has been installed at a nearby site to measure the reference ground motion for the building.

The building description and the sensor layout for the building are included in the Center for Engineering Strong Motion Data (CESMD) at <http://www.strongmotioncenter.org>. Strong-motion data from this building as well as other buildings will be available immediately after a significant earthquake. Data from previous earthquakes are also archived at the CESMD Data Center.

San Francisco - 62-story Residential Bldg

(CSMIP Station No. 58389)
 (NSMP Station No. 8389)

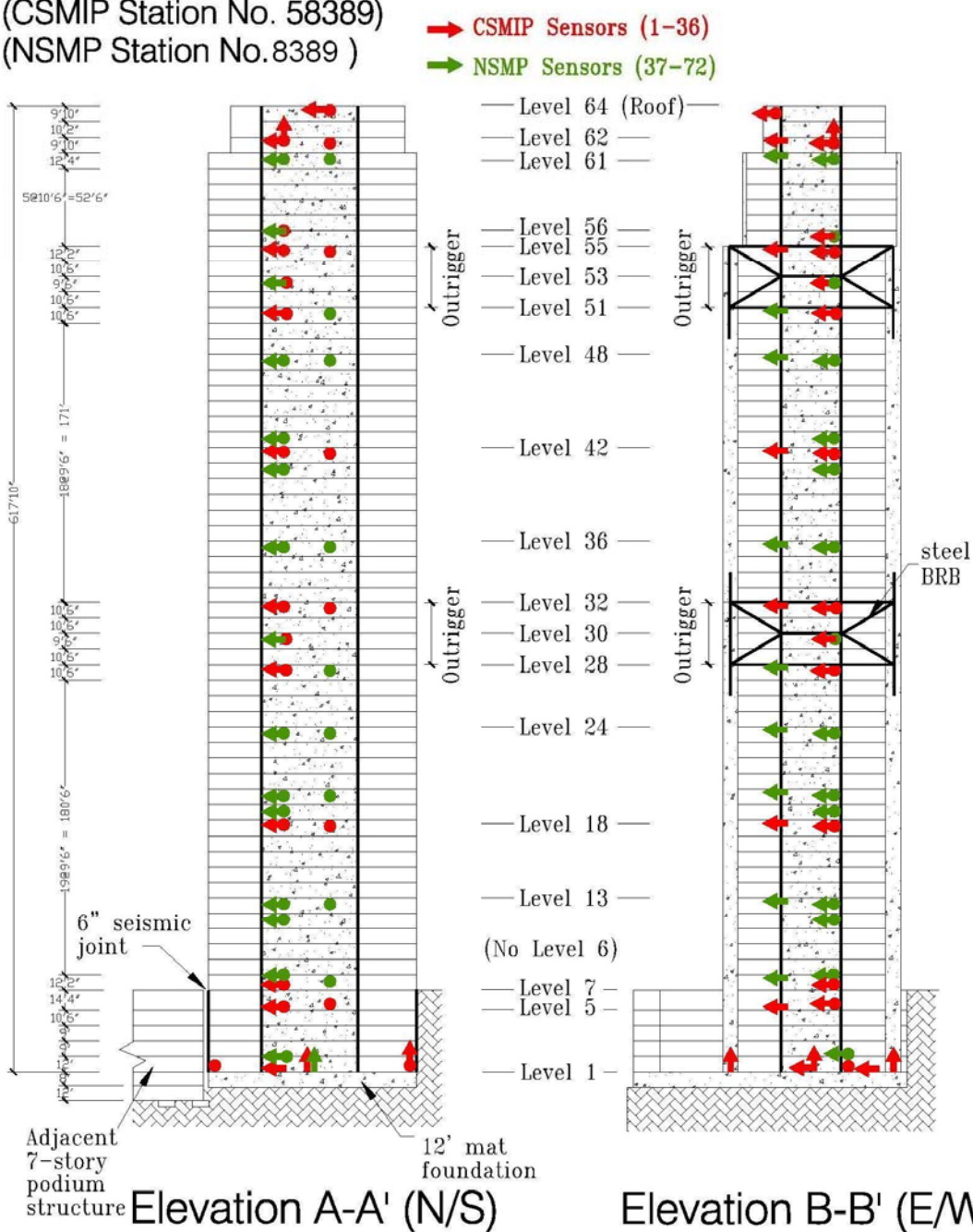


Figure 3. Elevation views showing the locations of the 72 sensors installed in One Rincon Hill Tower. (Arrows indicate sensing direction; solid circles indicated out of the page).

The primary objective of instrumentation for this building is to measure sufficient seismic data so that the response of the building to earthquake ground shaking can be studied. Although there are limitations on the locations for the sensors, in general, the more sensors that are installed, the more information that can be obtained.

The building foundation is a concrete mat with a thickness of 12 feet under the core shear walls. The motions of this rigid concrete mat are measured by six sensors including three horizontal and three vertical sensors. As shown in Figure 3, these six sensors were installed at strategic locations at Level 1 so the six components of rigid body motions can be determined or computed from these sensors. These six components include three translational motions and three rotational motions (i.e., two rocking and one torsional) of the building base.

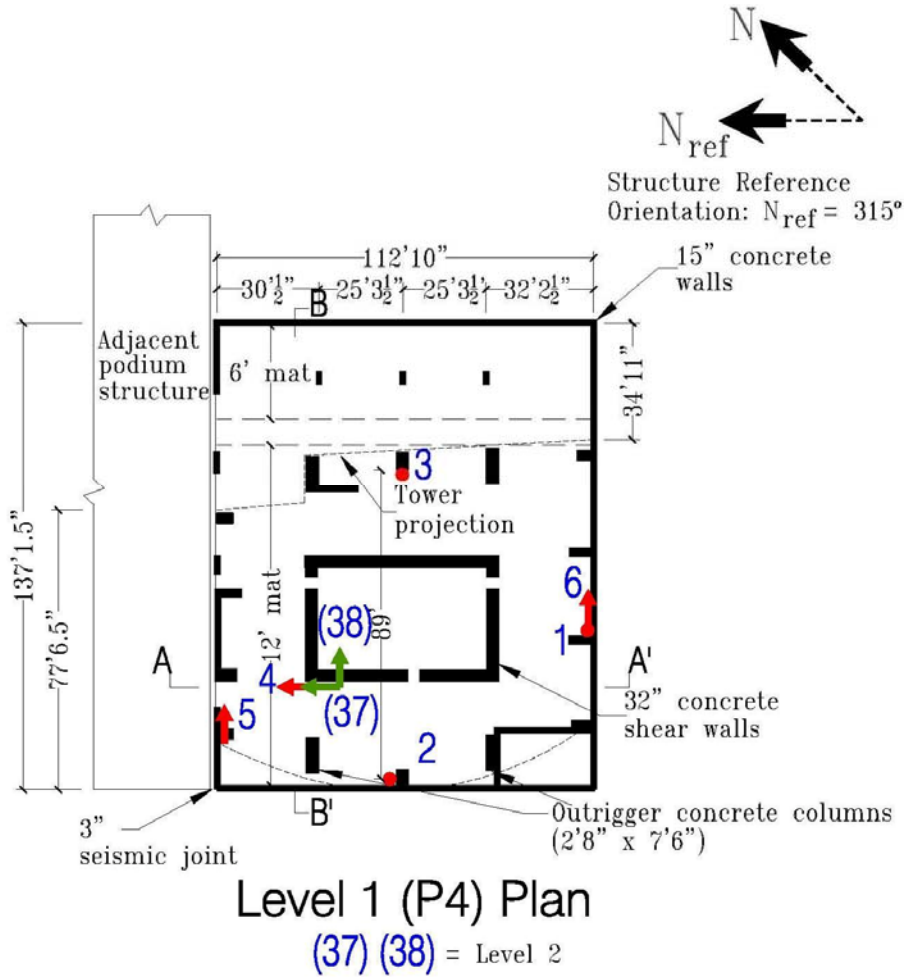


Figure 4. Sensor Locations at Level 1 to measure translational and rotational motions of the concrete mat foundation.

The remaining sixty-six sensors were installed in the upper stories of the superstructure. Sixty five sensors measure the lateral motions at 25 floor levels and one sensor measures the vertical motion at Level 62, which supports the water tanks. These sensors are located at the floors where seismic force resisting elements are changed or where the plan setbacks occur. Specifically, these floors are Level 5, 18, 28, 32, 42, 51, 55, 61, and 62 (Figure 3). These levels are instrumented with 3 sensors to measure the translational and torsional motions of the floor. Level 64 (roof) with only floor slab at the center core is instrumented with 2 sensors (Figure 5). Levels 8, 13, 20, 24, 36, and 48 are also instrumented with three sensors allowing better determination of the mode shapes. The remaining nine levels (Levels 2, 7, 12, 19, 30, 41, 43, 53,

and 56) are instrumented with two sensors only. Consecutive floor instrumentation allows direct computation, without interpolation, of the inter-story drift from the data recorded at the two adjacent floors. Figure 6 shows the sensor locations at Levels 28, 30 and 32 at the lower outrigger beam connection. Similar sensor locations also occur at Levels 51, 53 and 55, at the upper outrigger beam connection.

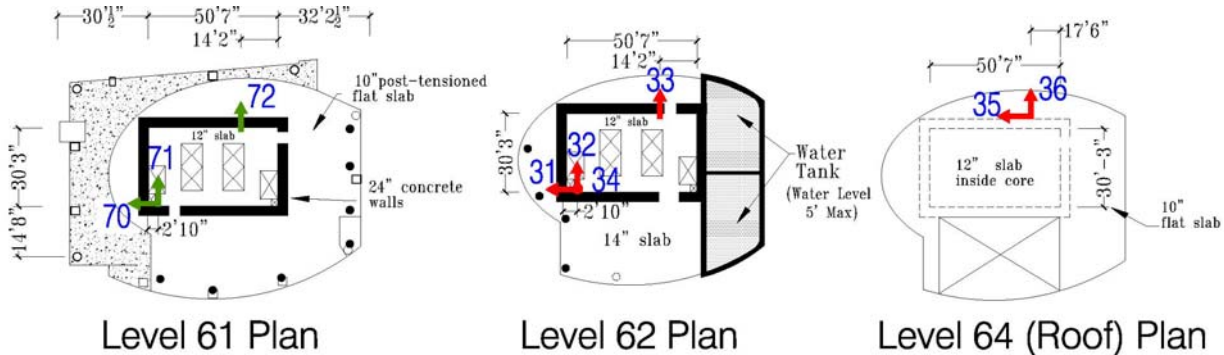


Figure 5. Sensor Locations at Levels 61, 62 (with water tank) and 64 (roof).

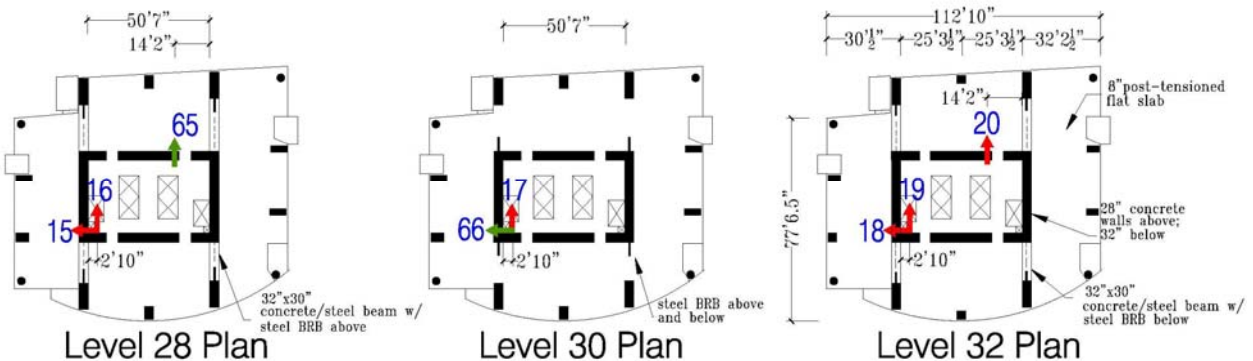


Figure 6. Sensor Locations at Lower Outrigger Frame connections at Levels 28, 30 and 32.

The records from this instrumentation will provide information on the input base motion and the response of the structure at different levels. Key parameters of the structural response, including modal periods and damping ratios for the first few modes, the base shear, inter-story drifts, and base rocking motion can be computed from the records.

Ambient Vibration Data

After the instrumentation in the building was completed, several sets of ambient data were taken by manually triggering the system. Each set of ambient data has duration of 2 to 5 minutes. The sampling rate is 200 samples per second. With all the data from 72 sensors, each set has a significant amount of data. More rigorous analyses of these sets of ambient data can be

performed by using detailed system identification methods to obtain modal frequencies and mode shapes. The results of a collaborative study are presented in a separate paper (Celebi et al, 2012).

Simple analyses can be performed on the ambient data from any upper floors to obtain modal frequencies. For discussions in this paper, only one set of ambient data (about 2 minutes long), from three sensors (Channels 31, 32 and 33) at Level 62 are considered. The acceleration time history data from these three channels are shown in Figure 7. The accelerometers installed in the building can record motions with frequencies from zero to 100 Hz. The accelerations are dominated by extremely high frequencies and the building fundamental motions are embedded in the records.

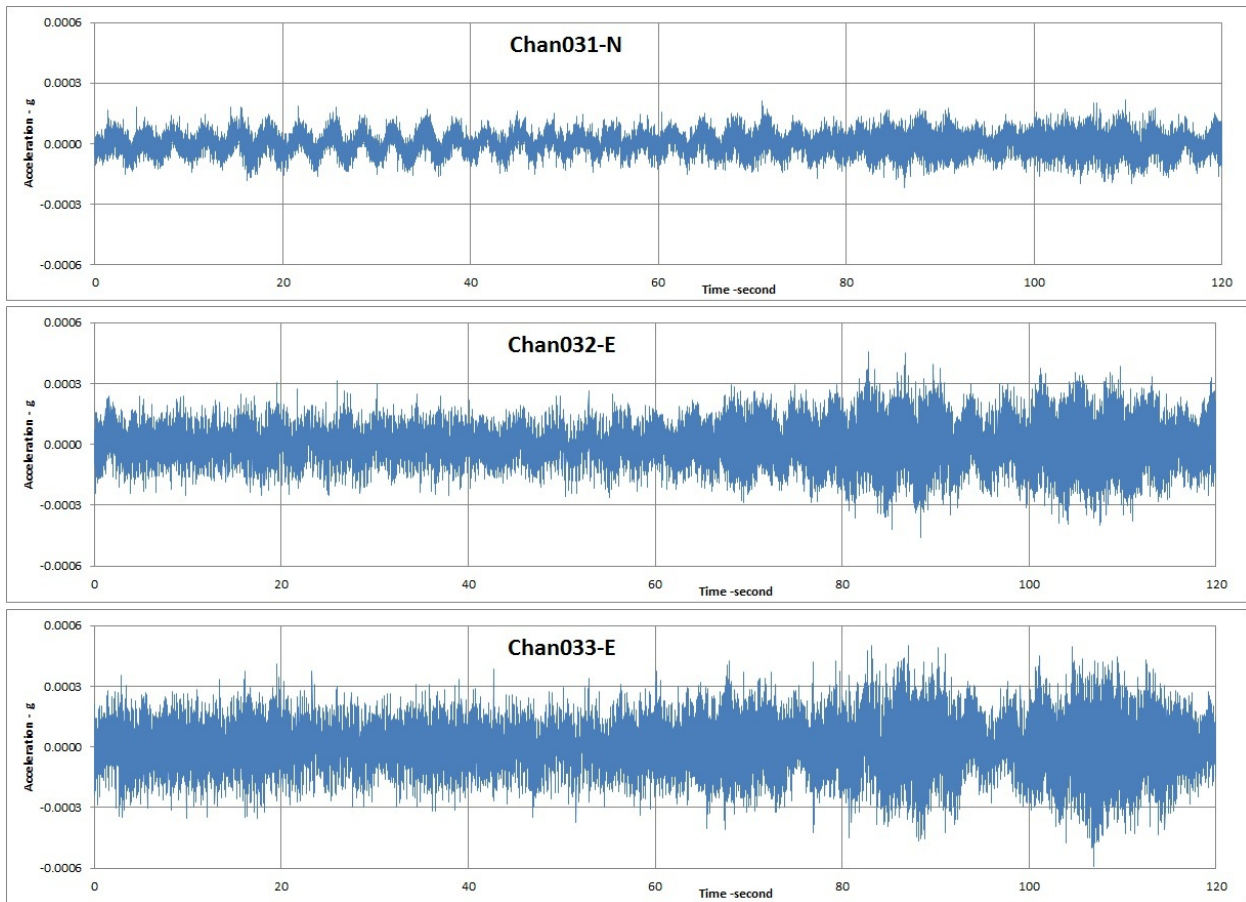


Figure 7. Ambient acceleration data from Sensors 31, 32 and 33 on Level 62 of the One Rincon Hill Tower.

To enhance the translational motion of the floor in the East direction and minimize the contribution of torsional motion, Channels 32 and 33 were averaged together. On the other hand, the difference of Channels 32 and 33 was obtained to enhance the torsional motion and minimize the translational motion in the East direction. The 120-second record was divided into 12 10-second windows. The Fourier transform of each window was then computed. The Fourier amplitudes of the 12 windows were summed and averaged. The results are shown in Figures 8, 9 and 10. The average spectra from Figures 7, 8 and 9 are re-plotted in Figure 11.

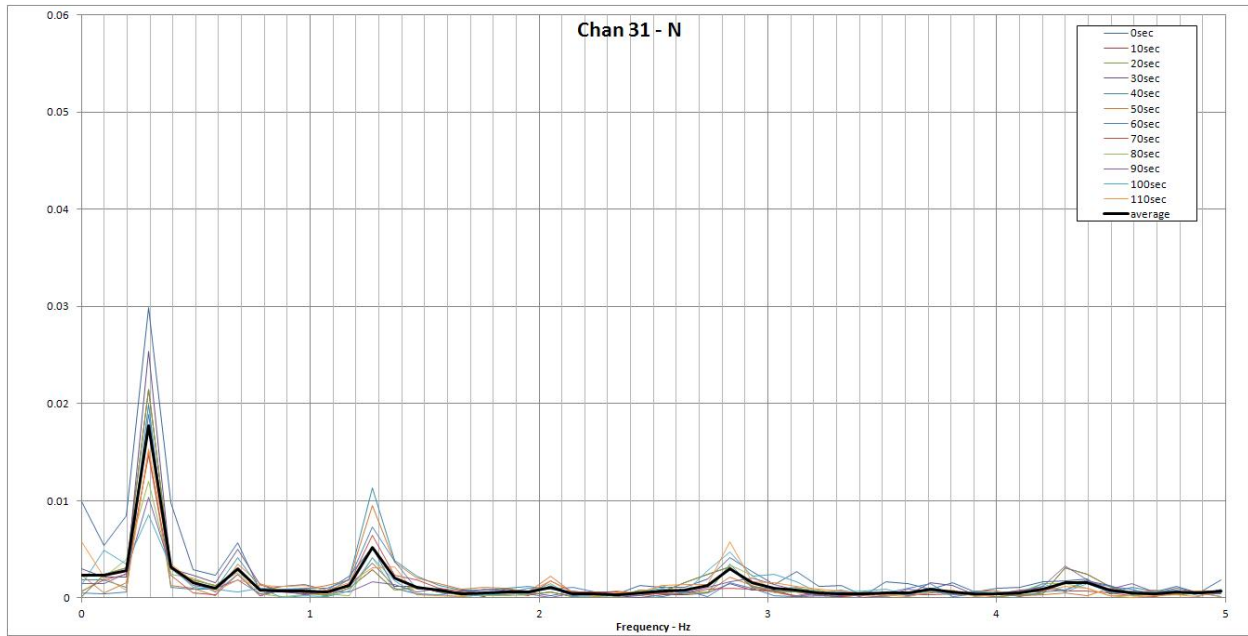


Figure 8. Fourier amplitude spectra of 12 10-second windows of the ambient data from Channel 31 in the north direction, and the average of the amplitudes. The translational modes are shown at near 0.3, 1.3 and 2.8 Hz, and the torsional modes at near 0.7 and 2.1 Hz.

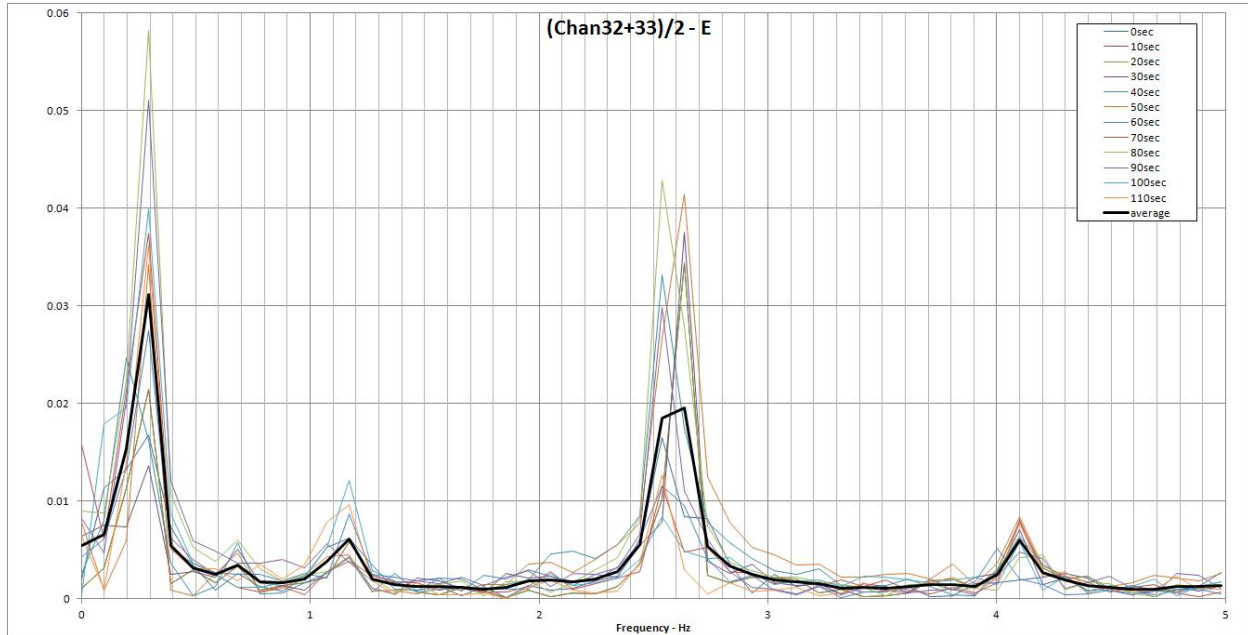


Figure 9. Fourier amplitude spectra of 12 10-second windows of the ambient translational motion from the average of Channels 32 and 33 in the east direction, and the average of the amplitudes. The translational modes are shown at near 0.3, 1.2, 2.6 and 4.1 Hz)

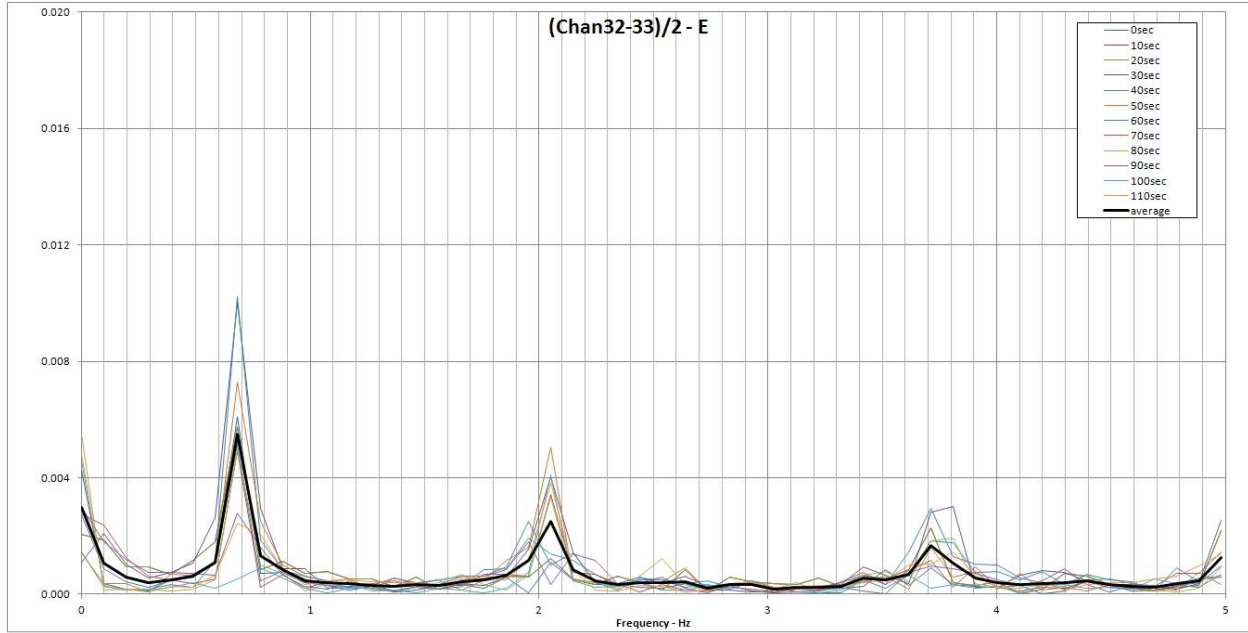


Figure 10. Fourier amplitude spectra of 12 10-second windows of the ambient torsional motion from the difference of Channels 32 and 33 in the east direction, and the average of the amplitudes. The torsional modes are shown at near 0.7, 2.1 and 3.7 Hz.

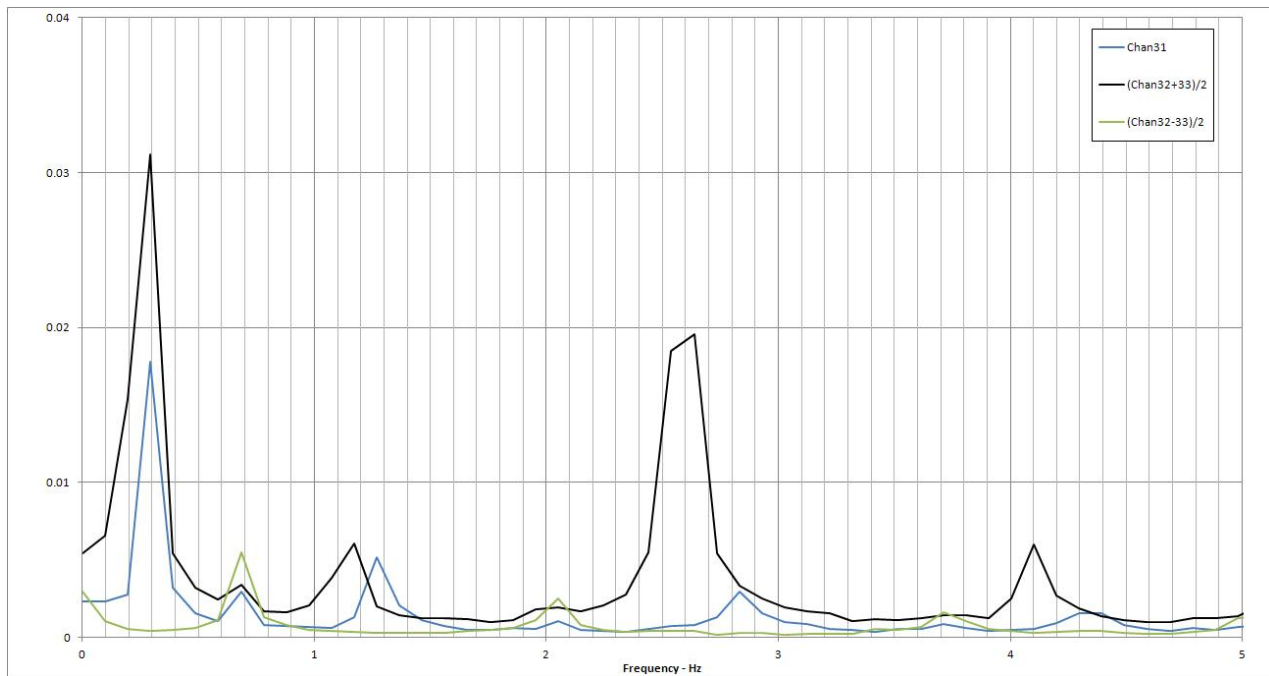


Figure 11. Average Fourier amplitude spectra of the ambient data from Channel 31 (N), and the average (translational motion) and difference (torsional motion) of Channels 32 (E) and 33 (E).

The simple analysis reflected in Figures 8 to 11 indicates that the frequencies of the first three fundamental modes are at about 0.3 Hz (N-S), 0.3 Hz (E-W) and 0.7 Hz (torsion), or 3.3 sec, 3.3 sec and 1.4 sec, respectively. The fundamental period of about 3.3 seconds can also be estimated from the velocity records shown in Figure 12, which were integrated and processed from the acceleration records shown in Figure 7. Furthermore, Figure 8 shows higher modes in the north-south direction at about 1.3 and 2.8 Hz. For the east-west direction, Figure 9 shows higher modes at about 1.2, 2.6 and 4.1 Hz. The mode of 2.6 Hz is predominant in the spectra shown in Figure 9 or 11. Higher torsional modes occur at about 2.1 and 3.7 Hz as shown in Figure 10. These modal parameters correspond to the linear response of the building to small ambient excitation and can serve as the baseline model for the building response to earthquakes. The fundamental period of 3.3 seconds is relatively short for a 62-story building, for which the building structure is subjected to very low level of excitation. This period is expected to be longer during earthquake shaking.

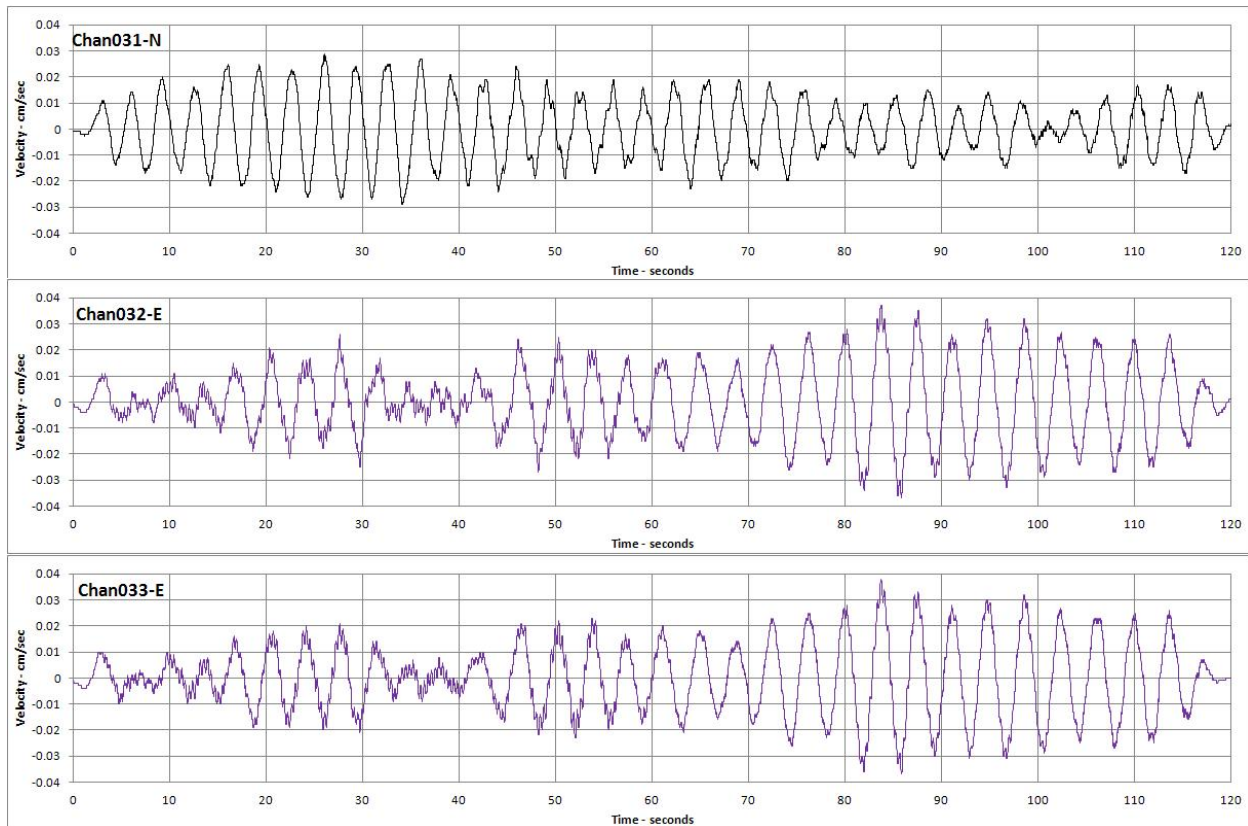


Figure 12. Velocity time histories integrated and processed from the acceleration data recorded by Sensors 31, 32 and 33 shown in Figure 7. A frequency band of 40 Hz to 6 seconds was used.

The velocity time history ambient records from selected sensors along the height of the building are plotted in Figure 13 for the east-west direction and in Figure 14 for the north-south direction. The beat phenomenon can be observed in the east-west direction, caused by the coupling between the building structure and the liquid damper system. The beat phenomenon has been observed in most combined structure-liquid damper systems (Yalla and Kareem, 2001).

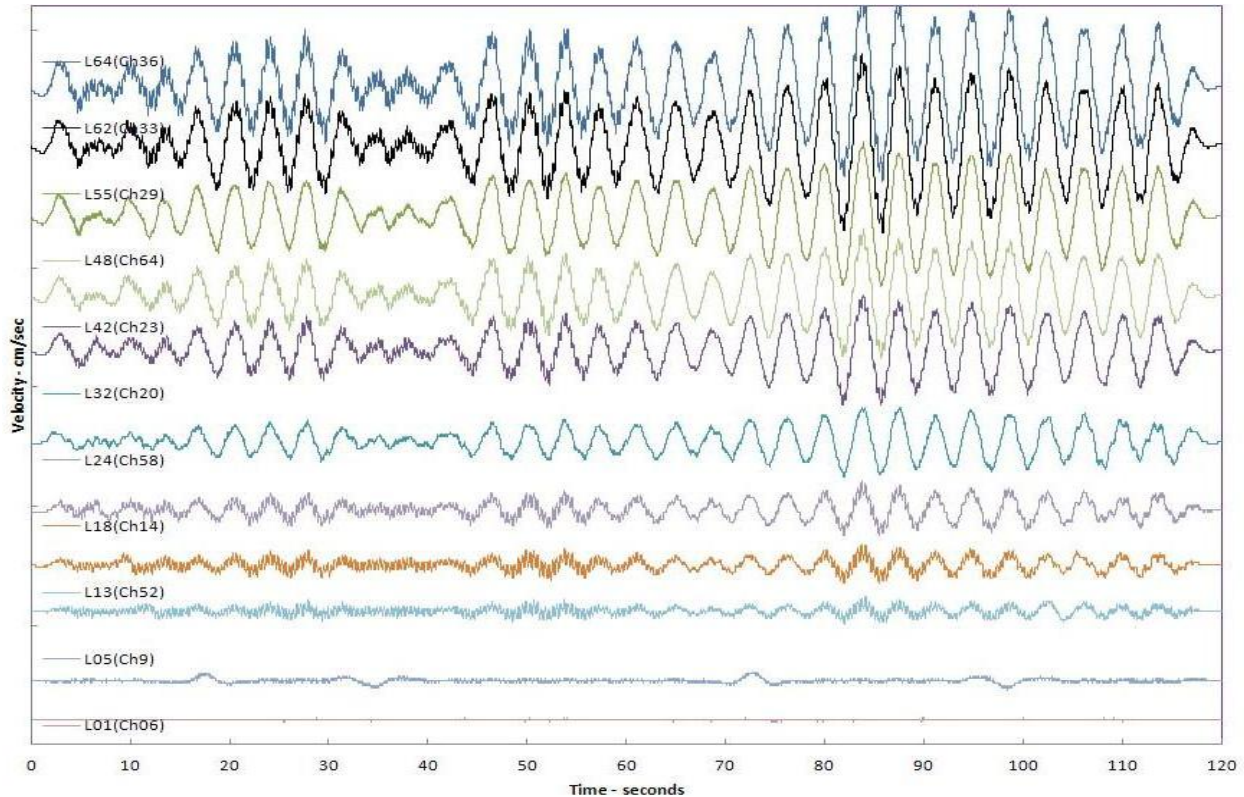


Figure 13. Velocity ambient records from selected sensors in the east-west direction, along the height of the building.

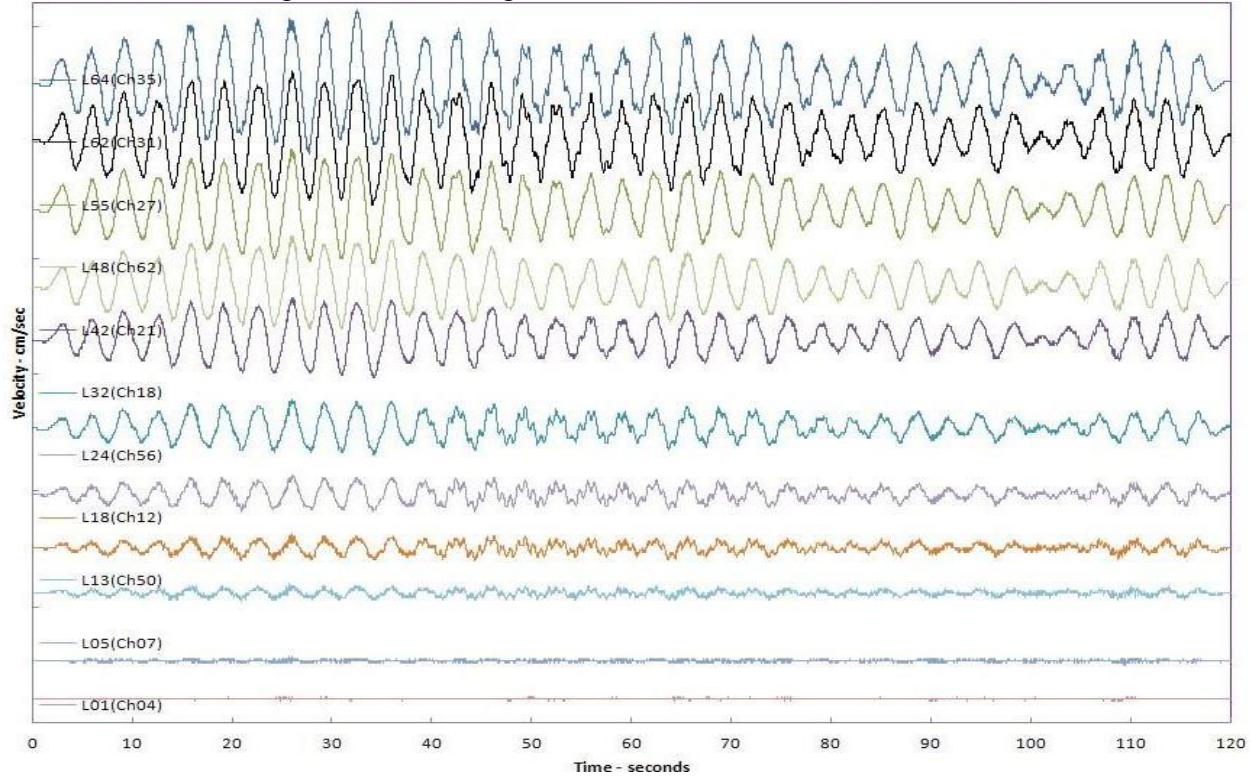


Figure 14. Velocity ambient records from selected sensors in the north-south direction, along the height of the building.

Summary

The One Rincon Hill Tower in San Francisco was jointly and extensively instrumented by the California Strong Motion Instrumentation Program of the California Geological Survey and the National Strong Motion Program of the U.S. Geological Survey in 2012. The instrumentation system can be manually triggered to record ambient vibration data. It will record building seismic response data from which the building performance can be understood and the effectiveness of the performance-based seismic design can be assessed after future significant earthquakes. The recorded data will be available so that the near-real-time data can be used for post-earthquake evaluation of the building performance.

Acknowledgement

The California Strong Motion Instrumentation Program of the CGS and the National Strong Motion Program of the USGS extend their appreciation to the Home Owners Association which permitted and cooperated in the installation of strong-motion equipment in the One Rincon Hill Tower. Beverly Wilson, general manager of One Rincon Hill Association, Ben Irving, building engineer and Jeff Sell, construction project manager, provided valuable assistance. Dr. John Parrish, State Geologist of the CGS and Dr. Tom Brocher, Director of the USGS Earthquake Science Center, coordinated the efforts of the two agencies. Drs. Joe Fletcher and Erol Kalkan of the USGS National Strong Motion Program developed the locations for 36 additional sensors. CSMIP also extends its appreciation to members of the Strong Motion Instrumentation Advisory Committee and its Buildings Subcommittee in recommending the building for instrumentation. Dr. Farzad Naeim of John A. Martin & Associates, Prof. Jack Moehle and Dr. Yousef Bozorgnia of the Pacific Earthquake Engineering Center reviewed and commented on the sensor locations proposed by CSMIP.

The instrumentation was made possible through the efforts of CSMIP engineers and technicians who planned and installed the instrumentation. The assistance of Deputy Director Hanson Tom of the City of San Francisco Department of Building Inspection was important in obtaining the City's support. CSMIP staff D. Swensen and E. Kalkan (now with the USGS) assisted with engineering; the instrumentation was installed by R. Schoengarth, S. Fife, J. Filak, D. Leiser, and A. Bollinger.

References

Celebi, M. Huang, M., Shakal, A., Hooper, J., and Klemencic, R. 2012, "Ambient Response of a Unique Performance-Based Design Building with Dynamic Response Modification Features," *Proceedings of SMIP12 Seminar on Utilization of Strong-Motion Data*, Sacramento, California, October 2, 2012.

Klemencic, R., Fry, J.A., and Hooper, J.D., 2006, "Performance-Based Design of Tall Reinforced Concrete Ductile Core Wall Systems," *Annual Meeting of the Los Angeles Tall Building Structural Design Council - Alternative Procedures for Design of Tall Buildings*. p. 122-32

Post, N., 2008, "San Francisco's 590-ft Skyscraper Lifts Seismic Design Stature," in Engineering News Record, January 21, 2008, p. 22-26.

Post, N., 2012, "Program Expected to Validate Extreme Seismic Engineering," in Engineering News Record, June 11, 2012, p. 16.

Klemencic, R. 2008, "Performance Based Seismic Design - Rising," in STRUCTURE magazine, June 2008, p. 10-13.

Treadwell & Rollo, Inc., 2004, "Updated Geotechnical Investigation, One Rincon Hill, 425 First Street, San Francisco, California," dated February 20, 2004.

Yalla, S. and Kareem, A., 2001, "Beat Phenomenon in Combined Structure-Liquid Damper Systems," in Engineering Structures, 23, 2001, p. 622-630.

AMBIENT RESPONSE OF A UNIQUE PERFORMANCE-BASED DESIGN BUILDING WITH DYNAMIC RESPONSE MODIFICATION FEATURES

Mehmet Çelebi¹, Moh Huang², Antony Shakal², John Hooper³ and Ron Klemencic³

¹Earthquake Science Center, USGS, Menlo Park, CA 94025

²California Geological Survey, Sacramento, CA 94814

³Magnusson Klemencic Associates, Seattle, WA 98101

Abstract

A 64-story, performance-based design building with reinforced concrete core shear-walls and unique dynamic response modification features (tuned liquid sloshing dampers and buckling-restrained braces) has been instrumented with a monitoring array of 72 channels of accelerometers. Ambient vibration data recorded are analyzed to identify modes and associated frequencies and damping. The low-amplitude dynamic characteristics are considerably different than those computed from design analyses, but serve as a baseline against which to compare with future strong shaking responses. Such studies help to improve our understanding of the effectiveness of the added features to the building and help improve designs in the future.

Introduction

A new, landmark building decorates the panorama of San Francisco, CA. Completed in 2008, the 64-story tall and slender building with reinforced concrete shear-wall core (hereafter referred to as “the building”) is described as the tallest building in the United States designed using performance-based seismic design (PBSD) procedures (*written information by MKA, 2012*) and applying unique structural dynamics modification features such as buckling restrained braces (BRBs) and tuned liquid sloshing dampers (TSD). These features qualify the building also as being the tallest performance-based seismic design (PBSD) in the world using BRBs (*written information by MKA, 2012*).

The purpose of this paper is to introduce an extensive seismic instrumentation project recently completed cooperatively by California Strong Motion Instrumentation Program (CSMIP) of California Geological Survey (CGS) and the National Strong Motion Project (NSMP) under the Advanced National Seismic Systems (ANSS) managed by United States Geological Survey (USGS). This instrumentation project includes a 72-channel seismic monitoring system of this station (Station no. CSMIP 58389; NSMP 1871) that streams real-time acceleration data from multiple floors starting at Level 1 (Basement Parking Level P4) up to Level 64 (roof).

Recognizing that there is no known data from such a unique design, we obtained ambient vibration data on demand from the installed monitoring system to understand the behavior of the

building, with the caveat that behavior during stronger shaking during strong earthquakes or high winds may be different than that from low-amplitude ambient shaking. In particular, the response of the building during strong shaking is expected to be significantly altered by the special structural features described above. Thus, the dynamic characteristics identified from ambient response of the building will be the baseline elastic response. The scope of this paper includes a description of the building, the monitoring system, and a discussion of the building behavior as inferred from the response analyses ambient data. Finite element model analyses are not included, but references are made to those performed by the designers. The structural instrumentation process and more details of the building are provided in a separate paper by Huang and others (2012).

In this paper, we used spectral analyses techniques as described in Bendat and Piersol (1980) and coded in public domain software, Matlab (Mathworks, 2012). We also used system identification techniques to extract mode shapes and associated frequencies and damping.

The Building

Figure 1 shows a Google Earth[©] 3-D street view of the building in close proximity to another San Francisco landmark, the San Francisco Bay Bridge (SFBB). The west anchorage structure for suspension cables of the SFBB is approximately 100 m from the building, and thus may be a significant source of vibration for the building.

In Figure 2, a rendering of the building and its main skeletal core shear wall and “outrigger” BRB system are shown, as well as two vertical sections showing distribution of the 72-channel accelerometer array. The total height of the building is 188.31 m (617.83 ft).

Figure 3 depicts several typical floor plan views displaying core shear walls, “outrigger” columns, orientations and approximate locations and of installed accelerometers and also the tuned liquid sloshing damper pools at the 62nd level. The plan views also show the true north and reference north (hereinafter referred to as NS). A typical floor area of this condominium building is approximately 880 m² (9500 ft²). The thickness of the core shear walls from Level 1 (Parking Level 4) to the 32nd Level is 81.3 cm (32”), from 32nd Level to 55th Level is 71.3 cm (28”) and from 55th Level to the top of the building is 61.0 cm (24”). Thus, with these shear-walls, the wall-to-floor area percentages change from ~ 2.4-3.9%, making the building one with considerably higher wall-to-floor percentages and comparable to average percentages of the shear-wall buildings in Chile that performed well during the 1985 Valparaiso (M=7.8) and 2010 Maule (M=8.8) earthquakes. Outrigger concrete column thicknesses generally follow those of the core shear wall and are generally 2.29 m (7.5’) wide. If the outrigger and other columns are considered, the lateral force resisting elements (columns and walls) to the floor area percentages increase by about 35 % providing the building a comparatively large stiffness and strength. In general floor slabs are 30.5 cm (12”) throughout the core but changes to 20.3 cm (8”) outside of the core.

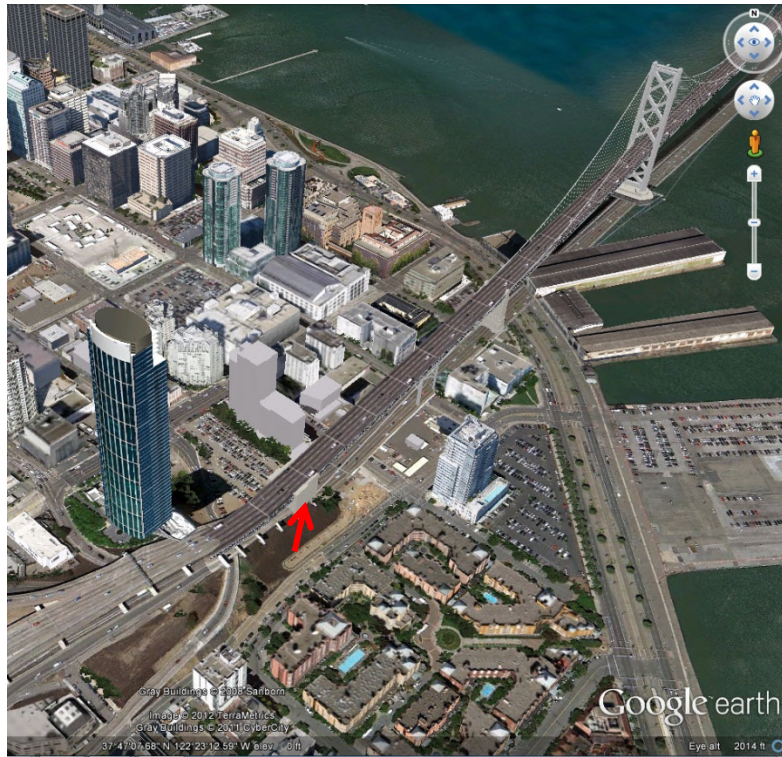


Figure 1. Google Earth[©] street view showing the building (left center) and vicinity, and the west end of the San Francisco Bay Bridge (SFBB). Arrow points the west anchorage structure of the SFBB, which is approximately 100 m from the building.

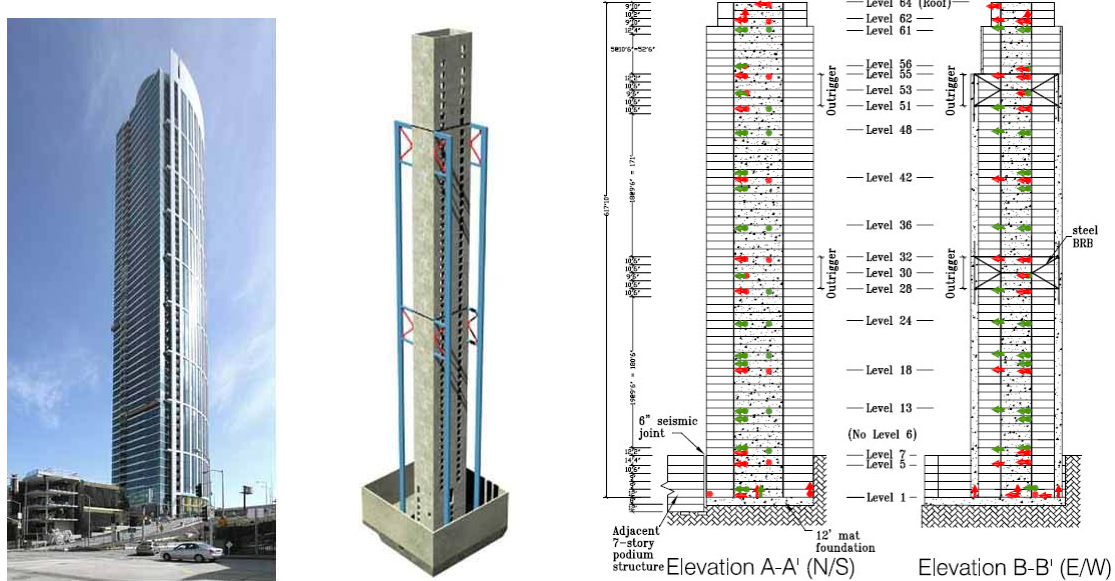


Figure 2. (Left) Rendering of the building and its skeleton core shear wall, outrigger columns and BRBs, and (Right) Vertical sections of the building showing locations of the accelerometers along the height of the building (www.stongmotioncenter.org, last visited July 29, 2012). Red and Green colors refer to channels installed by CSMIP and USGS NSMP respectively.

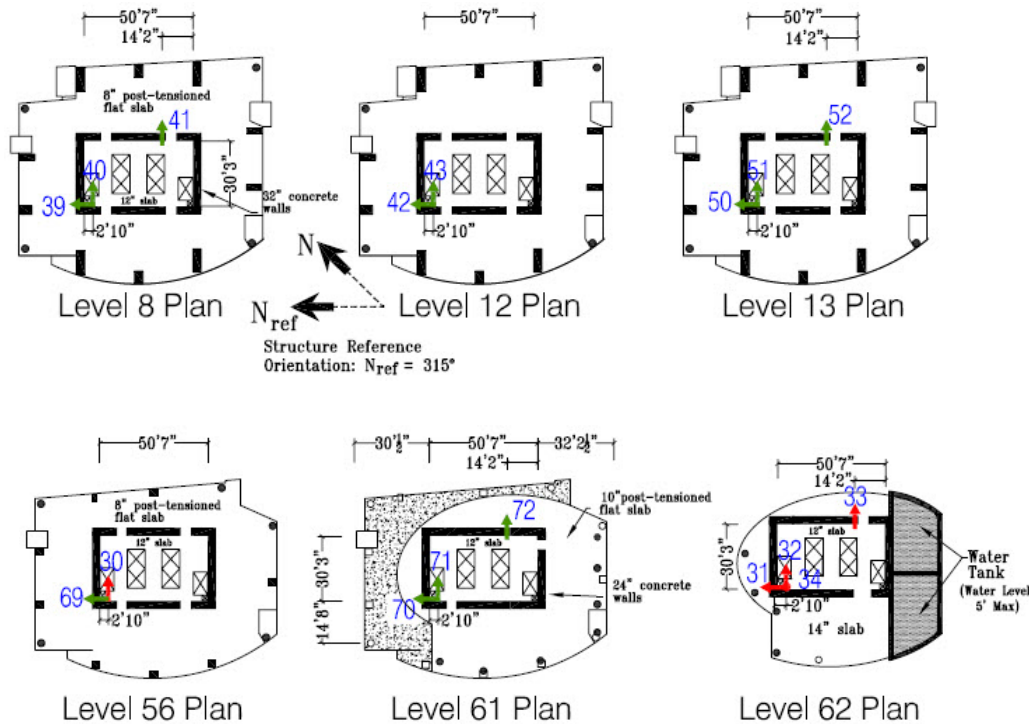


Figure 3. Typical plan views exhibiting sensor locations, general dimensions and the core shear wall and outrigger columns (www.stongmotioncenter.org, last visited July 29, 2012).

The building has a 3.7 m (12') mat foundation on Rincon Hill of San Francisco. The area has a geological formation described as a clastic sedimentary outcrop of sandstone and shale (Schlocker, 1974). Fumal (1974, 1991) confirms this description as sandstone and shale of Franciscan assemblage and provides an average 30-meter shear wave velocity, $V_s=745\pm140$ m/s for Rincon Hill. With assumption of 30 m depth for this average shear wave velocity, a short site period $T_s \sim 0.16$ s can be computed. However, the actual period for such a site is possibly much shorter, which, of course, is also much shorter than the fundamental period of a 64-story building, even with the response modification features, and clearly indicates that site effects will not be a significant factor in the responses of the building.

During design of the building, Design Basis Earthquake (DBE) and Maximum Considered Earthquake (MCE) levels of analyses were performed for 5 % damped spectra corresponding to 10% probability of exceedance in 50 and 100 years, respectively. For DBE elastic analysis, an FEM model of the building was subjected to a DBE spectrum scaled to San Francisco Building Code (SFBC) Section 1631.5. Corresponding Zero Period acceleration for DBE and MCE are 0.505g and 0.602g respectively. The two design response spectra are shown in Figure 4 (*written information by MKA, 2012*). Both response spectrum and non-linear time-history analyses have been performed by the designers. Ground motions recorded at select stations during seven large earthquakes with magnitudes ranging from 6.9 (1989 Loma Prieta, Los Gatos PC station) to 7.9 (2002 Denali, Pump station 10) have been used for non-linear

analyses. For base shear evaluation at DBE level, SFBC period equation 30.8: $T=C_t(h_n)^{.75}$ for $h_n=577.33$ ft was computed as 2.36 s ($f=0.42\text{Hz}$). According to SFBC, this can be increased by 30% to $T=3.06$ s ($F=0.327\text{ Hz}$). These values are compared with other data-identified characteristics later in the paper.

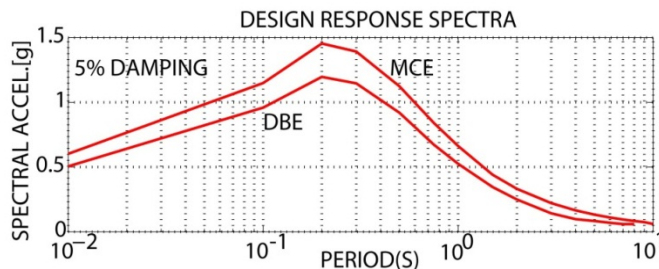


Figure 4. Design Response Spectra for DBE and MCE.

Seismic Instruments and Summary of Ambient Data

Through an agreement, CSMIP and NSMP collaborated in instrumenting the building. There are 72 channels of accelerometers distributed throughout the building to capture its translational, torsional and vertical motions, and specifically to measure the motions at the levels where the outrigger BRBs and tuned liquid sloshing dampers are located. Table 1 displays cross reference of the horizontal accelerometers at different levels. Four vertical channels (1-3 at Level 1 and 34 at Level 62) are not listed in the table. Due to the underlying geology, and the tall and slender design of the building, soil-structure interaction (*e.g.* rocking) is not expected.

The accelerometers used in the building are Kinematics Episensors¹ with $\pm 4\text{g}$ full-scale recording capability and the recorder system is a Kinematics Granite⁴. The accelerometers are powered via cables from the recorder with ± 12 volt DC, and have a power consumption of 1.6 amperes and ± 2.5 volt output range. The analog signals from the sensors are digitized at a very high sampling rate within the recorder, and then digital data are multiplied by a calibration constant based on the voltage output and decimated with application of an anti-alias filter to the desired sampling rate. USGS obtains and serves the digitized data at 200 samples per second.

General information on structural monitoring procedures and suggestions for deployments of accelerometers can be found in COSMOS (2001) and Çelebi (2004). The choice of locations for sensors is not based on mathematical formulas or computations.

Data used in this paper were obtained on demand from the monitoring system of the building. Table 2 summarizes the recording intervals and length of the data. We used four of these data sets in this paper to infer the behavior of the building and repeatability of the results

¹ Mentioning commercial names in the manuscript is for information only and does not indicate endorsement of the manufacturer or the products.

during low-amplitude ambient motions. The largest peak amplitude of acceleration among all the data sets is <1.5 gal.

Table 1. Distribution and labeling of horizontal channels along the height of the building.

Level	H(m)	H(ft)	Channel Numbering (used in analyses)		
			NS	EW1	EW2
1	0	0	37	38	6
5	12.34	40.5	7	8	9
7	16.71	54.83	10	11	
8	20.41	67	39	40	41
12	32	105	42	43	
13	34.9	114.5	50	51	52
18	49.38	162	12	13	14
19	52.27	171.5	44	45	
20	55.17	181	53	54	55
24	66.75	219.66	56	57	58
28	78.33	257	15	16	65
30	84.73	278	66	17	
32	91.13	299	18	19	20
36	103.72	337	59	60	61
41	117.7	384.5	46	47	
42	120.1	394	21	22	23
43	122.99	403.6	48	49	
48	137.46	451	62	63	64
51	146.46	480.5	24	25	67
53	152.55	500.5	68	26	
55	159.46	523.17	27	28	29
56	162.67	533.67	69	30	
61	179.22	588	70	71	72
62	185.21	607.83	31	32	33
64	188.31	617.83	35		36

Table 2. Summary of ambient data recorded on demand from the monitoring system.

Date(MMDD)/Time(HHMM)	Length of Data, s	Raw Data (Samples Per Sec)
06011459	120	200
06012159	120	200
06040921	120	200
07022012	240	200
07030159	298	200

Data Analyses

Time-History Plots of Sample Data Set

Figure 5 shows time-history plots of accelerations and displacements for the data set obtained on July 2, 2012. In these plots, accelerometer channel organization described in Table 1 (translational NS, EW1 and EW2 alignments and torsional [EW1-EW2]) are used.

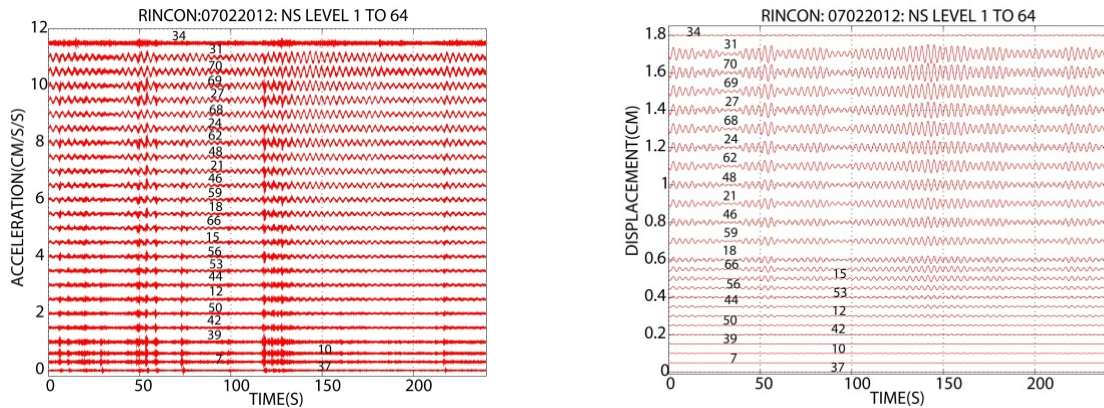


Figure 5a. Time history plots of accelerations (left column) and displacements (right column) of translational (NS) motions for data set of July 2, 2012.

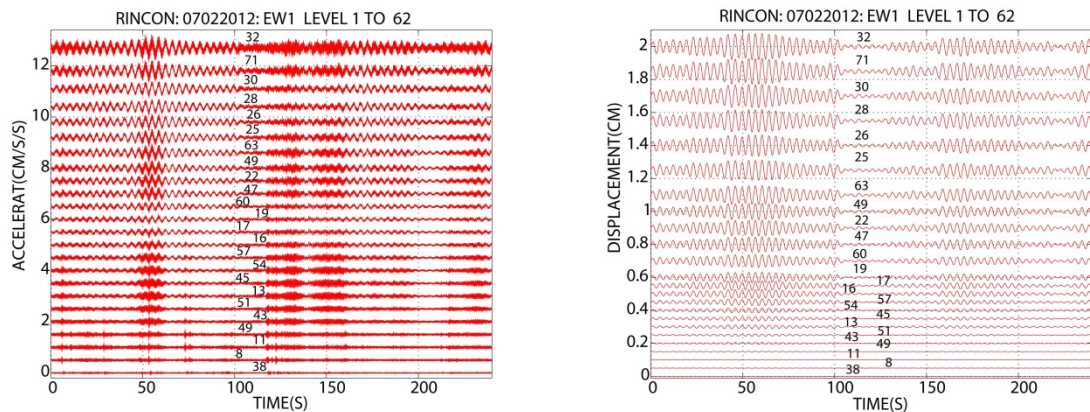


Figure 5b. Time history plots of accelerations (left column) and displacements (right column) of translational (EW1) motions for data set of July 2, 2012.

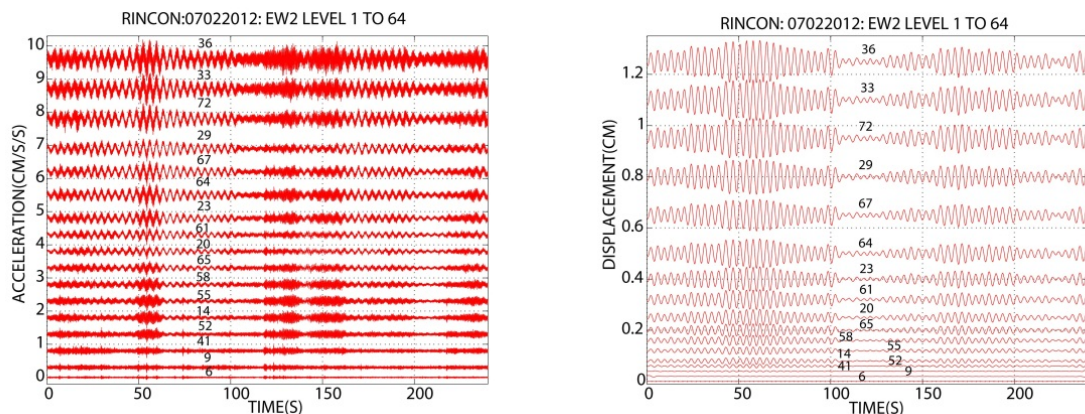


Figure 5c. Time history plots of accelerations (left column) and displacements (right column) of translational (EW2) motions for data set of July 2, 2012.

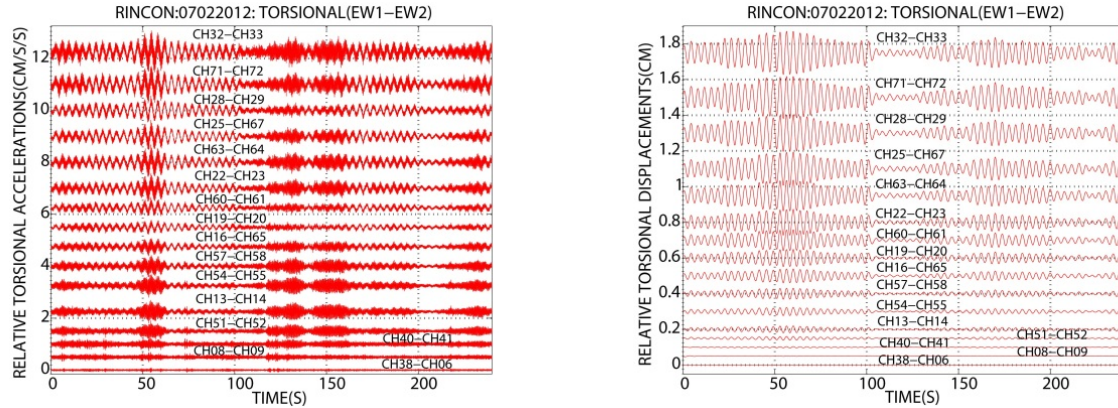


Figure 5d. Time history plots of relative torsional accelerations (left column) and relative torsional displacements (right column) of motions for data set of July 2, 2012.

Spectral Analyses

Due to space limitations, detailed spectral analyses of only the data set 0604212 are presented. Summary cross-spectrum (S_{xy}), phase angle and coherency plots for other data sets are also provided to exhibit repeatability in identification of translational and torsional modal frequencies.

Figure 6 shows at least five modes in perfect to near-perfect coherence and consistent phase angles corresponding to the 1st, 2nd, 3rd, 4th and 5th modal frequencies for the translational (NS, EW1 and EW2) and torsional modes.

Summary cross-spectra plots for four data sets are provided in Figure 7 and confirm that the identified frequencies are consistent for all four data sets.

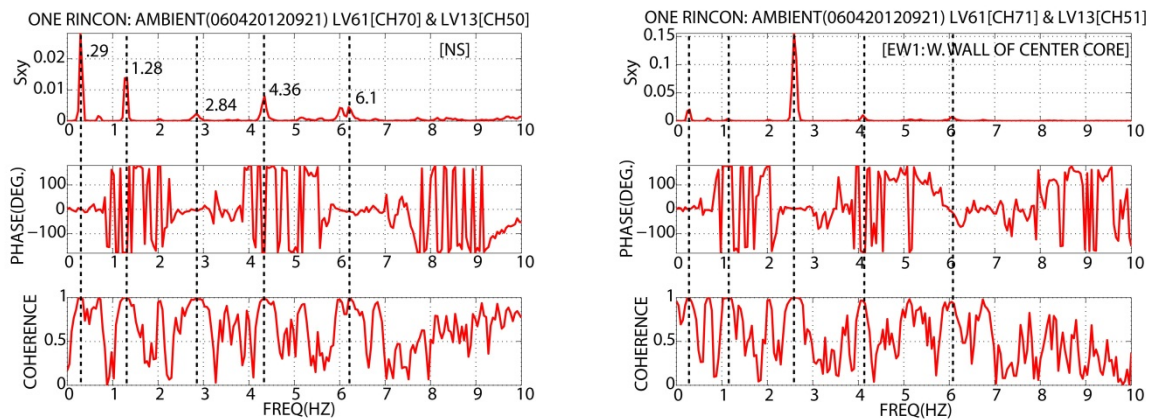


Figure 6a. Using data from Levels 61 and 13, cross-spectra, phase angle and coherency plots identify modal frequencies for (a) left: NS direction, (b) right: EW1 direction using channels aligned with west end of core shear wall.

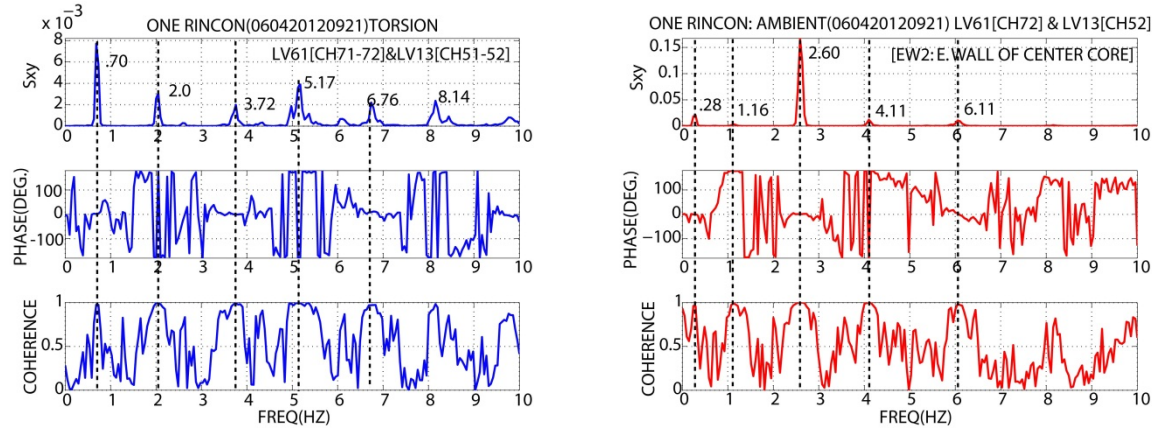


Figure 6b. Using data from Levels 61 and 13, cross-spectra, phase angle and coherency plots identify modal frequencies for (c) left: torsion using data from levels that have two EW parallel channels (EW1-EW2), and (d) right: EW2 direction: using channels aligned with east end of core shear wall.

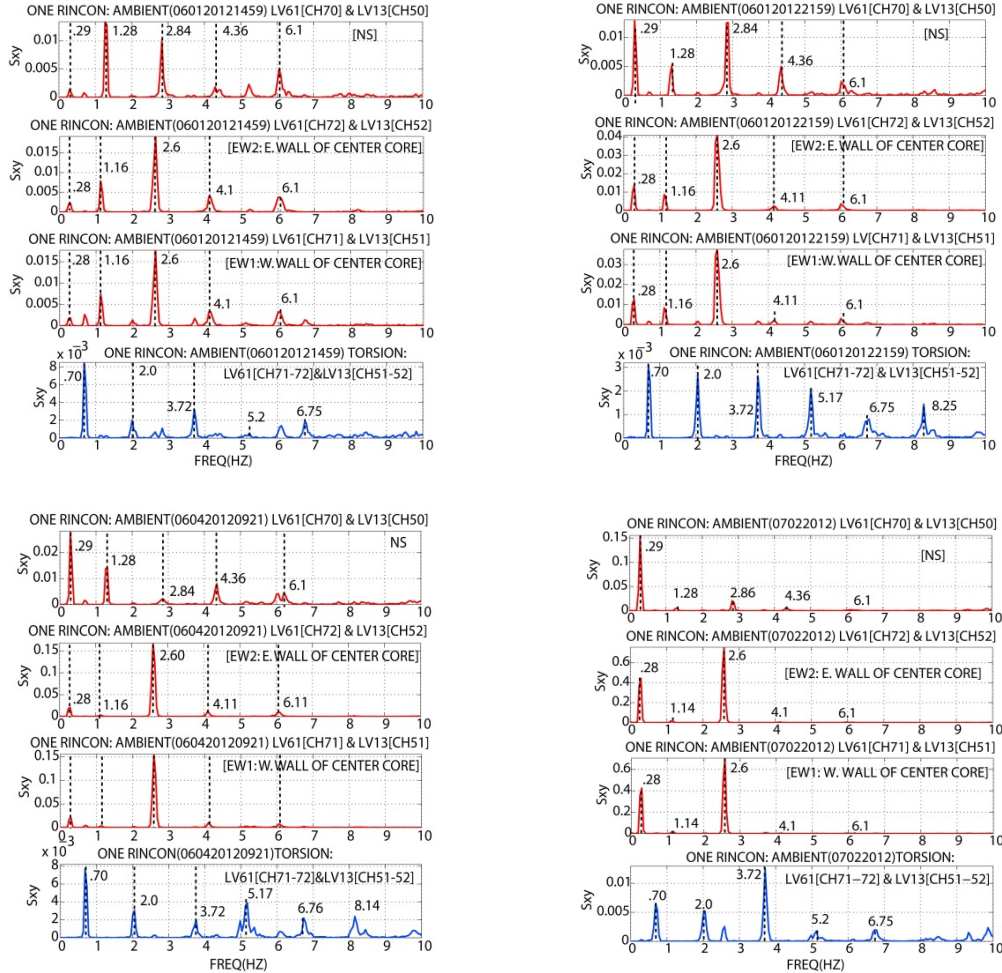


Figure 7. Summary cross-spectral amplitudes for translational (NS, EW1 and EW2) and torsional motions.

System Identification, Extraction of Modal Shapes, Frequencies and Damping

System identification analysis was performed using the ambient data to identify and/or validate key frequencies and compare them with those determined by spectral analyses. In this study, we used measured data from the building as output to estimate a predefined number of order of state-space model using subspace method as coded within Matlab (Mathworks, 2012). Further details of background of this method are not repeated herein as they are provided in many publications including Matlab (2012), Ljung (1999), van Overschee and De Moor (1996) and Juang (1994).

Corresponding to only the 06041459 data set, five mode shapes and corresponding frequencies and damping ratios for each of the output data identified with NS, EW1, EW2 and EW1-EW2 (torsion) directions accelerations listed in Table 1 are presented in Figure 8.

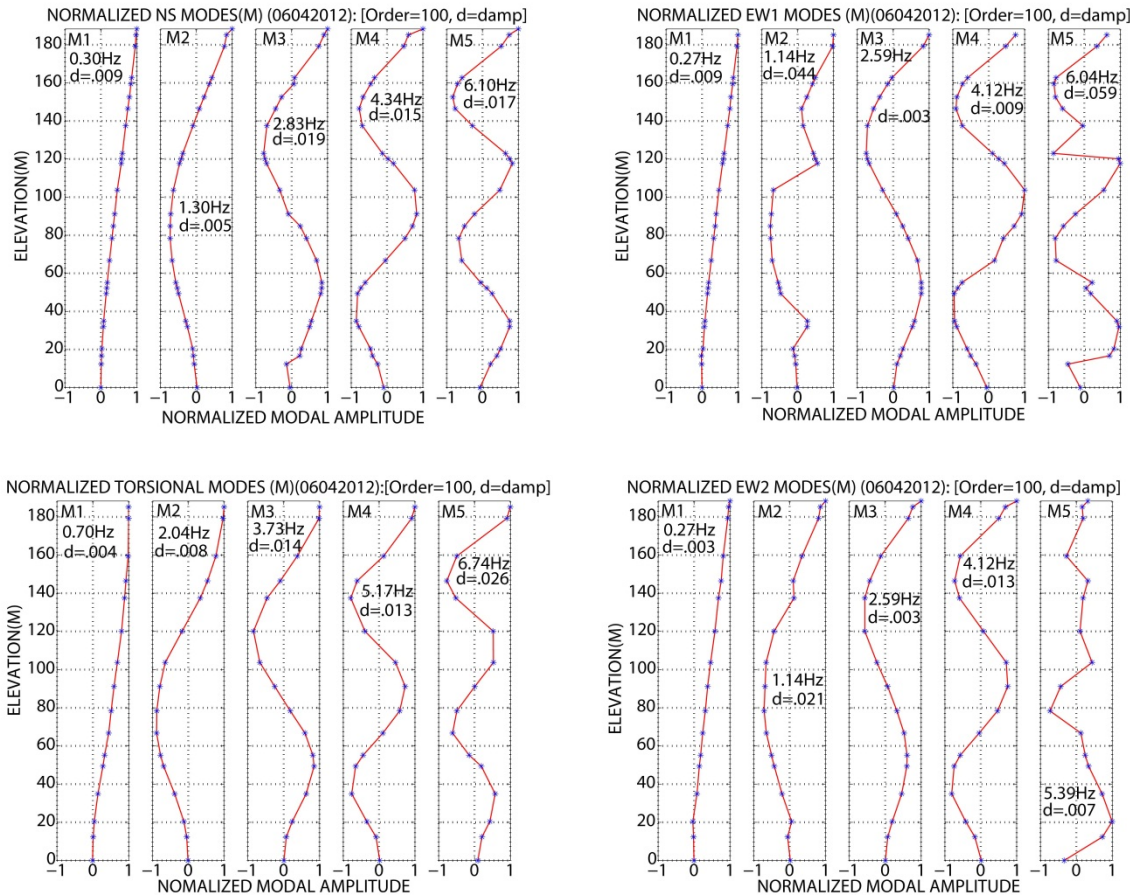


Figure 8. Identified modal shapes, frequencies and damping percentages for NS, EW1, EW2 and torsion (EW1-EW2) for data set 06042012.

As shown in this figure, the mode shapes conform reasonably to expectation with some irregularities at higher modes. The modes shapes do not indicate any alterations due to BRBs or TSDs.

Compilation and Comparison of Dynamic Characteristics

Dynamic characteristics identified from ambient data are compared to those computed during design analyses as summarized in Table 3.

Table 3. Comparison of Dynamic Characteristics of the Building.

Code [SFBC Section 1630.2 Equation 30-8] (<i>written comm. MKA, 2012</i>)					
$T=C_t(h_n)^{75} = 2.36s$ ($f=.42Hz$) [increased 30 % to 3.06 s or .327 Hz]					
DBE Level Elastic Analysis (<i>written comm. MKA, 2012</i>)					
Mode	NS	EW	Torsion		
1	4.91s .204Hz	5.51s .182Hz	2.26s .443Hz		
MCE Level Non-Linear Analyses (<i>written comm. MKA, 2012</i>)					
1	4.53s .221Hz	5.04s .198Hz	1.86s .538Hz		
Ambient Data : Spectral Analyses (<i>This study</i>)					
Mode	NS	EW	Torsion		
	T(s)/f(Hz)	T(s)/f(Hz)	T(s)/f(Hz)		
1	3.45 .290	3.57 .280	1.43 .700		
2	.781 1.28	.862 1.16	.5 2.0		
3	.352 2.84	.385 2.60	.269 3.72		
4	.229 4.36	.244 4.10	.192 5.2		
5	.164 6.10	.164 6.10	.148 6.75		
Ambient Data: System Identification (<i>This study</i>)					
Mode	NS	EW(*)	Torsion		
	T(s)/f(Hz)	ξ (%)	T(s)/f(Hz)	ξ (%)	T(s)/f(Hz)
1	3.33 .300	.9	3.70 .270	.3-.9	1.43 .700
2	.769 1.30	.5	.877 1.14	2.1-4.4	.490 2.04
3	.353 2.83	1.9	.386 2.59	.3	.268 3.73
4	.230 4.34	1.5	.243 4.12	.9-1.3	.193 5.17
5	.164 6.10	1.7	.166-.186 5.39-6.04	.59-.7	.148 6.74
(*) Note: Variations in EW direction is due to two analyses on EW1 & EW2 line-up of data					

Discussion and Conclusions

To serve as a baseline for future data analyses, be they low-amplitude or strong shaking, ambient data were recorded on demand from this building with unique dynamic characteristics modification features such as BRBs and TSDs. At the recorded level of low-amplitude shaking (maximum accelerations < 1.5 gals), dynamic characteristics (periods, mode shapes and damping percentages) have been identified using well-known spectral analyses and system identification techniques and are summarized in Table 3.

The NS, EW and torsional periods (frequencies) for the first five modes obtained by spectral analyses and system identification techniques as described herein are similar. The first modal damping percentages (<1%) are low, as can be expected from ambient motions and observed in previous studies (Çelebi, 2004, Çelebi and others, 2012). The mode shapes of the building appear to be normal, which suggests that at these low-amplitude levels of shaking, the aforementioned BRB and TSD features contributed very little if any to its behaviour.

However, as might be expected, the ambient fundamental periods (frequencies) are considerably different from those computed by using the code formula and from DBE level elastic and MCE level analyses. This may be explained by the fact that, during the DBE and MCE level analyses, BRB and TSD characteristics were considered. For example, although linear elastic material behaviour have been assumed in the DBE analyses, and nonlinearities by the actions of the dynamic response modification features (tuned liquid sloshing dampers and buckling restrained braces) were included in the MCE analyses that alter the dynamic characteristics discussed, the fact that the results from MCE level analyses do not match with those from ambient data analyses is therefore not surprising.

As discussed earlier in the paper, future strong shaking data to be retrieved from the state-of-the-art seismic monitoring array of this building will be the main test to assess its behavior, performance and effectiveness of the dynamic response modification features integrated into the building. The results from the ambient data presented herein will serve as a baseline for comparison for any other result obtained using data at higher level of shaking.

Acknowledgements

Data used in this study were obtained on demand by CSMIP from the seismic monitoring array of the building. The array was designed by CSMIP and NSMP staff and deployed as a collaborative effort between CSMIP and USGS. Thanks are due to Chris Stephens, Manager of Strong Motion Data Center of NSMP (USGS) for diligently processing some of the data. The home owners association of the building and the design engineering company, MKA provided requisite information to carry out this study. Thanks are due to Roger Borcherdt and Chris Stephens for review of the paper.

References

- Bendat J. S. and Piersol, A. G. (1980). *Engineering Applications of Correlation and Spectral Analysis*. John Wiley and Sons, New York, N.Y.
- Çelebi, M.(2004). Structural Monitoring Arrays – Past, Present and Future, PROC. NATO SFP Workshop on Future Directions on Strong Motion and Engineering Seismology, Kusadasi, Izmir, Turkey, May 17-21, 2004. *in* Future Directions in Strong Motion Instrumentation (eds. P. Gulkan and J. Anderson), NATO Science Series: IV. Earth and Environmental Sciences, Kluwer Academic Publishers, v. 58, pp. 157-179.
- Çelebi, M., Toksöz, N., and Büyüköztürk, O. (2012). Rocking behavior of an instrumented unique building on the MIT campus identified from ambient shaking data, paper submitted to Earthquake Spectra.
- COSMOS. (2001). Proceedings of Invited Workshop on Strong-Motion Instrumentation of Buildings, CP-2001/04.
- Fumal, T. (1978). Correlations between seismic wave velocities and physical properties of near-surface geologic materials in the southern San Francisco Bay region, California, USGS Open-File Report 78-1067.
- Fumal, T. (1991). A Compilation of the Geology and Measured and Estimated Shear-Wave Velocity Profiles at Strong-Motion Stations that Recorded the Loma Prieta, California, Earthquake, USGS Open-File Report 91-311.
- Huang, M., Shakal, A., Petersen, C., Çelebi, M., Hooper, J., and Klemencic, R. (2012). Strong Motion Instrumentation of a 62-story concrete core residential building in San Francisco, Proc. SMIP12 Seminar on Utilization of Strong-Motion Data, Sacramento CA. Oct. 2, 2012.
- Juang, J. N. (1994). *Applied System Identification*, Prentice Hall, Upper Saddle River, NJ. 394 pages.
- Ljung, L. (1987). *System Identification: Theory and User*. Prentice hall, Englewood Cliffs, NJ.
- Mathworks. (1988 and newer versions). Matlab Users Guide. System Identification Toolbox for use with Matlab, The Mathworks Inc., South Natick, MA.
- Schlucker, J. (1974). Geology of the San Francisco North quadrangle, California: U.S. Geological Survey Professional Paper 782, 109 p.
- Van Overschee, P. and De Moor, B. (1996). Subspace identification for linear systems. Kluwer Academic Publishers, Dordrecht, The Netherlands.

HOSPITAL SEISMIC SAFETY PROGRAM AND STRONG MOTION INSTRUMENTATION

Chris Tokas and Roy Lobo

Office of Statewide Health Planning and Development
Sacramento, California

Abstract

The need for functioning hospitals after a major earthquake is obvious and rarely disputed. While emergency field hospitals, medical tents, and air-lifts to available facilities are often used to supplement for damaged hospitals, they will never provide a sufficient substitute. Only modern health care facilities, located within the damaged region and capable of functioning at full capacity can adequately provide the needed medical assistance.

The Health and Safety code requires insofar as practicable California hospital buildings to continue to provide services after a disaster and designed and constructed for forces generated by earthquake, gravity, and wind. While the expected operational performance of new hospital buildings can be estimated with a reasonable degree of accuracy, the performance of existing structural, non-structural and operational components are more difficult to ascertain. The degree of nonstructural damage or inherent structural damage can be difficult to ascertain immediately after a seismic event. Current seismic codes have come a long way since the start of seismic design. However there is a large inventory of the hospital buildings that predate modern seismic codes. Even hospital buildings designed with modern seismic codes have not been seriously tested in a large urban earthquake. With practical and monetary limits to laboratory testing, it makes sense to instrument hospital buildings to determine actual performance in an earthquake. There is also a need for use of the instrument recordings to provide automated damage indicators in these instrumented hospital buildings. Such instrumented damage indicators are required to supplement the traditional visual inspections immediately after a seismic event to make quick and reliable decision on whether to evacuate damaged buildings.

Hospital Seismic Safety Program

The 1972 Seismic Safety Act

The Hospital Seismic Safety Act (HSSA) as originally proposed called for the immediate strengthening or replacement of all hospital buildings that did not meet the modern standards. However, it was quickly realized that this was an economic impossibility. The proposed law was changed to apply only to new hospital buildings and existing hospital buildings undergoing substantial structural remodel or expansion and, therefore, all hospitals licensed at the time were “grandfathered” in – that is, they were not required to meet the new statewide standards. The intent was to bring any building whose useful life was being extended by a modernization program up to the modern seismic standards. However, the rate of retrofitting or replacing pre-

73 hospital buildings was much too slow. The unexpected result was to maintain the existing facilities as they are and build new facilities as needed.

In Northridge Earthquake of January 1994, several of these older hospitals sustained significant damage. Hospitals built in accordance with the standards of the Seismic Safety Act resisted the Northridge earthquake with minimal structural damage, while several facilities built prior to the act experienced major structural damage and had to be evacuated. It must be noted that certain nonstructural components of the hospitals did incur damage, even in facilities built in accordance with the structural provisions of the Seismic Safety Act.

Table 1. Performance of all hospital buildings in the Northridge Earthquake at 23 hospital sites with one or more yellow or red tagged buildings.

Type of Damage	Number (%) of Buildings	
	Pre Act	Post Act
Structural Damage		
Red tagged	12 (24%)	0 (0%)
Yellow tagged	17 (33%)	1 (3%)
Green tagged	22 (43%)	30 (97%)
Nonstructural Damage		
Major	31 (61%)	7 (23%)
Minor	20 (39%)	24 (77%)
Total Buildings	51	31

The lessons from the Northridge Earthquake clearly showed that the majority of California's hospitals located in regions of highest seismicity do not comply with the new "functionality" standards and their expected performance during a major earthquake varies from moderate damage to complete collapse. The California Legislature clearly understood that a program was needed to require hospitals to improve the seismic resistance of their existing buildings in a phased and prioritized manner with the ultimate goal of full strengthening or replacement. The legislative response was Senate Bill (SB 1953), which required that all hospitals meet statewide seismic safety standards. SB 1953 Seismic Retrofit Program

SB 1953 was introduced on February 25, 1994. It was signed into law on September 21, 1994 and became effective on September 22, 1994. The bill was an amendment of the Hospital Seismic Safety Act (HSSA) of 1983.

The first step in the retrofit program was the seismic evaluation of individual buildings. The evaluation placed each building in a Structural Performance Category (SPC), and a Nonstructural Performance Category (NPC). There are five levels of each performance category. The combined SPC and NPC rating of a building constitutes its overall seismic performance category. Buildings assigned to the Seismic Performance Category 1 (SPC 1) were built before the 1973 standards were enacted and assumed to pose a significant risk of collapse and public danger.

The SPC's were based on a plan as expressed in the law. Buildings which represent a "potential risk of collapse or pose a significant loss of life" have been required to be closed, retrofitted, or removed from acute care use by January 1, 2008. There is a provision in the law which allows delays in compliance with the 2008 deadline. The provision says, "A delay in this

deadline may be granted by the office upon a demonstration by the owner that compliance will result in a loss of health care capacity that may not be provided by other general acute care hospitals within a reasonable proximity". This was further defined in the California Administrative Code to be a maximum of five years thereby moving the compliance dead line to 2013. Almost all hospitals but 13 have applied and received this extension.

In the last few years several legislative mandates (due to economic pressures as well as other factors) amended the HSSA to allow for various extension paths to the January 1st 2013 seismic compliance deadline while leaving the compliance requirements for the full compliance date of 2030 unchanged.

Hospitals with buildings in the SPC 1 category (those in most danger of collapsing in an earthquake or other natural disaster) must be upgraded or removed from service by January 1, 2013, 2015, or 2020 – depending on the path they have chosen. The parameters and requirements for these paths are explicitly defined in the various legislatively amendments by SB 306, SB1661, SB 499, SB 608 and SB 90 made to the HSSA. There are a few variations for specific circumstances, but those dates are the significant extensions authorized by law.

The latest amendment is SB 90 which authorizes the Office of Statewide Health Planning and Development (OSHPD) to provide hospitals with an extension of up to seven years on an existing seismic safety deadline provided certain requirements are met. OSHPD would consider requests for extensions on a case by case basis based on the following criteria: (1) structural integrity of the building; (2) community access to care if the hospital building were to close; and (3) financial capacity of the hospital to complete the construction projection.

Early indications on SB 90 extension requests are that only about one third of the applicants are applying for the full seven year extension. The others extension requests vary from a couple of months to full seven years.

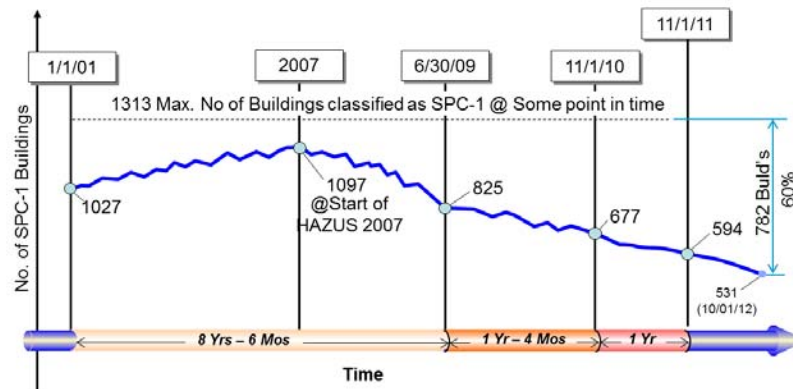


Figure 1 Rate of Removal of dangerous buildings (SPC-1) from the General Acute Care Hospital Building inventory.

That being said, hospitals are making progress. The numbers show that the program has come a long way. Thus, California hospitals indeed are safer today, but there is still work to do.

The final steps will occur between years 2013 and 2030. The law requires the buildings to be in substantial compliance with the Act by January 1, 2030 and all general acute care hospitals must be able to remain operational beyond that point in time.

During this 17 year period, retrofitting and new construction is expected to reach substantial compliance, that is, buildings housing patients will not collapse in a damaging seismic event and the systems serving critical care will continue to function in a design level earthquake.

Looking back at the first steps of the program as well as looking ahead at the approaching 2013 deadline it is imperative to point out how much progress has been achieved. While the critics may point out that not enough progress has been made, 60% of hospitals buildings rated as more dangerous have already been reclassified as SPC-2 or higher by retrofit or analysis. Some have been removed and many more will be added to that list by January 2013.

There are various paths to full operational compliance as the law allows for a “phased in” approach to meet the 2030 deadline while allowing interim deadlines. The seismic compliance regulations prior to 2007 required a full seismic evaluation of the buildings to be performed. This path appeared not to be achieving the desired results, and a new risk based approach had to be adopted.

Risk Based Seismic Evaluation of Pre 1973 Hospital Buildings Using the HAZUS Methodology.

The seismic evaluation of the existing hospital buildings yielded a surprisingly large number of buildings that required either retrofit or replacement and which constituted a large proportion of all acute care hospital buildings in California.

After careful evaluation of the SPC-1 hospital building inventory, it became obvious that all the SPC-1 buildings do not represent the same risk to life due to a major earthquake. Even though all hospital buildings were evaluated using the same regulatory requirements, the analysis varied highly with respect to sophistication and accuracy since the seismic evaluations were performed by different engineers across the state.

OSHPD, keenly aware of the cost of retrofitting, attempted to require only the absolute minimum and give as much flexibility as possible for compliance. It is important to point out that OSHPD has looked for ways to lessen the impact of the seismic retrofit program without jeopardizing safety. That has been achieved by constantly re-examining the program and realigning it by adopting policies to provide flexibility in its implementation, or by looking forward at the national level to adopt state of the art seismic retrofit standards.

In 2005, after careful evaluation through a variety of options, OSHPD selected the HAZUS earthquake loss estimation methodology as a tool to re-examine and assess the seismic risk for each SPC-1 hospital building. Utilizing the HAZUS methodology would rank the SPC-1 buildings based on their relative risk, thereby enabling the policy makers to implement “*Worst First*” *Compliance with the Hospital Seismic Safety Requirements*. The results of such a re-examination would allow hospitals to focus their resources appropriately on the “worst buildings first”.

The HAZUS methodology may be implemented using “default” engineering parameters that affect building performance. However, the default values were developed for “generic” model building types and they are not generally applicable to individual buildings. Furthermore, the HAZUS default damage functions are appropriate for fairly regular buildings, but tend to underestimate damage in buildings with “significant structural weaknesses”. A significant structural weakness is an attribute that causes the building to perform significantly worse than average. While building-specific analysis are not feasible for assessing the seismic risk of each SPC-1 hospital building, it was recognized that more appropriate engineering parameters that affect building performance should be developed to better represent the types comprising the SPC-1 building inventory. OSHPD augmented the algorithms of the HAZUS default parameters, thus permitting the appropriate adjustment in order to account for significant structural weaknesses where they occur.

The HAZUS/AEBM methodology provided the California hospital seismic compliance program the tools needed to examine and assess the seismic risk of each building individually in order to identify buildings that most likely will experience a catastrophic failure in the event of an earthquake and thereby focus on available resources to retrofit such buildings first.

Currently 319 buildings have been reclassified as SPC-2 using the HAZUS 2007 regulations and 58 buildings have been reclassified to SPC-2 using the HAZUS 2010 regulations. There are still 531 SPC-1 buildings in our inventory that are either to be reclassified or can no longer provide acute care services.

The OSHPD Seismic Instrumentation Program for Hospital Buildings.

The California Strong Motion Instrumentation Program (CSMIP) was established following the 1971 San Fernando Earthquake to increase the limited set of data on strong earthquake shaking. The CSMIP authorities emanate from the Public Resources Code, Section 2700:

There is hereby established in the State of California a strong-motion instrumentation program for the purpose of administering the program and of acquiring strong-motion instruments and installing and maintaining such instruments as needed in representative geologic environments and structures throughout the state.

However, Section 2709.1 of the Public Resources Code states the following:

- (a) *No strong-motion instrumentation shall be installed pursuant to this chapter in the structural types identified in subdivision (b) unless funds proportionate to the construction value as called for under Section 2705 are received from organizations or entities representing these structural types, or the instrumentation is specifically called for by the Seismic Safety Commission in urgency situations.*
- (b) *The structural types subject to this section include all of the following:*
 - (1) *Hospitals.*
 - (2) *Dams.*
 - (3) *Bridges.*
 - (4) *Schools.*
 - (5) *Powerplants.*

OSHPD under the authorities of the HSSA and specifically section 129680(d):

. . . It is further the intent of the Legislature that the office, with the advice of the Hospital Building Safety Board, may conduct or enter into contracts for research regarding the reduction or elimination of seismic or other safety hazards in hospital buildings or research regarding hospital building standards.

has created the Hospital Building Instrumentation Program under contract with the CSMIP for the installation, maintenance, and monitoring of seismic instrumentation of hospital buildings. The primary goal of the program is not that much different than those reported by several authors in a variety of engineering journals and publications: Learn from earthquakes by materializing all the steps of the scientific methodology: observation, hypothesis, prediction of the consequences of that hypothesis, and observations to test those predictions. *"Predictive modeling is at the heart of building engineering. Predictive modeling is central to everything earthquake engineers do from post-earthquake investigations to retrofitting buildings, to designing buildings to performance base engineering"* [Stepp 2002].

There are three main approaches to evaluate seismic behavior and performance of structural systems: 1) Laboratory testing, 2) Analysis of mathematical models using Computerized Simulation methods, and 3) Real world laboratory.

The merits of each approach have been enumerated and debated repeatedly by many authors of earthquake engineering publications and journals. In the case of earthquake engineering, laboratory experimentation can be used to test many hypotheses. However, laboratory testing is infeasible because of size, cost etc., so the best option is to take advantage the real world laboratory of earthquake experience.

The problems with the real-world laboratory are that earthquakes occur infrequently. Therefore in optimum test areas (seismically prone areas) we have selected hospital buildings with varying seismic resistive systems, installed integrated arrays of instruments to measure, and capture the ground motion at the selected site near the subject building as well as the response of the structure to the subject ground motion.

The data gathered from a well-designed hospital instrumentation program will satisfy in part the goals of the HSSA with regards to earthquake engineering research by providing the basic source data to improve understanding of the behavior and potential for damage of such structures under the forces generated and imposed by catastrophic earthquakes. As a result of this understanding, design and construction practices can be modified so that future earthquake damage is minimized and the objectives of the HSSA are fully met – continuous operation.

Hospital buildings are instrumented through two separate paths: 1) Required instrumentation under the California Building Code (CBC) provisions and 2) Hospital Building Safety Board (HBSB) - Instrumentation Committee recommendation and selection process.

CBC Requirements for Hospital Building Instrumentation.

Section 1615A.1.40 of the CBC requires the following for hospital building instrumentation:

Earthquake Motion Measuring Instrumentation and Monitoring. [OSHPD 1 & 4] . . .

For buildings with a seismic isolation system, a damping system or a lateral force resisting system (LFRS) not listed in ASCE 7 Table 12.2-1, earthquake motion measuring instrumentation and monitoring shall be required. . . .

Instrumentation: *There shall be a sufficient number of instruments to characterize the response of the building during an earthquake and shall include at least one tri-axial free field instrument or equivalent. A proposal for instrumentation and equipment specifications shall be forwarded to the enforcement agency for review and approval. The owner of the building shall be responsible for the implementation of the instrumentation program. Maintenance of the instrumentation and removal/processing of the records shall be the responsibility of the enforcement agency.*

Furthermore Section 3415A.1 states the following:

Earthquake recording instrumentation of existing buildings. *All owners of existing structures, selected by the enforcement agency for the installation of earthquake-recording instruments, shall provide space for the installation and access to such instruments. Location of said instruments shall be determined by the enforcement agency. The enforcement agency shall make arrangements to provide, maintain, and service the instruments. Data shall be the property of the enforcement agency, but copies of individual records shall be made available to the public on request and the payment of an appropriate fee.*

Hospital Buildings with seismic isolation and or passive energy dissipation are required by the CBC to be instrumented. Different types of applications of such systems will perform differently. Instrumentation provides the opportunity to reveal which type of such systems is more effective than others. OSHPD wants to promote buildings with new and innovative seismic resistant systems of predictable seismic response and behavior. However, occasionally designs of hospitals buildings are submitted for review that use such seismic resistance systems (deemed as experimental) are not permitted by the CBC because the building code has not caught up with technology. In those cases, OSHPD under the provisions of “alternate means of compliance” permits such systems for hospital construction provided that such building will be instrumented prior to the issuance of the certificate of occupancy. Examples are Buckling Restrained Braced Frames, Steel Plate Shear Walls, new soil stabilization systems that become part of the building foundation, etc. In such cases, the owner is responsible for the cost of the instrumentation and installation with OSHPD responsible for the maintenance of the instrumentation and data retrieval through CSMIP.

Hospital Building Safety Board (HBSB) - Instrumentation Committee Recommendations and Selection Process.

The goal of OSHPD with the assistance of the HBSB Instrumentation Committee is to instrument with a sufficient array of sensors (including a free field) station two hospital buildings per year in addition to any buildings required to be instrumented by the CBC.

The committee works from a list of candidate hospital buildings that have been selected for instrumentation. The list of candidate hospital buildings has been formulated by the committee based on specific eligibility criteria. Some of eligibility criteria that the Committee considers in order to place a building on the list of candidate hospital buildings for instrumentation is as follows:

1. Close proximity to one or more of the many major California faults capable of generating a large earthquake(s) ($M>6.5$)
2. Sites w/ high probability of seismic event(s)
3. Type of structural system
4. Soil type (soft soil)
5. Tall interstory heights
6. Adjacency to other buildings (pounding)
7. Buildings with projecting wings
8. Template Buildings on the same site
9. Building system configuration (irregularities)
10. Seismically retrofitted buildings
11. Buildings reassessed from an SPC-1 level to an SPC-2 through the HAZUS methodology

Since the inception of the Hospital Building Instrumentation Program, fifty-five (55) hospital buildings have been instrumented. Each such instrumented building has a well optimized number of sensors placed at critical locations to generate meaningful data that characterizes the response of the subject buildings in order to help the scientific and engineering community in assessing design/analysis procedures thereby validating the mandates of the HSSA. Figure 2 illustrates one such hospital instrumentation scheme.

Figure 3 illustrates all locations of instrumented hospital buildings - CBC required and HBSB Instrumentation and Committee selected - superimposed on the California probabilistic hazard map depicting regions with PGAs greater than 20% in 20 years on alluvial soil conditions.

Why the Need for a Separate Inventory of Instrumented Hospital Buildings?

Based on the preceding discussion, California hospital buildings are different than other less essential occupancy buildings in the state. The California hospital buildings are separated into two major classifications: Pre-Act buildings and Post-Act buildings. Pre-Act buildings were permitted prior to March 7, 1973 and are not in compliance with the HSSA. Post Act buildings were permitted and constructed after March 7, 1973 and are in compliance with the requirements of the HSSA. Post-Act buildings possess higher strength and stiffness than typical buildings built in the same era under the requirements of the model code enforceable at that time. The response of hospital buildings will be very different than nonhospital building of the same era even though they are built of the same material, structural system engineering methodologies etc. Strong motion records from hospitals buildings tell the story of different performance. Figure 4 illustrates the recorded accelerations from a 1 story Hospital in Templeton during the San Simeon Earthquake of December 22, 2003. The building is Post Act vintage and despite the

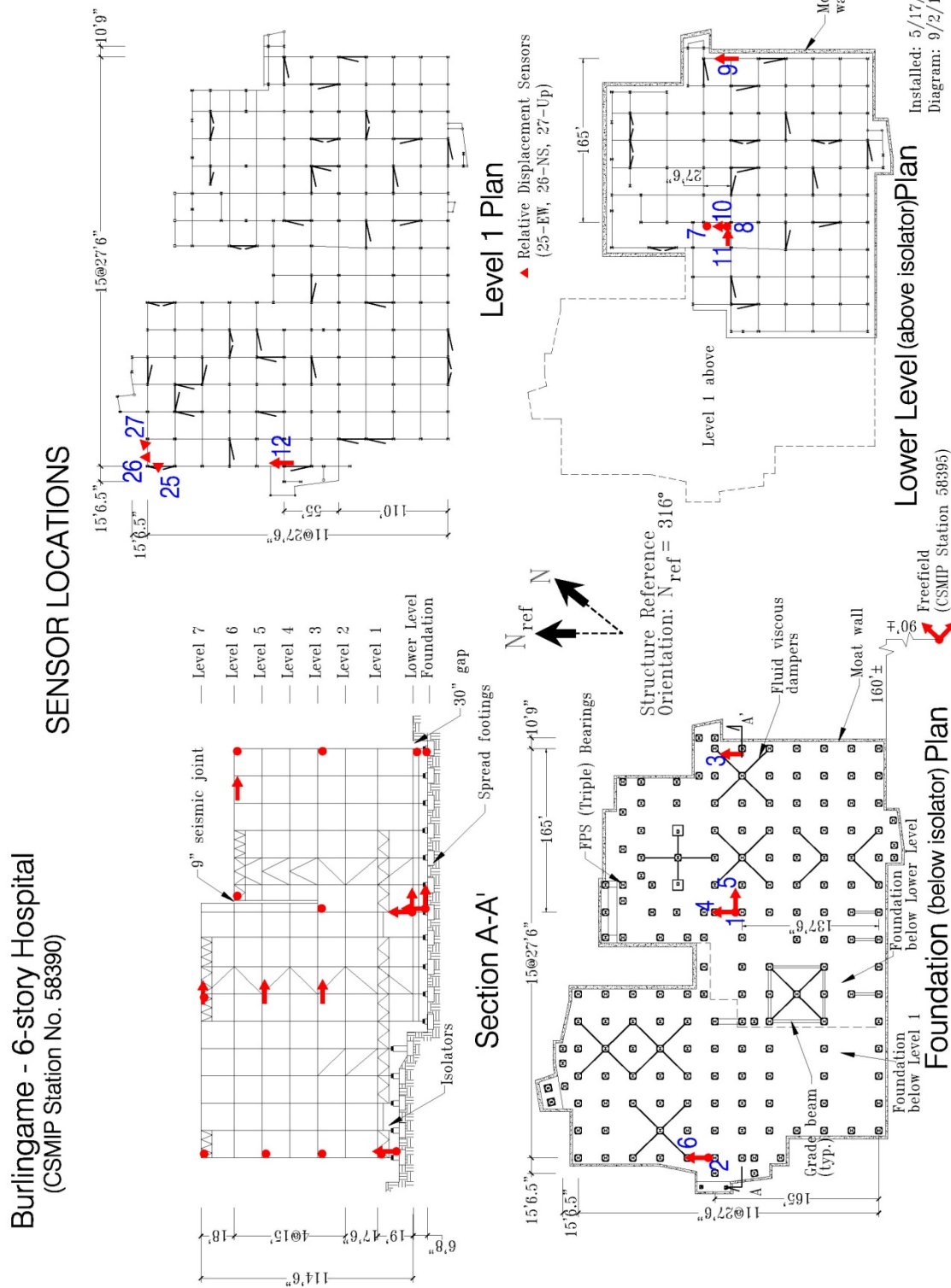


Figure 2. Example of Hospital Building Instrumentation Layout

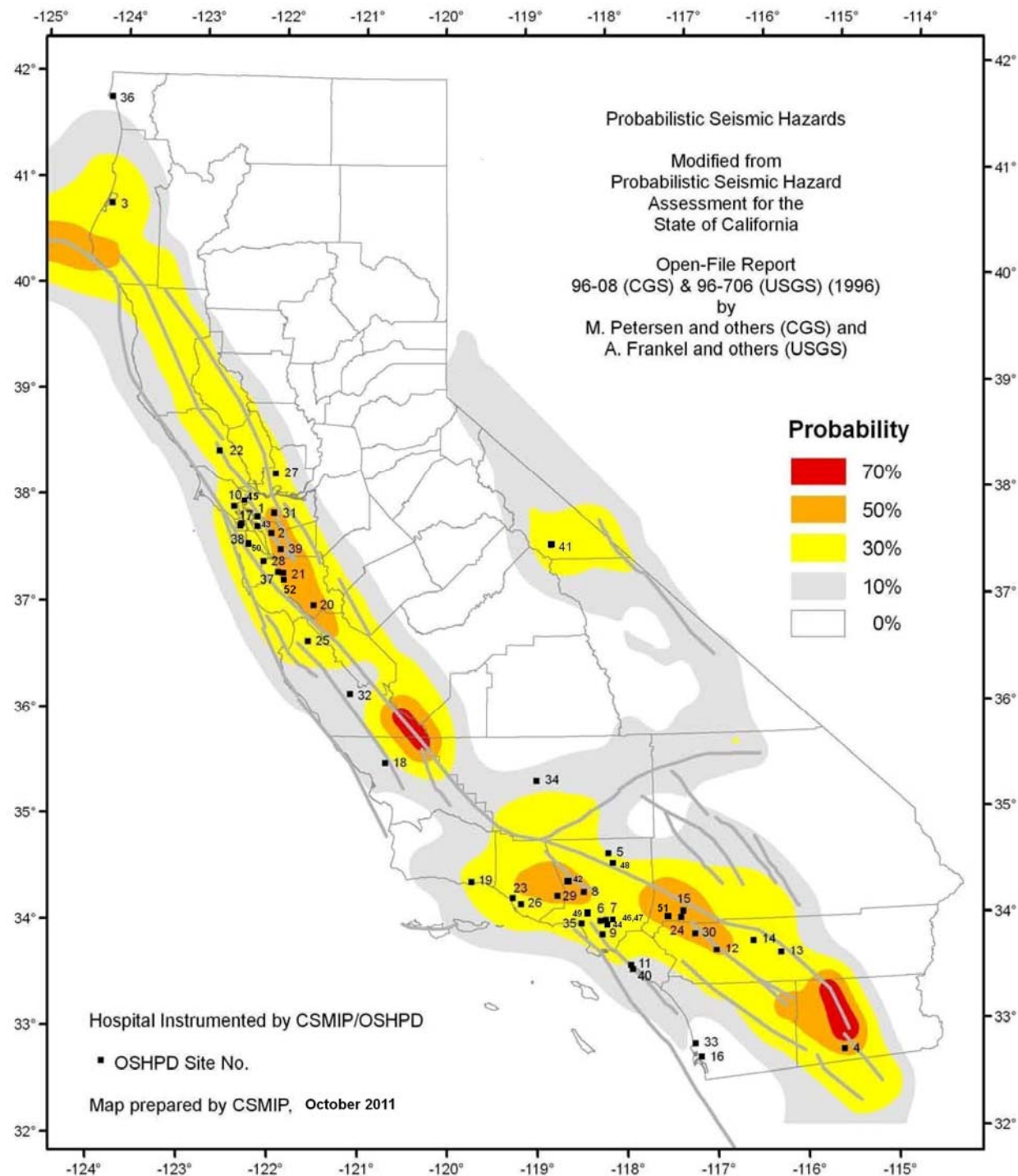


Figure 3. Instrumented Hospital Buildings by SMIP/OSHPD for sites with PGA > 0.2g in 20 years on alluvial soil conditions.

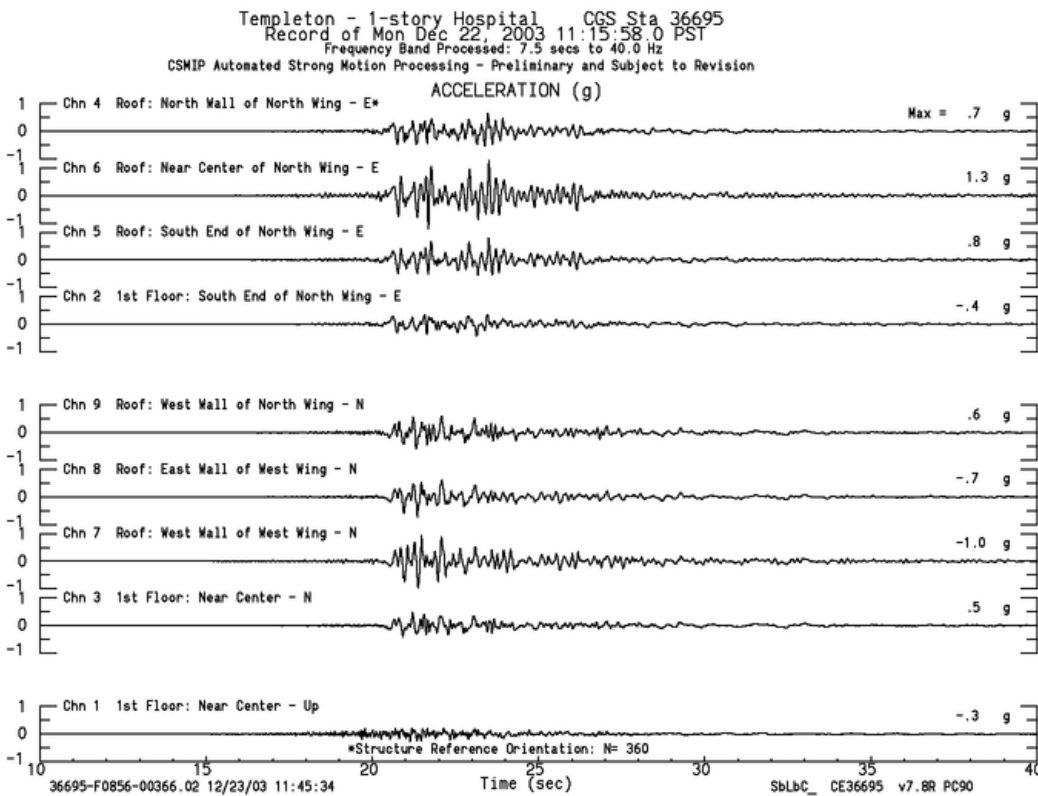


Figure 4. Recorded accelerations from the 1 story Hospital in Templeton during the San Simeon Earthquake of December 22, 2003

strong demand from the ground motion, the structure had enough strength and did not suffer any structural damage during the earthquake.

More importantly hospital building instrumentation is one of the performance indicators validating the requirements of HSSA.

The HAZUS methodology has been recently used as a means to reclassify buildings from posing a significant risk of collapse and a danger to the public (SPC-1), to buildings that do not significantly jeopardize life, but may not be repairable or functional following strong ground motion (SPC-2). However, this HAZUS methodology is mostly untested in a strong seismic event; the need for seismic instrumentation becomes obvious. Because of the infrequent and unpredictable nature of when and where an earthquake will occur, it is important to start such preparation early, so that valuable information useful to develop earthquake protective technology is not lost.

Emergency Response

OSHPD has statutory authority (HSSA, Section 130025) and responsibilities in the event of a seismic event, or other natural or manmade calamity to activate its emergency response center and mobilize a specialized team of authorized representatives in order to examine the

hospital building structure(s) or systems affected by such an event. Furthermore the same section of the HSSA requires that:

. . . If, in the opinion of the office, the structural integrity of the hospital building or any system has been compromised and damaged to a degree that the hospital building has been made unsafe to occupy, the office may cause to be placed on the hospital building either a red tag, a yellow tag, or a green tag.

The California Seismic Instrumentation Program in general as well as the Hospital Instrumentation Program are an essential tool for the OSHPD emergency response and recovery operations. Seismic networks (CSIN) along with instrumented buildings provide OSHPD real time earthquake data to respond efficiently and effectively in a seismic event and carry out its statutory responsibilities.

Utilizing the ShakeMaps which are usually available within minutes of the occurrence of strong shaking along with strong motion records from instrumented buildings, specific GIS information that the office has developed over the years and other intelligence information collected from the field, the office can structure a very efficient plan of response to deploy its resources in the most effective manner. That means number assessment teams, which facilities first, etc. A recent example of such response is the latest significant seismic events in Brawley in South California on August 26, 2012.

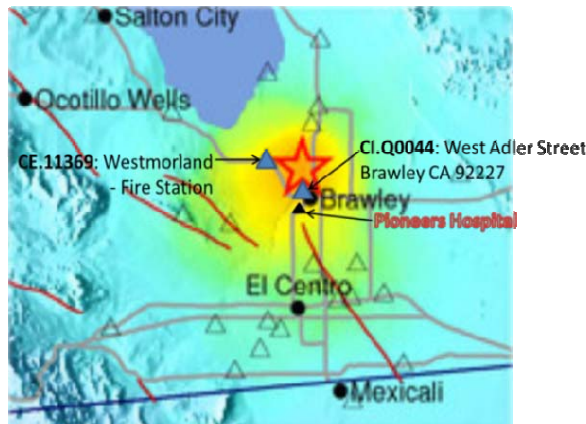


Figure 5. ShakeMap Brawley M5.5 Earthquake August 26, 2012

CI.Q0044: West Adler Street, Brawley CA 92227	Agency: Southern California Seismic Network				
Lat: 32.9860 Lon: -115.5469 Distance: 3.0 km from source					
Intensity: 7.8 Location: 345 West Adler Street, Brawley CA 92227					
Station Comp	Max Vel (cm/s)	Max Acc (%g)	PSA: 0.3 sec (%g)	1.0 sec (%g)	3.0 sec (%g)
01.HNN	39.6971	45.1719	98.6657 -T	42.7503	6.5662
01.HNE	36.0459	28.7961	70.3703 -T	19.7977	10.2899
01.HNZ	11.2906	49.2668	30.9127 -T	6.8925	4.5785

Figure 6. Strong Motion Record, Station SCSN-CI.Q0044, Brawley M5.5 Earthquake August 26, 2012

Having the appropriate strong motion information along with detailed structural system information (Steel SMRF Systems used in the subject hospital buildings) focused the OSHPD post-earthquake assessment team on what to look for and the recommendations to make to the hospital owner for a detailed post-earthquake evaluation report.

Conclusions

1. Looking back at the first steps of the hospital seismic safety program as well as looking ahead at the approaching 2013 deadline it is imperative to point out that significant progress has been achieved.
2. The hospitals are making progress. California hospitals indeed are safer today, but there is still work to do.
3. The HSSA requires hospitals to be in substantial compliance with the HSSA by January 1, 2030 and all general acute care hospitals must be able to remain operational beyond that point in time.
4. The hospital seismic instrumentation program is monitoring the pulse and health of the HSSA.
5. Performance based engineering is the next step in the profession. The hospital instrumentation program will give the capability to the earthquake engineering community to validate the predictions of risk analysis tools such as HAZUS and PACT.

References

Office of Statewide Health Planning and Development (1995). "The Northridge Earthquake: A report to the hospital building safety board on the performance of hospitals in the Northridge Earthquake of January 17, 1994." OSHPD, Sacramento, California.

Tokas, C.V. and Schaefer, K. (1999). "The Seismic Safety Program for Hospital Buildings in California, Part 1: Seismic Performance Requirements for New Hospital buildings", Workshop on Seismic Design and Retrofitting of Hospitals in Seismic Areas, Florence, Italy, October 21-22, 1999.

Tokas, C.V. and Schaefer, K. (1999). "The Seismic Safety Program for Hospital Buildings in California, Part 2: The Seismic Retrofit Program for Existing California Hospitals." Workshop on Seismic Design and Retrofitting of Hospitals in Seismic Areas, Florence, Italy, October 21-22, 1999.

Huang, M. and Tokas, C.V. (2004). "Recorded Response and Observed Performance of a Wood-Frame Hospital Building During the 2003 San Simeon Earthquake", in *Proceedings of SMIP04 Seminar on Utilization of Strong-Motion Data*, Strong Motion Instrumentation Program, Sacramento, May 17, 2004, p. 125-136.

Tokas, C.V. and Lobo, R.F. (2009). "Risk Based Seismic Evaluation of Pre 1973 Hospital Buildings Using the HAZUS Methodology", Paper presented and published in *Proceedings of the ATC & SEI Conference on Improving the Seismic Performance of Existing Buildings and Other Structures*, San Francisco, December 2009.

Stepp, J. C. (2002). "Strategies and Criteria for Selecting Buildings for ANSS Strong-Motion Instrumentation", Strong Motion Instrumentation Program, California Geologic Survey, Sacramento, 2004.

Celebi, M. (2000). "Seismic Instrumentation of Buildings", Open File Report 00-157, USGS, Menlo Park, California, 2000.

Porter, K. A. (2002). "Learning from Earthquakes: a Survey of Surveys", Earthquake Engineering Research Institute, Oakland, California, 2002

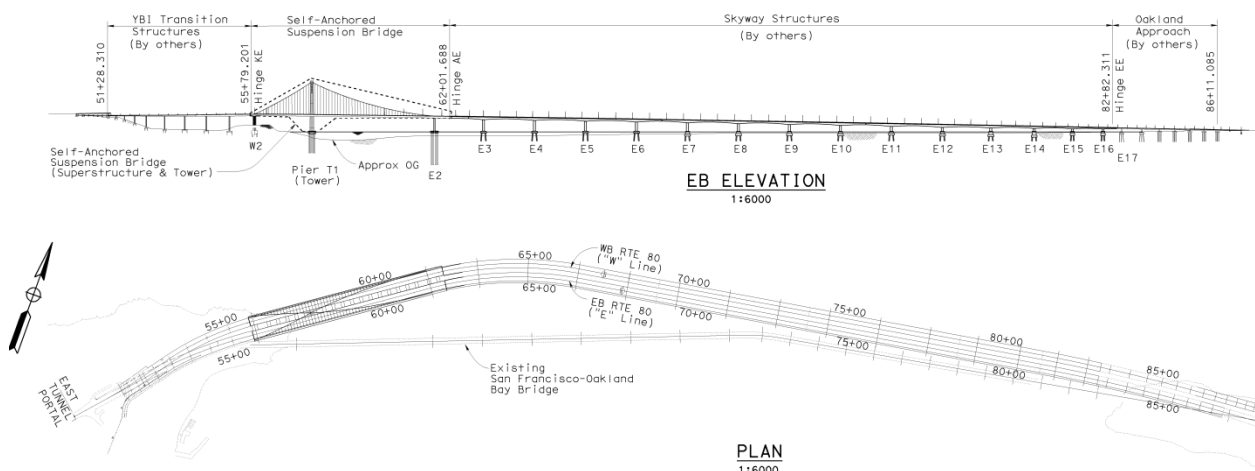
SAN FRANCISCO-OAKLAND BAY BRIDGE NEW EAST SPAN: CONSTRUCTION PROGRESS AND CHALLENGES

Brian Maroney

California Department of Transportation
Sacramento, California

San Francisco-Oakland Bay Bridge: New East Span

The new Bay Bridge East Span is comprised of four major structures. From west to east they are: (1) the Yerba Buena Island Transition Structure, (2) the Self-Anchored Suspension Bridge, (3) the Skyway, and (4) the Oakland Touchdown Approach. The entire East Span is being targeted for opening on Labor Day weekend of 2013 (more information is available at <http://www.baybridgeinfo.org>). The entire structure is 3.5 km (2.2 miles) long.



The Yerba Buena Island Transition Structure (YBITS)

461 meters long; cast-in-place concrete box girders; several outrigger bents; under construction. This section will be instrumented with 28 sensors.

The Self-Anchored Suspension Bridge (SAS)

623 meters long with a 385m main span and a 180m back span. A unique signature structure with a 160m tall tower that is comprised of 4 steel shafts connected with steel shear links, and steel box girders connected by steel cross beams; under construction. This bridge is being instrumented with 86 sensors.

The Skyway

2,085 meters long; 4 concrete frame structures separated by hinges with steel pipe beams; 452 pre-cast concrete segments; 3-cell concrete box girders; construction completed in April 2008. Instrumentation of this structure with 73 sensors has been completed and is online.

The Oakland Touchdown Approach (OTD)

330 meters long; cast-in-place concrete box girders; phase 1 construction completed in June 2010, phase 2 under construction. The approach has been instrumented with 12 sensors. A geotechnical array with 15 sensors, to a depth of 160 meters, has been installed at a site southeast of the approach.

